CONSTRAINING THE BODY FOR BETTER FORCE-TRACKING ANALYSIS

A Thesis

Presented to the Faculty of the Graduate School

of Cornell University

in Partial Fulfillment of the Requirements for the Degree of

Master of Science

by

Megan Elizabeth Thompson

May 2008

ABSTRACT

My work has two goals: to develop a method capable of comfortably isolating a single group of muscles to improve *in vivo* human muscle testing and to investigate how well humans can track target force profiles.

I designed, built, and tested a system for isolating leg-extensor muscles (muscles that lift the lower leg) and for measuring knee extension forces during an interactive tracking experiment featuring computer feedback. The chair was designed to isolate the leg-extensor muscle and to eliminate movement by forming rigid connections to the body. When properly constrained in the chair, the maximum movement observed during "fixed" leg angle experiments was a leg rotation of 1°.

In the first force-tracking experiments, the test subject tracked a periodic target force function at a fixed leg angle. In the second experiments, the subject attempted to match a constant, ramp, or sine wave force profile as her leg angle was being oscillated from 90° to 120° by a motor. Target wave frequencies for the fixed-angle experiments were 0.10 Hz, 0.25 Hz, 0.50 Hz, 1.00 Hz, and 2.00 Hz; for variable-angle experiments: 0.25 Hz, 0.50 Hz, or 1.00 Hz.

Among fixed-angle tests, the lowest RMS error was 4.12%, and the highest was 23.86%. The best variable angle result, obtained while tracking a constant force, was 9.06%. Error was considerably lower for fixed-angle experiments than it was for variable-angle experiments–the lowest measured error in variable-angle tests was similar to the highest error in fixed-angle tests. Results generally improved with increasing target force magnitude and worsened with increasing target and forcing frequency. For fixed-angle tests, conducting additional tests improved accuracy but not precision; the opposite was true for variable-angle tests.

BIOGRAPHICAL SKETCH

Megan earned her B.S. in Mechanical Engineering at Clemson University, graduating summa cum laude. While there, she completed three co-op rotations with Michelin, as well as an honors research project with Professor Jay Ochterbeck. In her first co-op rotation, Megan worked with the quality control group to improve repeatability and reproducibility of quality testing methods. In her second rotation, Megan worked with the Michelin prototype tire shop, helping design mechanisms to aid in tire production. Megan spent her third co-op rotation working with Michelin's original French division in Claremont-Ferrand, France. There, she designed components for a new, proprietary extruder. In her senior year, Megan completed a senior design course, helping to improve a proprietary production method (again for Michelin). She also worked with Jay Ochterbeck on an honors research project seeking to better understand and utilize loop heat pipes.

At Cornell University, Megan began her graduate studies with Professor Nicholas Zaberas, working to create mesascale computational materials models for use in multiscale material modeling. Megan later joined Professor Andy Ruina's Human Locomotion and Robotics Laboratory, where she researched the mechanical properties and capabilities of muscles in humans, *in vivo*. While at Cornell, Megan also spent two semesters organizing and managing the Machines and Organisms weekly seminar.

I dedicate this thesis to Judson, whose patience and encouragement has helped me work through this process, and to my parents and brother.

ACKNOWLEDGEMENTS

I have been humbled to work with a large collection of great minds throughout my education. First, I would like to thank the head of my academic committee and my graduate studies advisor, Professor Andy Ruina, who introduced me to human locomotion studies, helped to guide my research, and provided support throughout this process. His optimism, keen mind, and sense of humor have also been great boons in my research.

I would also like to thank Professor Francisco Valero-Cuevas, who taught me the basics of muscle physiology and who always had great suggestions for furthering my research. Members of Professor Valero-Cuevas's lab were often equally helpful: I would especially like to thank Madhu Venkadesan, Lisa Toth, Alicia Velázquez, Manish Kurse, and Kevin Keenan for inspiration and friendship.

Professor Mike Thompson has a great mind and is a helpful committee member. Through his patience, I understand thermodynamics and computational materials science far better than I would have had I been left to my own devices.

When I was at Clemson, Professors Imtiaz Haque, J. Leo Gaddis, Paul Frank, and Jay Ochterbeck were great sources of encouragement and inspiration. Before then, back in high school, Mr. Bryan Coburn, my Advanced Placement Computer Science teacher, was an excellent fan and supporter of women in science and engineering.

I'd like to thank the other members of Professor Ruina's Human Locomotion and Robotics Laboratory for their support, friendship, encouragement, and aid. Without the help of Edgar Rios and Jason Cortell, in particular, I would not have been able to finish my studies.

Finally, I'd like to thank the National Science Foundation for making my graduate studies possible through their funding.

TABLE OF CONTENTS

LIST OF TABLES

LIST OF FIGURES

CHAPTER 1

INTRODUCTION

One way to better understand locomotion is to investigate the relationship between energy expenditure and muscle activity. By collecting force, velocity, and position data through *in vivo* human muscle tests, and by investigating how humans respond to dynamic variations in muscle position and loading, we can develop an improved understanding of muscle mechanics not necessarily determinable in animal- or *in vitro* testing. If energy expenditure data, such as heart rate, temperature, and oxygen uptake, are recorded while the test subject performs muscle exercises, we can begin to hope to find a relationship between muscle mechanics and muscle energy use. If we then assume people and animals use as little energy as possible to accomplish goals, then once we have determined which muscles are used in human locomotion activities, we may be able to predict how a person would move. Such locomotion predictions would require us to perform an energy optimization routine on all the muscles involved in the motion and to have developed a working understanding of muscle mechanics at the system level. The first step in developing such locomotion predictions is to understand the performance capabilities and the mechanics of *in vivo* muscle.

From Blix's first investigations into muscle modeling in 1874 as reported in [Norssell, 2000] to modern studies that decompose myoelectric signals into motor-unit specific action potential trains [de Luca and Mambrito, 1987], much work has been conducted to understand the properties and capabilities of the human machine. Many scientists and engineers have committed their lives to learning more about muscle, but one issue remains largely unstudied: the properties and mechanics of human muscle *in vivo*. Although developing and applying constraints

to limit motion during human testing applications is often mentioned in the literature, there seems to be little information about the performance of these isolation devices. A means to gain this understanding is through force-tracking experiments. This thesis attempts to address the force-tracking abilities of humans and to present an apparatus for isolating the leg extensor muscles.

Understanding human force resolution and capabilities could also aid our ability to design realistic virtual environments, where the properties of the human system can be exploited for performance gains [Tan et al., 1994]. Physical therapy applications are also a possibility, as knowing how accurately a normal, healthy person can produce and maintain a particular force under given conditions could allow therapists to better evaluate their patients.

The development of a muscle isolation chair is necessary not only to facilitate the force-tracking experiments, but also to enable future research into muscle energetics. The major goals in developing "the chair"—the muscle isolation chair—are to isolate the leg extensor muscles and to prevent motion of the body.

This thesis begins with a literature review and background information about muscle anatomy, physiology, and modeling. Next, the development and features of the muscle isolation chair are described. Subsequently, the fixed-angle force-tracking methodology, experiments, and results are described. Then the variable-angle force-tracking experiments and methodology are discussed. Finally, a discussion section compares and contrasts experimental results.

CHAPTER 2

LITERATURE REVIEW AND BACKGROUND INFORMATION

2.1 Contraction dynamics

A. V. Hill, who won the Nobel Prize in Medicine or Physiology for his muscle research, developed the basic model for muscle force production still used today. Hill used a thermopile to measure the energy released from frog sartorius muscles during *isometric* (contractions in which the length of the muscle remains unchanged) and *isotonic* (contractions in which the muscle contracts under a constant tension) contractions. Hill's work revealed that muscle released energy in two different ways: as heat proportional to the distance the muscle shortened and as mechanical work [Hill, 1938].

Because the heat produced by a contraction is proportional to the change in length of the muscle, this energy term could be represented as though it were a work term, ax. The proportionality constant, a has units of force and depends on both the size (in particular, on the cross-sectional area) of the muscle and the strength of the contraction [Hill, 1938].

Hill's experiments showed that while changes in the speed of the muscle contraction affect the heat rate–as the heat rate is inversely proportional to the load,– the total energy is constant. Thus combining the mechanical work term with the heat of shortening term resulted in Hill's famous equation relating muscle force to velocity:

$$(P + a)(v + b) = (P_0 + a)\, b = \text{constant} \tag{2.1}$$

where P is the force of contraction, P_0 is the maximum isometric force, v is the velocity of shortening, and a and b are constants.

Investigating the viscoelasticity of muscle tissue in the context of his energy experiments, Hill concluded that active muscle can be modeled as a two-component system consisting of a contractile element governed by Eq. 2.1 in series with a purely elastic element [Hill, 1938], as shown in Fig. 2.1. This concept is still prevalent in many modern muscle models [Zajac, 1989, Wilkie, 1950, Buchanan et al., 2004].

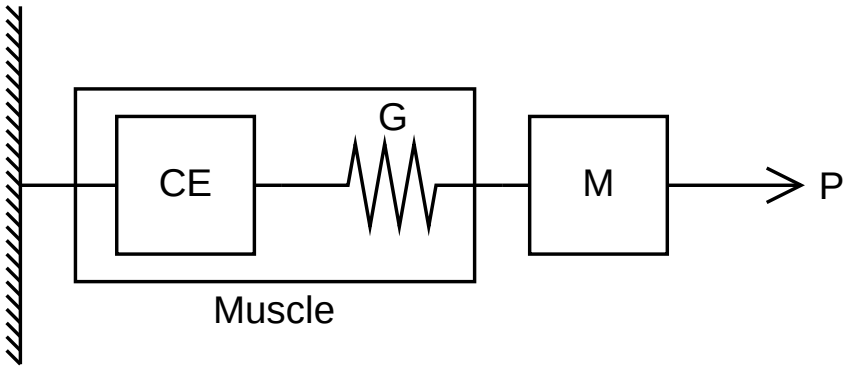

Figure 2.1: Schematic of Wilkie's model of active muscle contraction. The muscle itself consists of a contractile element, *CE*, in series with an elastic element, *G*. The entire muscle is then in series with an inertial term, *M*.

After conducting a series of *in vivo* isometric and isotonic experiments seeking to model the force-velocity behavior of human muscles *in vivo*, Wilkie [Wilkie, 1950] applied Hill's model to include interaction with an inertial term and the series elastic term originally proposed by Hill. If a muscle performing an isotonic contraction is assumed to act against an inertia along with the constant load, then the force exerted by the muscle becomes:

$$P = F + M\frac{dV}{dt} \tag{2.2}$$

where P is the total load exerted by the muscle; F is the isotonic load; M is the mass of the inertial load, and V is the measured velocity [Wilkie, 1950].

Substituting Eq. 2.2 into Eq. 2.1 yields [Wilkie, 1950]:

$$\frac{(P_0 + a)\, b}{v + b} - a - F = M\frac{dv}{dt}. \tag{2.3}$$

When the series elastic term is included, the measured velocity becomes the sum of the velocity of contraction and the velocity of the series elastic element: $V = v + G\frac{dP}{dt}$, where v is the velocity of contraction, and G is the compliance of the elastic element. The force-velocity relationship becomes [Wilkie, 1950]:

$$v + GM\frac{d^2v}{dt^2} = \frac{(P_0 + a)\, b}{F + M\,(dv/dt) + a} - b \tag{2.4}$$

Thus, in an isometric muscle contraction, the active element shortens at a rate:

$$V = \frac{(P_0 + a)\, b}{P + a} - b, \tag{2.5}$$

and the passive element lengthens at a rate of $G\frac{dP}{dt}$. The compliance of the series elastic element is thus [Wilkie, 1950]:

$$G = \frac{(P_0 + a)\, b}{P + a} - \frac{b}{dP/dt}. \tag{2.6}$$

Most modern models of contraction dynamics assume a form similar to the one shown in Fig. 2.2. Muscle force is assumed to result from the contributions of a passive element, PE (representing tendon compliance), and an active, contractile element, CE. The force in the active muscle component is assumed to be a function of muscle activation, length, and velocity. Hill's equation is typically modified to determine the effect of the contractile element [Zajac, 1989]. The series elastic element, or SEE, shown in Fig. 2.2 represents the muscle series elastic element.

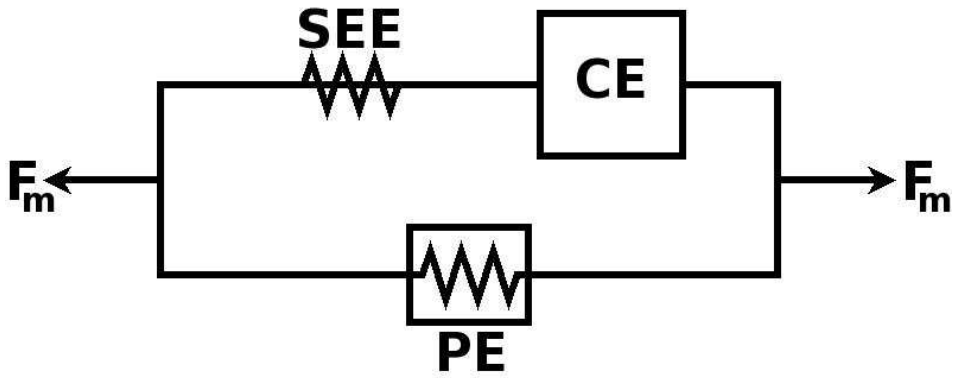

Figure 2.2: Modern Hill-type model for muscle contraction dynamics. The muscle is composed of active and passive components that act in parallel. The passive component is modeled with an elastic element, *PE*. The active component consists of a contractile element, *CE*, in series with an elastic element, *SEE*

Many muscle models neglect the SEE because, compared to the energy storage capability of tendons in most muscles, the contribution of the SEE is negligible [Zajac, 1989].

2.2 Tracking experiments

Examples of *in vivo* human force-tracking experiments seem somewhat rare in the literature. In real and in virtual settings, contact force helps drive human motor performance and influences the human sense of proprioception—the perception of the location, orientation and movement of one's own body and parts. Thus, in addition to research done by physiologists and kinesiologists, haptics researchers have studied the ability of the human machine to track forces through their work on design considerations for controllers.

Broadly defined, haptics is the study of touching behavior. In engineering, haptics research is generally focused on developing virtual environments that feel realistic to users. To create realistic virtual settings that are affordable and that work within the realm of current hardware limitations, haptics researchers seek to exploit the limits of human perception [Tan et al., 1994]. In order to develop and use these exploits, scientists and engineers must first identify and understand the limits of human sensing. Haptic devices are generally used to either measure the location and orientation of users' hands and the contact forces they apply or to emulate real forces and positions within a virtual environment [Tan et al., 1994].

Understanding how well humans can control or track a force is one potential area to exploit the human system to provide a more realistic virtual setting. Much research has been done to investigate the Just Noticeable Difference (JND) of weight sensing in humans [Tan et al., 1994, Srinivasan and Ruina, 2006], but much less work has been done to investigate human force-tracking precision and accuracy. In this thesis, "force-tracking" refers to the ability of a person to generate a force or a series of forces that matches a target force or a series of target forces. For force-tracking experiments, the subject is not concerned with position and is only attempting to contract his or her muscles in order to match a predefined target. Tan *et al.* conducted one such experiment. After determining the maximum sustainable force attained by each of three test subjects at the fingers, the hand, the wrist, the elbow, and the shoulders, Tan asked the test subjects to attain and maintain a force equal to approximately half of their maximum sustainable force. Three trials were conducted for each joint, and only the steady-state portion of the resulting force data was considered. Subjects were allowed to rest between each trial. Force-tracking resolution, reported as the standard deviation of the recorded force, was found to range from 0.71% to 3.35%. In general, reso-

lution improved (the percentage decreased) the closer to the body (more *proximal* the joint in question was [Tan et al., 1994].

While Tan *et al.* were interested in how force-tracking resolution depends on the distance from the center of the body to the joint in question, Kilbreath and Gandevia studied how force-tracking abilities varied among the different muscles of one small area. Kilbreath and Gandevia tested force-tracking capability of two hand muscles and of two thumb muscles. When subjects attempted to match forces when lifting weights with two thumb muscles–the *flexor pollicis longus* (FPL) and the *adductor pollicis* (AP), they were more precise than they were in weight-matching experiments using two hand muscles–the *first dorsal interosseous* (FDI) and the *flexor digitorum profundus* (FDP). The coefficient of variation ($100 \cdot \frac{stddev}{mean}$) was 13.5±4.0% for the best performing muscle, the FPL, and 17.6±6.6% for the worst performing muscle, the FDP. The tests performed by Kilbreath and Gandevia also showed that accuracy improved as the weight to be matched increased, with a c.v. of 19.1% at 2.5% MVC and a c.v. of 12.9% at 50% MVC [Kilbreath and Gandevia, 1993].

Kilbreath and Gandevia studied how well the same person could identify a given force with four different hand and thumb muscles. Tan et al. approached force-matching experiments by determining that joints that are closer to the body (more *proximal* joints) had better force-matching precision than joints that are farther from the center of the body (*distal* joints). Neither Tan *et al.* nor Kilbreath and Gandevia studied how well humans could track a changing force profile. Srinivasan and Chen investigated how well people can control normal fingerpad contact forces. Test subjects used the index finger of their dominant hand to press on a glass plate outfitted with a load cell. Subjects were given constant visual feedback on a computer screen and were asked to track constant forces, ramp forces, and sine

waves. Constant force tracking was the most accurate. For constant force tests, the target force ranged from 0.25 N to 1.5 N in 0.25 N increments. Error in the constant force tests was independent of target force level and ranged from 2.6% to 15.6%. The ramp forces being tracked had slopes of 0.04 N/s, 0.069 N/s, and 0.110 N/s, and the tests ended when the target force reached 1.4 N. The force rate was found not to impact the test results. Absolute error was found to be higher for the ramp-tracking tests ($\varepsilon = 0.054$ N) than for the constant-force tests ($\varepsilon = 0.039$ N). Sine waves were tracked for two periods. Three frequencies, 0.0541 Hz, 0.0952 Hz, and 0.143 Hz, were tested. For each frequency, three sine-wave tracking tests were completed with amplitudes of 0.5 N, 1.0 N, and 1.5 N. Error in sine-wave tracking ranged from 0.043 N in an 0.5 N amplitude, 0.043 Hz test to 0.135 N in a 1.5 N amplitude, 0.143 Hz test. In general, error increased with both increasing frequency and with increasing force amplitude. The tests at the lowest amplitude, however, showed little deviation as the frequency increased [Srinivasan and Chen, 1993].

The tests conducted by Tan *et al.* and by Kilbreath and Gandevia provide results that can be compared to the force-tracking results in this experiment. Tan *et al.* further suggest that tracking forces with the leg extensor muscles should produce better results than tracking a force with the calves would. Kilbreath and Gandevia suggest that force tracking may actually be more difficult when the required exertion is smaller. The experiments conducted by Srinivasan and Chen parallel the tests I conducted on the leg extensor muscles and are thus very useful to my work. For a comparison of my results with those obtained by Srinivasan and Chen, refer to Sec. 4.4.

CHAPTER 3

DEVELOPMENT OF A MUSCLE GROUP ISOLATION CHAIR

Accurately measuring the force exerted by a muscle or a group of muscles on humans *in vivo* is facilitated by both a rigid contact point between the test subject and the measurement apparatus and by isolation of the muscle or muscle group in question from the effects of other muscle groups. In the literature, however, it is not uncommon to find tests where minimal or no constraints were used [Srinivasan and Chen, 1993, Tan et al., 1994, Slifkin et al., 2000, Doke et al., 2004]. A number of experimenters use simple straps, joint cups, or bracing boards, but these rarely discuss whether these restraints were sufficient to ensure negligible error [Alkner et al., 2000, Allum and Young, 1976, Wilkie, 1950, Weerakkody et al., 2003, Brockett et al., 1997].

In Peyton's inertia experiments, each test subject gripped a handle while resting his or her elbow in an elbow cup. The elbow cup was connected to the handle via square aluminum tubing, forming a rigid connection between the device and the test subject. Peyton reported that the device was tested to determine whether it needed additional restraints and that the device performed adequately as designed. Test subjects were, however, asked to grip the handle with just enough force to maintain a rigid forearm (more force would engage the muscles of the shoulder and back, skewing results). In his conclusions, Peyton found that the accuracy of his results could have been improved by reducing the interference of other muscles, which would have required a test apparatus that improved the coupling between the arm of the test subjects and the supports [Peyton, 1986].

The subjects in Doke's experiments that determined the energetic cost of swinging the leg struggled to maintain their upper-body posture during testing, even

though a support frame was used, and the subjects were able to brace themselves against a lumbar support [Doke et al., 2004].

De Luca and Mambrito designed a forearm and hand constraint for their research on motor-unit control. Their apparatus included a plastic cast to immobilize the wrist, hand, and fingers; and a polyester resin and styrene monomer cast that was custom fitted to each test subject to constrain the knuckle of the thumb. The custom cast was connected to a force transducer [de Luca and Mambrito, 1987].

3.1 Design objectives and considerations

The test apparatus was designed with the goal of creating a device that would constrain the body, isolating the leg-extensor muscles to enable better *in vivo* research. Because a variety of experiments were envisioned for use on the apparatus, the device needed to be as generic as possible and to be simple enough to allow for adaptations and enhancements later. The apparatus must adapt to a variety of test subjects. It should isolate the leg extensors while being as comfortable as possible. Test subjects using the chair would be performing a number of tests in which the apparatus controls the motion of one of their legs as they try to match a force; thus appropriate ergonomics were also of tantamount importance.

3.2 Specifications

The subject is seated and strapped into the chair. His or her leg is positioned in a leg swing attached to the chair, and a shin brace connecting the load cell (for fixed-angle tests) or the motor (for variable-angle tests) is attached to the shin brace.

Shoulder supports are then lowered, and their position is fixed, further preventing movement of the subject's upper body. A schematic of the device is shown in Fig. 3.1.

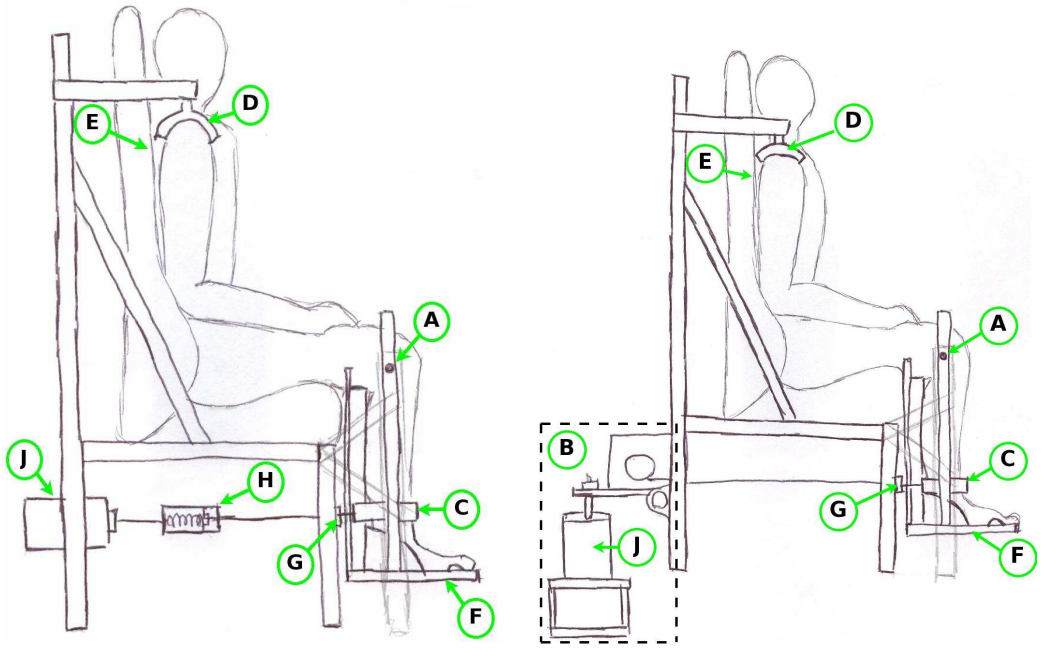

(a) Fixed-angle configuration *(b) Variable-angle configuration*

Figure 3.1: Schematic of the muscle isolation chair. (A) Axis of rotation of the leg; (B) Motor assembly (C) Shin brace; (D) Shoulder restraints; (E) Modified seat back; (F) Foot swing; (G) Cable connector; (H) Pretensioner; (J) Load cell

3.2.1 Structure

The chair's frame and structural support elements are made from perforated steel angle bracing. All open corners have been filed to protect passers-by from injury. Diagonal supports serve to add rigidity and to reinforce the chair. A racing seat is affixed to the steel structure, providing ergonomic seating for the test subject. The back of the racing seat was modified by replacing the foam cushions with plywood to provide rigid back support, while a plywood square was added to the seat to

help reduce the effect of compliance on the legs. The chair is equipped with a four-point racing harness used to reduce upper-body movement. The test subject holds an emergency stop button as (s)he participates in the experiments.

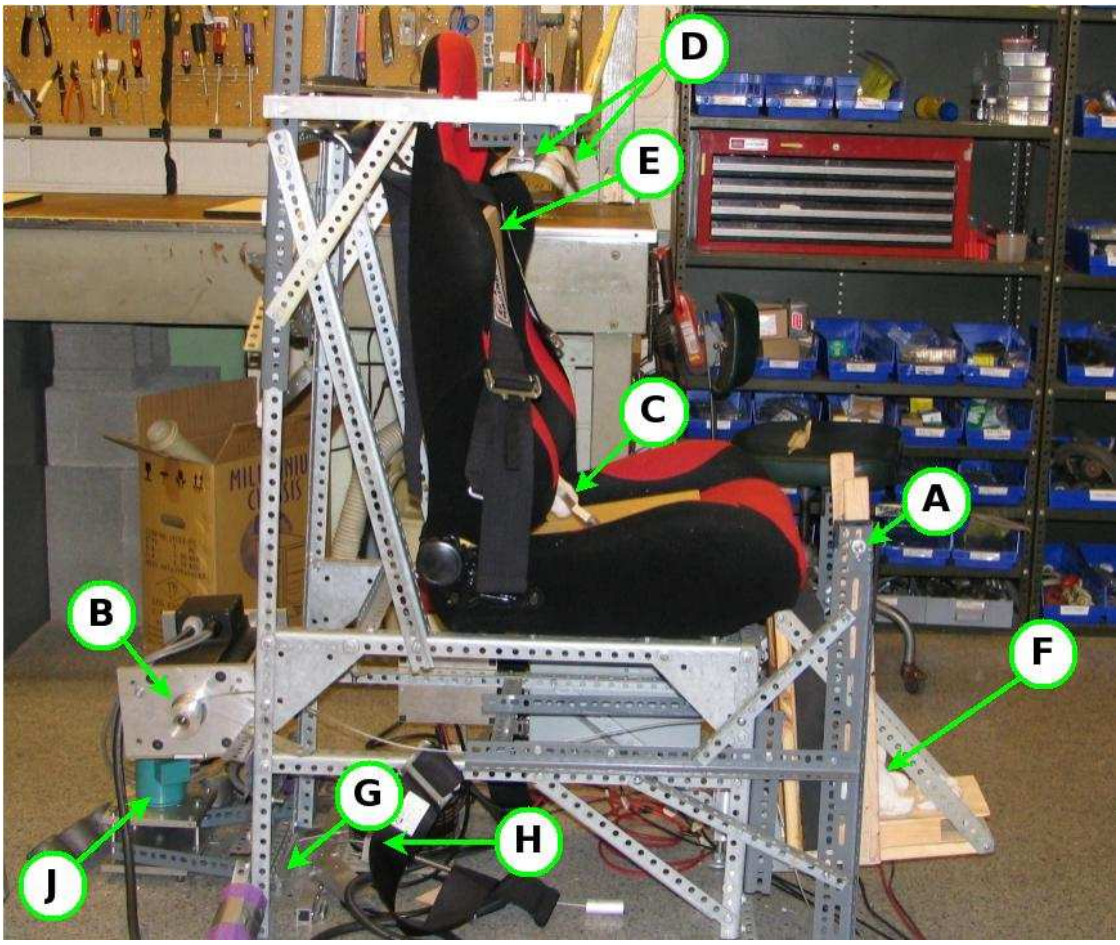

Figure 3.2: Muscle isolation chair. (A) Axis of rotation of the leg; (B) Motor assembly; (C) Shin brace; (D) Shoulder restraints; (E) Modified seat back; (F) Foot swing; (G) Cable connector; (H) Pretensioner; (J) Load cell

A leg swing structure was built to control the rotation and movement of the test subject's leg. The swing supports were made of steel angle bracing and were built up from the chair's support skeleton. The perforations in the vertical swing supports were aligned such that one of the holes would coincide with the approxi-

mate center of rotation of the test subject's knee. The swing itself was built from wood. Dense foam attached to the back of the leg swing provides the calf with support and helps push the shin forward into the shin brace. The test subject's foot was secured in the swing using toe and foot restraints, as described in Sec. 3.2.2. The leg swing can be seen in Fig. 3.3.

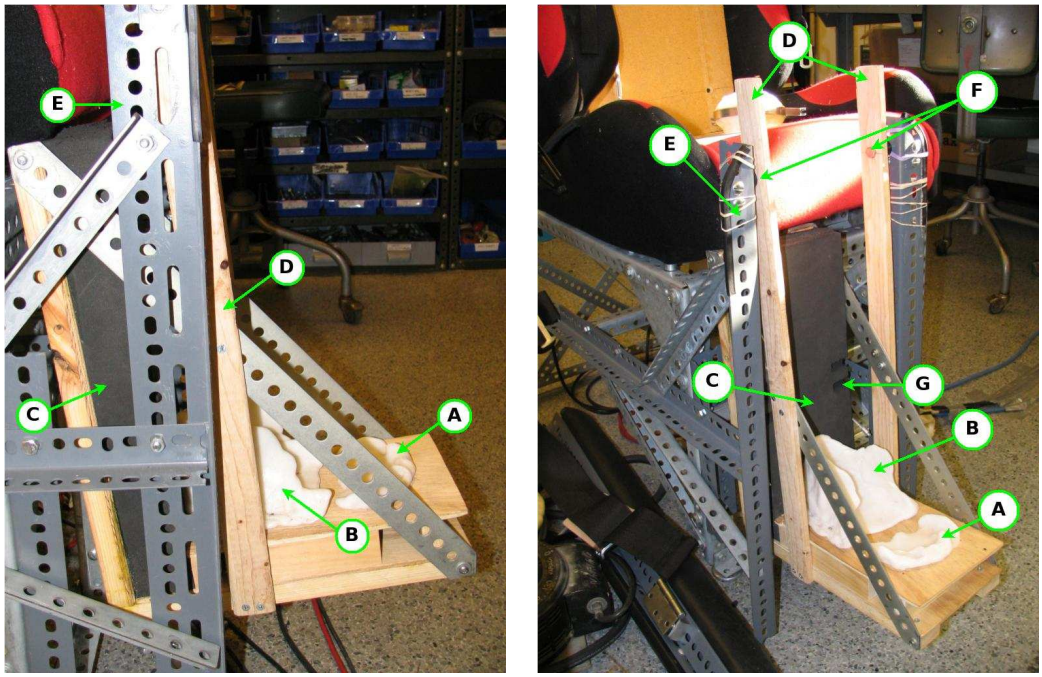

Figure 3.3: Leg swing structure used to control the motion of the test subject's leg. (A) Toe plate; (B) Heel cup; (C) Foam backing; (D) Swing rails; (E) Swing frame; (F) Axis; (G) Slot for shin brace

3.2.2 Restraints

In addition to the four-point safety harness, shoulder restraints, shown in Fig. 3.4 are used to limit upper-body motion. The shoulder restraints consist of a steel angle-brace frame to support the brace, two sets of nuts and bolts to lower and lock the restraints, and molded shoulder cups to grip the shoulder at the ball joint and the insertion point of the clavicle. The shoulder cups are molded from

a high-strength, low-melting-point plastic called "Friendly Plastic." This material melts at approximately 66°C and quickly cools so that it can be handled safely without injury. Each shoulder cup was custom-manufactured for the test subject. While the plastic was still pliable, it was forced into steel u-channel to form a connection to the governing structure. Although the Friendly Plastic melts at low temperatures, it can still be drilled with a bit of patience.

Figure 3.4: Molded plastic shoulder cups used to constrain movement of the torso.

The shin was connected to the load cell or motor via an aluminum shin brace, as shown in Fig. 3.5. The brace was designed using SolidWorks Inventor and was manufactured using a small CNC. The cable slots were machined by hand. An arch was used to ensure there could be a wide contact area between the leg and the brace, creating a better fit and improving comfort. Friendly Plastic was used to fit the brace to the test subject's shin. This resulted in a rigid connection between the front section of the tibia and the brace itself. Because the Friendly Plastic was

molded to each test subject's shin, the subject experienced little-to-no discomfort while performing the tests.

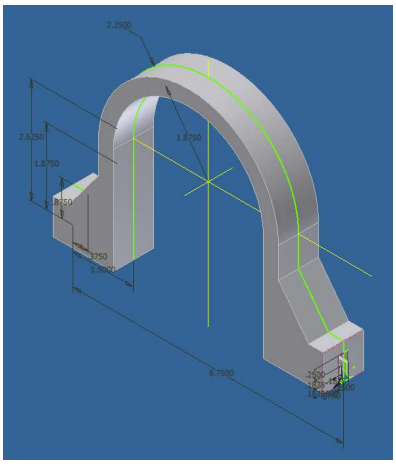

(a) Model of the shin bracket.

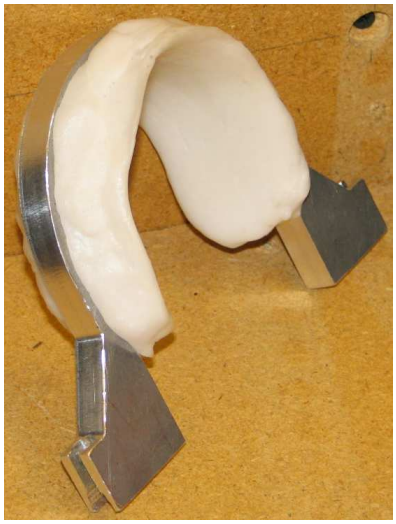

(b) Actual shin restraint.

Figure 3.5: Aluminum and molded plastic shin bracket used to connect the test subject to the load cell.

A heel cup was custom-molded from Friendly Plastic to ensure the test subject's foot was positioned correctly in the foot swing. This heel cup prevented lateral movement and circumduction of the ankle. Similarly, a toe plate was molded to prevent the test subject from sliding his or her foot forward in the swing. The toe plate featured indentations for the ball of the foot and for all the toes. A protrusion on the toe plate aligned with the space between the big- and second toe of the foot, securing the foot in place in a fashion analogous to a thong sandal. The heel cup and toe plate are shown in Fig. 3.6, while the finished foot swing is featured in Fig. 3.5.

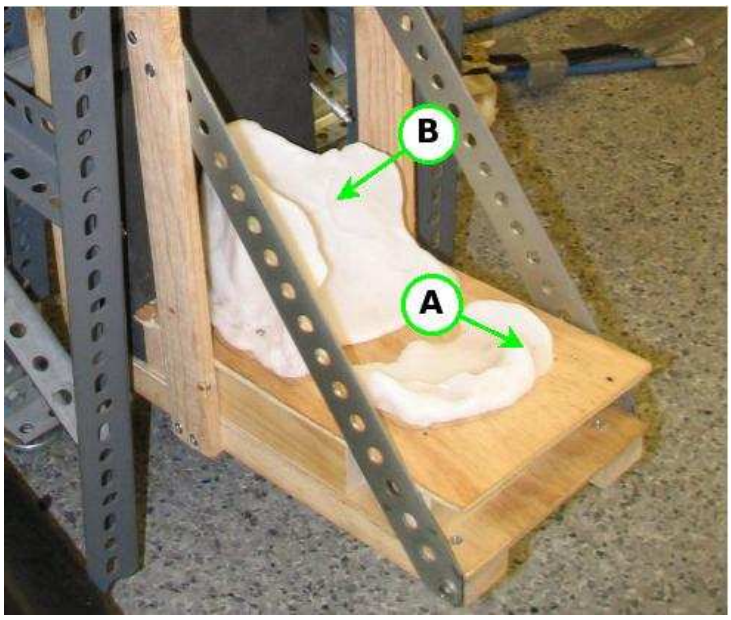

Figure 3.6: Heel cup and toe plate used to secure the test subject's foot. (A) Toe-plate protuberance used to help stop forward sliding; (B) Heel cup

3.2.3 Force and position input/output devices

Fixed angle test set-up

For fixed-angle tests, a load cell was used to record the force exerted by the test subject. The load cell was mounted to the chair support structure such that it was parallel to the ground and at an elevation that matched the distance from the shin brace to the ground. The load cell was connected to a 1/8-in. diameter steel cable via a threaded adapter. A pretensioning device was connected to the cable and set so that when the full pretension load was applied, the device acted as a rigid link. The cable was then threaded through an aluminum bar. A short cable extended from each end of the aluminum bar; these were inserted into the cable slots of the ankle brace. The complete load-cell assembly can be seen in Fig. 3.7.

The load cell output runs through an amplifier and is sent as an input to a LabVIEW control program.

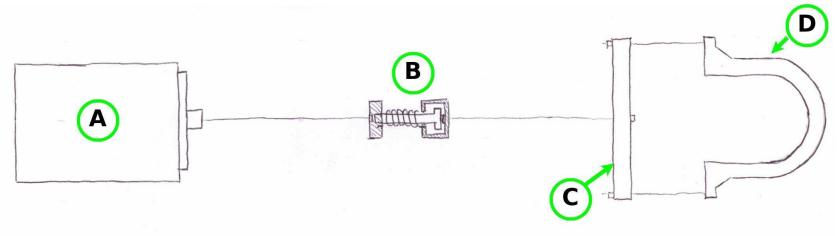

Figure 3.7: Schematic of the load cell assembly.

Variable-angle test set-up

A Baldor brushless AC servomotor was used to control the leg position during variable-angle tests. To enable the load cell to monitor force while the motor drives the position of the test subject's leg, the motor mount apparatus shown schematically in Fig. 3.8 was designed. A photograph of the motor mount is shown in Fig. 3.9

A 2-in diameter motor spool is attached to the motor to wind and unwind the cable, which is connected directly to the cable slots on the ankle bracket. As the motor turns, the cable is either wound or unwound, pulling the test subject's leg toward the chair or allowing the subject to extend his or her leg.

An Advanced Motion Controls servo drive controls the motor. The servo drive is controlled at a low level by servo drive software and at a higher level by a LabVIEW program. A Variac sets the maximum voltage applied to the motor, limiting the velocity of the test-subject's leg and thus serving as a safety feature.

The servo drive controller is a PID operating on the motor spool velocity. This controller was developed only to monitor and to weakly correct the motor's

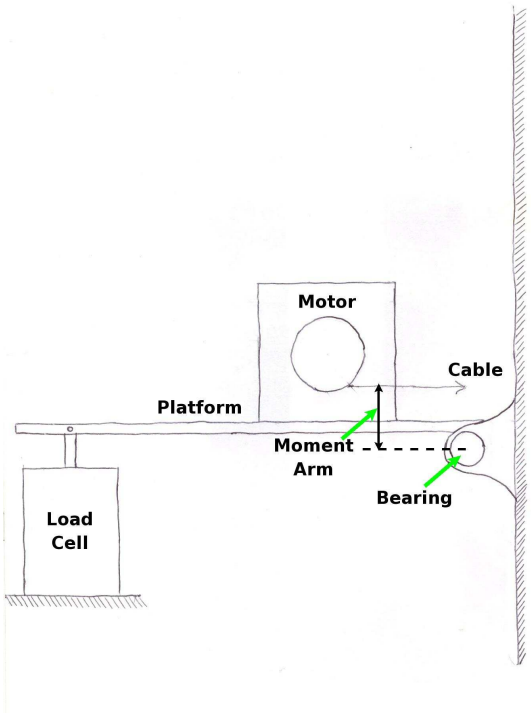

Figure 3.8: Schematic of the motor/load-cell mounting

behavior, allowing most of the control to be done by the LabVIEW program, where the control program could be custom-designed. The servo drive includes a position transducer serving as position feedback. The LabVIEW motor controller is shown in Fig. 3.10. It is a standard proportional controller with feed-forward.

3.2.4 Human-Computer Interface

The force-tracking experiments were conducted with the test subject secured in the muscle-isolation chair, as described earlier. A computer was positioned approximately 1 meter in front of the test subject in order to provide visual and audio feedback throughout the experiments. LabVIEW was used for all computer display elements.

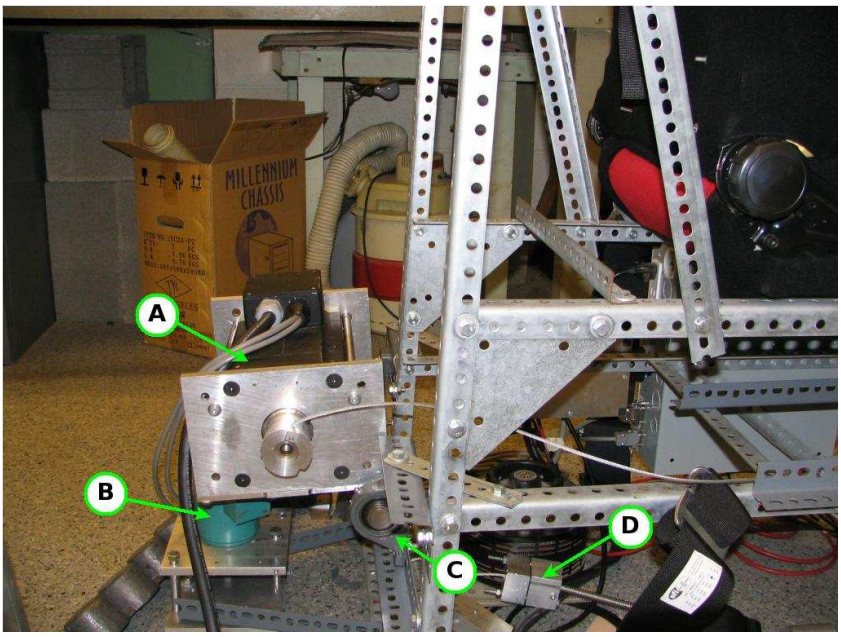

Figure 3.9: Motor mount setup used for variable-angle experiments (drive cable left unconnected). (A) Motor; (B) Load cell; (C) Mount bearing; (D) Pretensioner

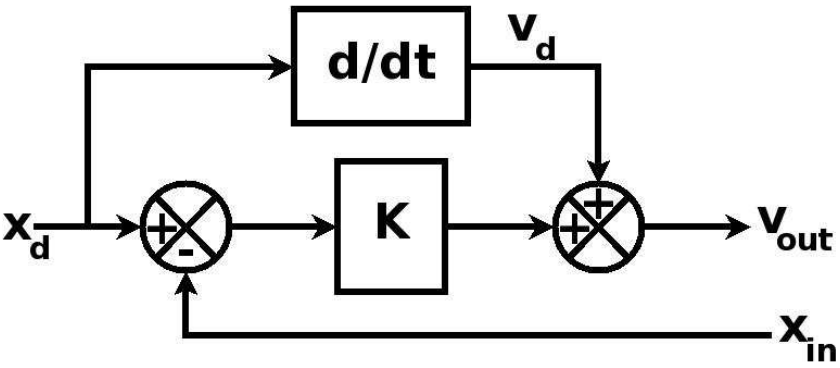

Figure 3.10: Proportional controller with feed-forward used to control the motor.

The LabVIEW feedback and control program consisted of three key components: a motor controller, a force-feedback interpreter, and a main organizational program. The motor controller was used only for variable-angle tests. Fixed-angle and variable-angle tests featured a different main program. Force feedback was the same for both fixed-angle and dynamic tests.

Force-feedback module

The force-feedback program module, shown in Fig. E.1, was designed to provide the test subject a clear and easy to interpret evaluation of his or her force-matching success throughout a trial. The load cell signal was imported, and the force data was converted from Volts to Newtons.

During the course of the experiments, test subjects were able to watch their performance on the computer monitor as well as to hear a metronome beating to the frequency of the wave. Furthermore, when the test subject reached a local maximum or minimum in her own force production, the speakers sounded a short beep in a different tone from that of the metronome.

The visual feedback shown on the monitor was generated in LabVIEW and consisted primarily of two graphs shown on the screen. The top graph provided an extended view of the force profile to be matched along with a pip representing the instantaneous force the user produced. The lower graph showed a time history of the desired and the user-produced force curves. To the right of the graphs, buttons indicate whether the user is producing too much or too little force (the tolerance used during testing was $\pm 10\%$).

A LabVIEW sound virtual instrument (VI) was used to provide audio feedback to the test subject. The program used the known local maxima and minima to sound a tone at each desired high and low point, acting as a metronome for the test subject. A simple exponential average was used to smooth instantaneous data to identify local maxima and minima in the force signal generated by the test subject. When the software registered the force signal at a local minima or maxima, a noise sounded with a slightly different tone than that of the metronome-simulator. In

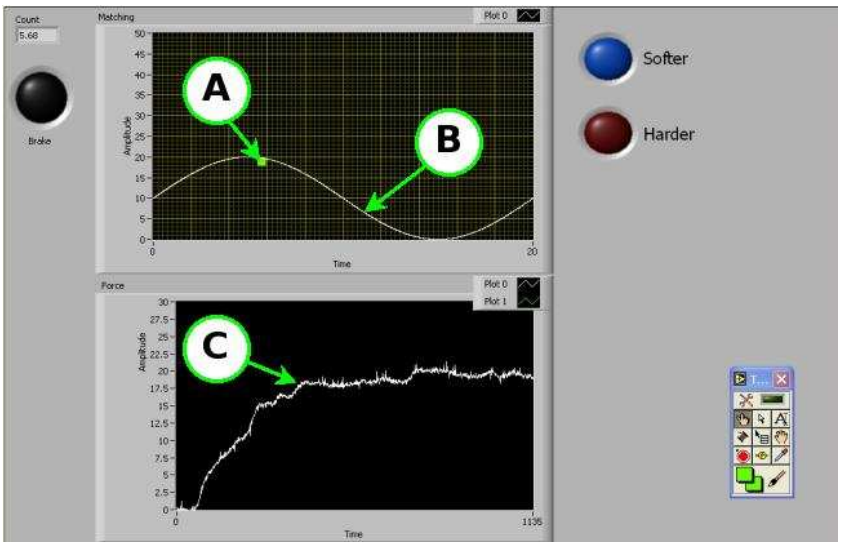

Figure 3.11: Screenshot of visual feedback provided by the LabVIEW program. (*Note: this was not taken during a tracking experiment.*) (A) Current force output measurement; (B) Target wave; (C) Force output history

this way, the test subject could attempt to minimize the delay between the two tones, thus matching the desired frequency.

Motor control module

As discussed in Sec. 3.2.3, the motor was controlled through a proportional controller with feed forward, as shown in Fig. 3.10. Throughout the experiments, current time, position, and target position data were recorded to file. The block diagram for the motor control program is shown in Fig. E.3. In LabVIEW, the velocity of the motor was controlled through the proportional controller with feed-forward, where:

$$\begin{aligned} v_{out} &= \frac{dx_d}{dt} + k\epsilon \\ \epsilon &= x_d - x_{in} \end{aligned} \tag{3.1}$$

where v_{out} is the velocity command sent to the motor, x_d is the target motor angle, x_{in} is the measured angle; k is the gain; and ϵ is the rotational error.

The combination of AMC controller and custom-built LabVIEW controller managed to limit normalized RMS error to less than 1% in all tests. Absolute error was less than 6 mm in all tests, as shown in Fig. 3.12.

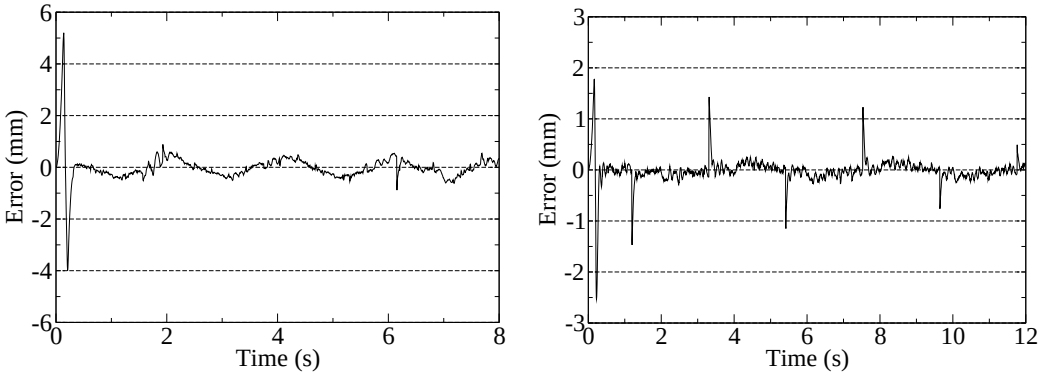

(a) *(b)*

Figure 3.12: Motor position-tracking error during variable-angle experiments. *(a)* shows the absolute error during a test in which the subject attempted to match a sinusoidal target force with a frequency of 0.25 Hz as the motor oscillated her leg at a frequency of 0.50 Hz. *(b)* shows the absolute error during a test in which the subject attempted to match a constant 100-N force as the motor oscillated her leg at a frequency of 0.25 Hz. *Note:* Actual displacement ranged from 0 cm to 12.7 cm.

The greatest source of tracking error occurred at the beginning of each trial. There was a delay of approximately 140 ms before the controller began to influence force-tracking. Once the controller activated the actual position output matched the target position within 300 ms, as shown in Fig. 3.13.

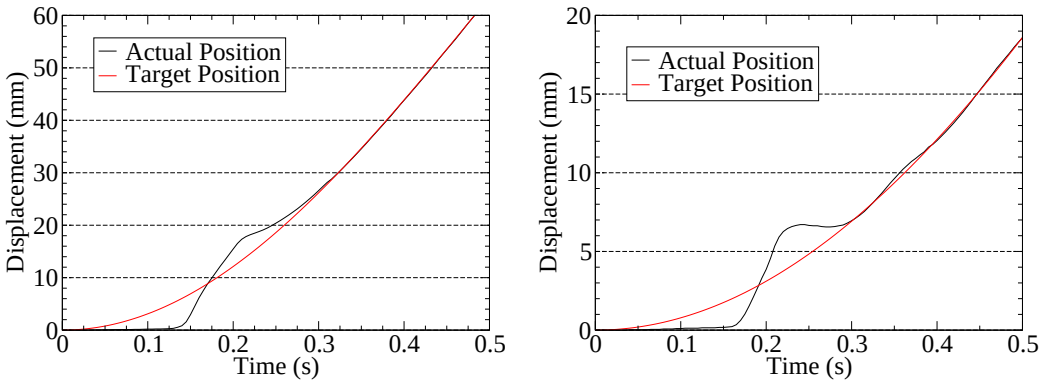

Figure 3.13: Motor response during the first 0.5-sec of a variable-angle experiment. *(a)* shows the motor response during a test in which the subject attempted to match a sinusoidal target force with a frequency of 0.25 Hz as the motor oscillated her leg at a frequency of 0.50 Hz. *(b)* shows the motor response during a test in which the subject attempted to match a constant 100-N force as the motor oscillated her leg at a frequency of 0.25 Hz.

Set-up and initialization options

Figure E.4(a) and (b) show the front panel for the fixed-angle and variable-angle tests, respectively. The main code block serves to initialize and organize calls to the force-feedback and motor-control modules. Both the fixed-angle and variable-angle version feature controls for the test frequency, sampling frequency, wave type, and test length. The user can further control the variable-angle program to ensure the correct range of motion of the test subject's leg.

CHAPTER 4

FORCE TRACKING EXPERIMENTS

Eventually, we would like to be able to predict human locomotion patterns using energy models and mechanics derived from *in vivo* human muscle tests. First, it is important to establish the mechanics and capabilities of the human machine. For this work, I chose to focus on the ability of humans to track forces. Not only is human force-tracking capability an attribute that has not received much attention in the literature, but it is also a good platform for conducting future muscle property and metabolism studies.

Although force matching has not been covered extensively in the literature, some work [Srinivasan and Chen, 1993] has been done to determine how well people can track normal forces using their fingerpads. Srinivasan and Chen asked test subjects to complete a series of tests in which the subjects attempted to match a constant, ramp, or sinusoidal target force function by pressing the pad of their dominant index finger against a load cell. Error was lowest when tracking constant force profiles (0.039 N) and was higher for both ramp profiles (0.048 N - 0.054 N) and sinusoidal profiles (0.043 N - 0.135 N) [Srinivasan and Chen, 1993]. As noted in Sec. 2.2, the work done by Srinivasan and Chen is highly relevant to my research. Not only were their methods similar to my own, but their results give me the opportunity to compare and contrast tracking difficulty under different conditions.

4.1 Methods

4.1.1 Setup and Protocol

I was the only test subject to participate in the force-tracking experiments. In all tests, I was seated in the muscle isolation chair, and my position was secured using the four-point seat belt. I positioned my leg in the swing and placed the custom-fit aluminum shin restraint over my shin. A labmate connected the shin restraint to the cable leading to the load cell. The shoulder restraints were then lowered and locked into place. See Fig. 3.1 for an illustration of my positioning in the test chair. For fixed-angle tests, the cable was connected to the pretensioning device described in Sec. 3.2.3, and a cable connected the other end of the pretensioning device directly to the load cell (Fig. 3.1*a*). For variable-angle tests (Fig. 3.1*b*), the cable was connected from the shin brace directly to the driving motor, which was connected to the load cell via the assembly described in Sec. 3.2.3.

Testing was divided into trials lasting no longer than 30 seconds each. For fixed-angle experiments, three trials were completed at each of four exertion levels, while five trials were completed for all three types of variable-angle test. I rested for 30-60 seconds between each trial and for 2-3 minutes between each set of trials. Exertion levels and waveform selection are discussed in the following section.

As I attempted to match a given waveform, I watched a computer monitor that displayed the target waveform along with both my instantaneous performance and my overall performance, as shown in Fig. 3.11. Audio feedback reinforced the frequency of the signal. Button indicators on the screen further reminded me to generate more force or to relax slightly, as shown in Fig. 3.11. My goal was to

maintain the pip representing the force I was generating as close as possible to the target force profile, as if I were playing a video game.

4.1.2 Waveform and frequency selection

Constant leg-angle experiments

Constant leg angle force-tracking tests were conducted using three different periodic functions: sinusoidal, square, and triangular waveforms. For each wave type, the test subject attempted to match the waveform with the frequency set to 0.10, 0.25, 0.5, 1.0, or 2.0 Hz and with the maximum target force set to 25%, 33%, 50%, or 66% of the subject's maximum voluntary contraction (MVC).

Because of time constraints and mild muscle soreness associated with the experiments, not all combinations of waveform and frequency were tested. Furthermore, the square waveforms were not attempted at frequencies above 1 Hz or at efforts above 50% of the test subject's MVC in order to minimize risk of injury. Table 4.1 shows the waveforms and frequencies that were tested.

Table 4.1: Experiments at different waveforms and frequencies

	25%	33%	50%	66%
0.05 Hz	sin		squ	sin
0.10 Hz	sin, squ	sin, squ, tri	sin, squ	
0.25 Hz	sin, tri	sin, squ	sin, squ	
0.50 Hz		sin, squ		
1.00 Hz		sin, squ		
2.00 Hz		sin		

During experimentation, the test waveform and frequency were selected randomly. For each test, the subject completed three 20- or 30- second trials, resting approximately 30 seconds between each trial and two minutes or more between each test. A total of 62 trials were completed.

Variable leg angle experiments

Force-tracking tests were conducted to attempt to meet constant, ramp, and sinusoidal functions. The test subject began each experiment with her leg forming a 90° angle with her thigh. The position amplitude was set such that the test subject extended her leg a maximum of approximately 30° with the vertical. The servo-motor and driver described in Sec. 3.2.3 forced the test subject's leg to follow a sinusoidal trajectory throughout the variable-angle experiments. Three frequencies were used in testing: 0.25 Hz, 0.50 Hz, and 1.00 Hz. Five trials were conducted for each test.

In the constant load test, the subject attempted to maintain a load of either 50 N or 100 N. In the ramp test, the subject attempted to match a ramp function with a slope of 6 N/s or 12 N/s over the course of a 8-second trial. The sine-matching tests were conducted with an amplitude of either 50- or 100N at target frequencies of either 0.25 Hz or 0.50 Hz. A total of 24 tests (120 trials) were conducted.

4.1.3 Data Processing Methods

Data was recorded in LabVIEW at a sampling frequency of 500 Hz and saved to a tab-separated plain-text file in columns corresponding to time, recorded force, and target force. Each 20- or 30-second trial was saved individually. This data was

plotted using xmgrace to view overall trends. Processing and analysis was completed using Octave. A number of Perl and Python scripts were used to automate the process. All code can be found in Appendix F.

Normalized root-mean-square (RMS) error was calculated for all experiments as follows:

$$\epsilon_{NRMS} = \frac{\sqrt{\frac{1}{N}\sum_{i=1}^{N}(x_d - x_i)^2}}{x_{max} - x_{min}} \tag{4.1}$$

where ϵ_{NRMS} is the normalized RMS error; x_d is the target force; x_i is the measured force; x_{max} is the maximum target force; and x_{min} is the minimum target force. For constant target forces, x_{min} was taken to be zero.

Fixed leg angle experiments

For the fixed-angle experiments, the data files were divided into files containing data for each period of the waveform, centered around the local maxima. Because the properties of the sine and triangle waveforms were similar to each other but not to those of the square waves, the waveforms were further analyzed separately.

Sine and triangle wave analysis methods

For sine waves, in addition to the overall normalized RMS error, the following data were extracted:

- *Rise lag (s)*: The delay between the midpoint of the rising portions of the target and experimental curves.
- *Fall lag (s)*: The delay between the midpoint of the falling portions of the target and experimental curves.

- *Standard deviation*: Measure of the precision of force-tracking forces.

$$\sigma = \sqrt{\frac{1}{N-1}\sum_{i=1}^{N}(x_i - \bar{x})^2} \tag{4.2}$$

  The standard deviation was generally normalized by the mean of the target waveform and expressed as a percentage.

Square wave analysis methods

Square waves were divided into three regions consisting of an initial low-force region, a high-force region, and a final low-force region. Relevant data extracted from square waves included:

- *Low (High) error (%)*: The relative difference between the target force and the experimental force for the initial low (or the entire high) region.
- *Low (High) standard deviation (%)*: The standard deviation of the force recorded over the initial low region, normalized by the average force recorded over the initial low (or the entire high) region.
- *Rise time (s)*: The time required to transition from the low region to the high region.
- *Fall time (s)*: The time required to transition from the high region to the final low region.
- *Lag (s)*: The delay between the midpoint of the rising portions of the target and experimental curves.
- *Overshoot (%)*: The relative difference between the maximum experimental force and the maximum target force.
- *Settling time (s)*: The time required for the overshoot to be corrected.

The overshoot was simply the relative error between the maximum target force ($F_{t_{max}}$) and the maximum recorded force (y_{max}):

$$\%_{os} = 100\left(\frac{y_{max} - F_{t_{max}}}{F_{t_{max}}}\right). \tag{4.3}$$

Settling time was determined by finding the time elapsed between achieving the maximum recorded force and reaching a force within one standard deviation of the average force for the high region.

Variable leg angle experiments

Because the trials in the variable-angle experiments lasted only eight seconds each, the sinusoidal data set was not separated by period. For all dynamics tests, absolute and percent error, median, standard deviation, and the first- and third-quartiles were computed over the course of each trial in addition to the total normalized RMS error. Processed data was sorted and compared according to frequency, wave type, trial number, and force.

4.2 Observations

4.2.1 Fixed-angle experiments

At the onset of each fixed-angle experiment, both third-party observers and the test subject noticed a deflection in leg angle of approximately 1° that resulted from a slight rotation of the test subject's hip, pressing her thigh into the seat. Once the force exceeded the preload by approximately 20 N, no further movement was

observed. The movement consisted almost entirely of downward vertical movement of the knee, indicating the test subject was able to rotate her leg into the chair despite the support of the leg swing. A small amount (3-5 mm) of lateral movement of the knee was observed in some, but not all trials. This movement was attributed to imperfect alignment of the test subject in the chair. No movement of the hips, torso, or shoulders was observed; however, the test subject reported pressure applied to her shoulders by the shoulder restraints in all tests. In tests above 50% MVC, this pressure caused the test subject mild discomfort and soreness that lingered for 1-4 hours after testing.

There were two reported challenges to performing the tests well: mental and physical fatigue. Physical fatigue had been expected, and attempts were made to minimize its effect by allowing plenty of rest between trials and by conducting testing over the course of several days, with rest days following days where higher % MVC tests were conducted. The test subject perceived that fatigue affected her test results after completing ten or more trials in one day. When the subject ended testing for the day and climbed out of the chair, she reported that her muscles felt similar to the way they felt after completing a long, challenging run or bicycle ride. This feeling subsided after 5-10 minutes in all cases. The test subject did not experience any quadriceps muscle soreness lasting more than four hours.

The test subject often found herself struggling with mental fatigue in the course of the experiments. In fact, she felt mental fatigue was far more significant a detriment to the force-matching exercise than physical fatigue. Boredom with the exercise was reported as a major source of mental fatigue. This challenge was felt most significantly in tests at high frequencies with low forces and at the end of test sequences. The subject sought to minimize mental fatigue by taking frequent

breaks both in and out of the chair and by thinking of the experiment as a video game or a personal challenge. The subject responded extremely well to support from friends and labmates.

Sine- and triangle-waveforms seemed easiest to track at 33%-50% MVC with a frequency of 0.25 Hz, while the test subject struggled most with sine- and triangle-waveforms at frequencies greater than 0.5 Hz. She also reported that the 66% MVC test at 0.05 Hz was among the hardest of all trials, as she struggled to increase the force slowly but smoothly.

Square waveforms provided a greater challenge than sine- and triangle-waveforms at all efforts and frequencies. Because lower frequency tests required maintaining the maximum force for longer amounts of time, while developing drastic changes in force application in short amounts of time for high frequency tests was also difficult, the tests performed at 0.25 Hz seemed a clear optimum. The test subject felt that the 50% MVC trials were easiest because overshoot was much easier to control at higher exertion levels.

4.2.2 Variable-Angle experiments

Compared to the fixed-angle tests, the test subject found force matching in variable-angle circumstances to be extremely challenging. As the subject's leg was moved more quickly, the test subject found it more difficult to match the desired force. Neither the test subject nor third-party observers noticed movement of the test subject's hips, shoulders, or torso, and overall, the test subject found the dynamic tests far more comfortable than the fixed-angle tests. The subject experienced less soreness and fatigue from all tests, but she complained that her

knee felt slightly achy. This slight knee pain was attributed to imperfect alignment of the axis of rotation of the swing with the (moving) axis of rotation of the test subject's leg. The test subject reported struggling most with tracking the 6 N/s ramp target force.

4.3 Results

4.3.1 Determining the maximum voluntary contractile force

The first step in conducting the force-tracking experiments was to determine the test subject's *maximum voluntary contractile force* (MVC) by completing a maximum exertion test. The MVC was then used to scale the target force waves in the fixed-angle experiments.

The test itself consisted of three trials, each of which included three separate attempts at an MVC. With the program started, one of the members of the lab would encourage the test subject to push as hard as she could. The force was held until it could not be maintained, and then the test subject relaxed. Several seconds later, another attempt was made. The test subject rested approximately 60 seconds between each trial. The results of the trial which produced the maximum force are shown in Fig. 4.1. The test subject's MVC was 568 N.

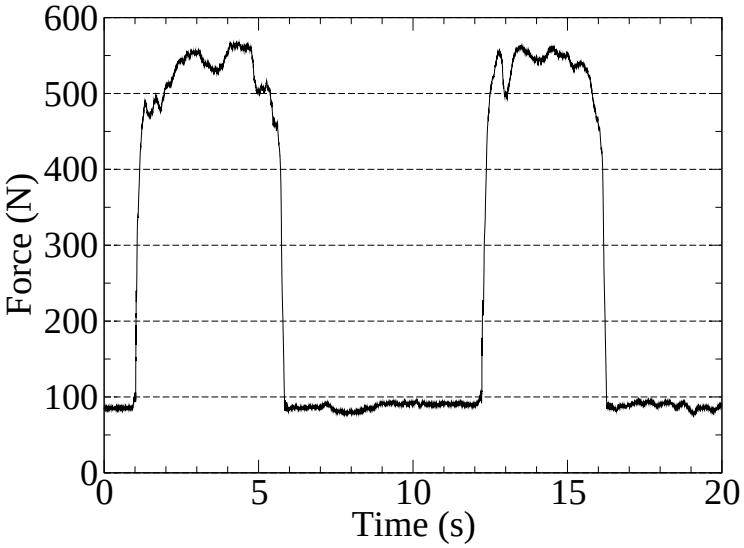

Figure 4.1: Maximum voluntary contraction. Subject pushed as hard as she could and then maintained as long as she could before relaxing and resting several seconds.

4.3.2 Fixed-leg-angle results

In general, the test subject was highly successful in tracking forces when her leg was held at a fixed angle. Figure 4.2 shows typical results obtained when tracking a square, sine, and triangle wave at 33% MVC at a frequency of 0.10 Hz. The results of all fixed-angle tests are shown in Table 4.2, which presents the mean normalized RMS error in addition to the normalized standard deviation for each fixed-angle experiment.

Table 4.2 shows the mean normalized RMS error and standard deviation for all fixed-angle experiments. In general, both error and standard deviation increased as the frequency increased. Too few triangle-matching experiments were completed to draw meaningful force-matching comparisons, but the results appear to be comparable to or slightly better than sine-matching experiments. Square waves were

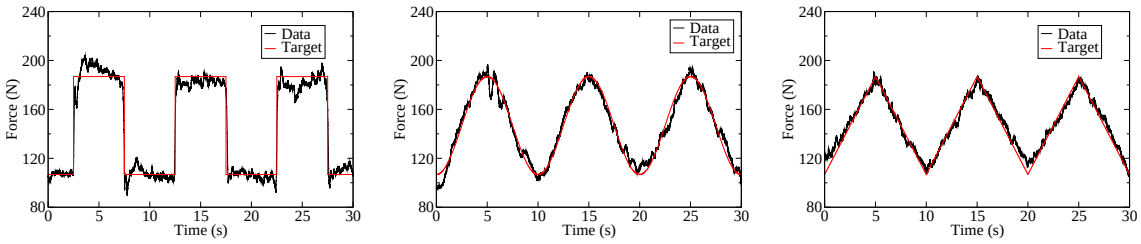

(a) Square *(b)* Sine *(c)* Triangle

Figure 4.2: Fixed-angle force tracking at 33% MVC and 0.10 Hz

consistently more difficult to track than sine waves at the same effort and frequency (at 33% MVC and a frequency of 0.50 Hz, the difference between square- and sine-wave normalized RMS error was only 2.4%, but on average, the normalized RMS error for square-wave tracking was 37% higher than that for sine-wave tracking.)

Sine and triangle waves

Figure 4.3 shows typical results of the waveform matching test at 33% MVC as the frequency was increased. It is difficult to analyze these graphs qualitatively, but it seems the error and lag both remained low until the frequency was increased above 0.5 Hz. The test subject reported difficulty tracking forces at a frequency of 2.0 Hz. Although force-tracking at 2.0 Hz was worse than force-tracking at lower frequencies, the normalized RMS error for 2.0-Hz sine-wave matching was only 16.23% with a standard deviation of 12.89%. Despite being given audio and visual feedback to aid in maintaining the correct force frequency, the test subject often did not consistently lag or lead the target force. Instead, the experimental data often transitioned from a period of leading the target curve to a period of closely following the target curve to finally lagging target curve. This is illustrated in Fig. 4.4.

Table 4.2: Fixed-angle force-tracking results

Target	*Error (%)*	*0.05 Hz*	*0.10Hz*	*0.25 Hz*	*0.50 Hz*	*1.00 Hz*
Squ. - 25%	Mean		13.41			
	Std. Dev.		2.25			
Squ. - 33%	Mean		7.76	8.99	10.78	23.86
	Std. Dev.		2.29	1.57	9.84	21.26
Squ. - 50%	Mean		7.39	9.17	9.56	
	Std. Dev.		2.16	2.53	13.98	
Sine - 25%	Mean	10.08	9.73	12.53		
	Std. Dev.	2.96	2.66	3.56		
Sine - 33%	Mean		6.36	7.65	10.53	13.46
	Std. Dev.		4.16	5.00	6.45	8.57
Sine - 50%	Mean		4.12	5.81		
	Std. Dev.		4.1	6.7		
Sine - 66%	Mean	3.13				
	Std. Dev.	5.54				
Tri. - 25%	Mean			12.69		
	Std. Dev			4.15		
Tri. - 33%	Mean		5.53			
	Std. Dev.		4.11			

The relationship between rise lag and frequency is shown in Fig. 4.5(a). There is more variation in the rise lag at lower frequencies than at higher frequencies. This result, however, is mostly an artifact of the way in which testing was completed. Because the subject could not see her force output until the test began, lag at the beginning of a trial was always relatively high. In a twenty-second test interval,

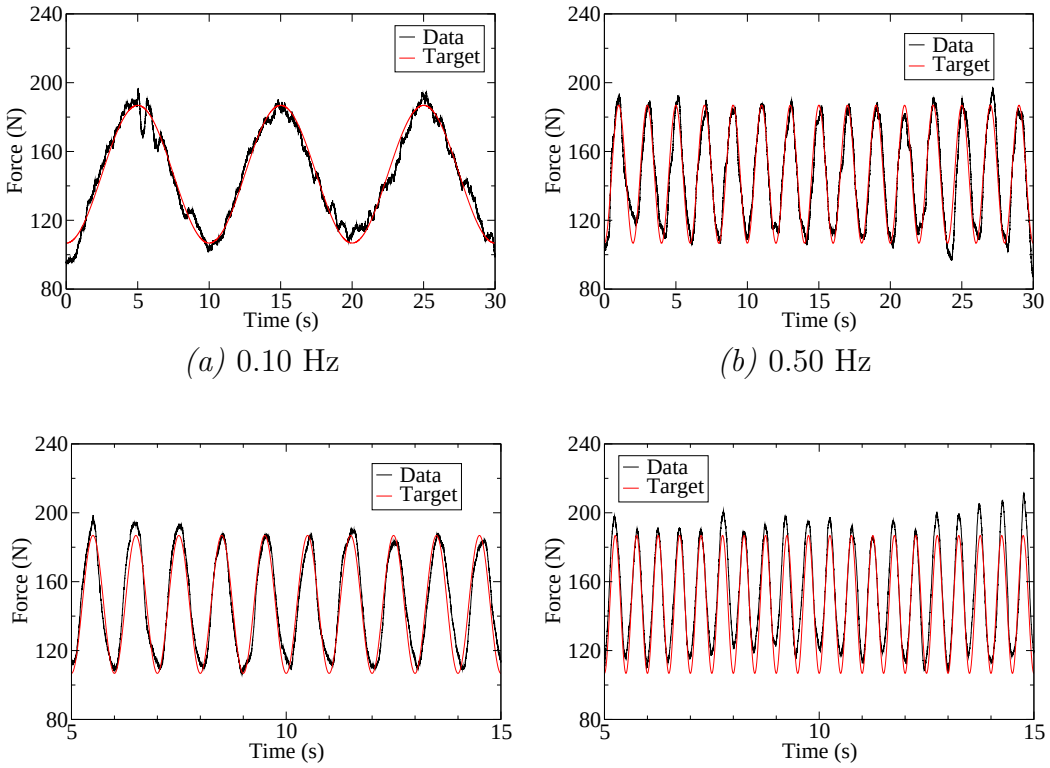

(a) 0.10 Hz *(b)* 0.50 Hz

(c) 1.00 Hz *(d)* 2.00 Hz

Figure 4.3: Typical results of fixed-angle sinusoidal waveform matching at various frequencies. See Fig. 4.4 for a clearer view of 2.00 Hz results.

there are fewer periods conducted at low frequencies to compensate for this initial error. The average rise lag was best at 0.5 Hz, where the data led the target curve by 1.3 ms.

Normalized RMS error from constant angle sine wave tracking experiments is plotted in Fig. 4.6. In most cases, error did not improve significantly as more trials were attempted. One notable exception, however, is the 2.00 Hz tracking test conducted at 33% MVC, where error improved from 35% in the first trial to under 20% in the third trial, as shown in Fig. 4.6(a). With a little practice,

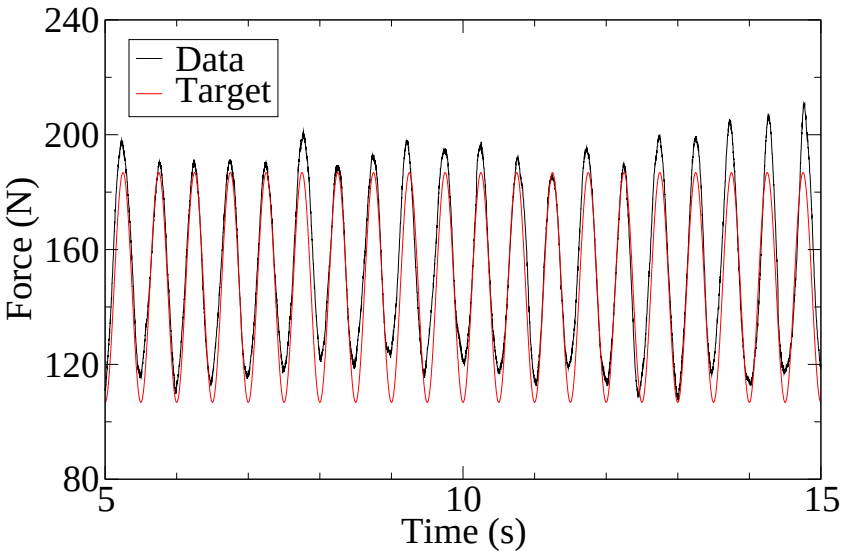

Figure 4.4: Sine-wave tracking at 33% MVC and a frequency of 2 Hz.

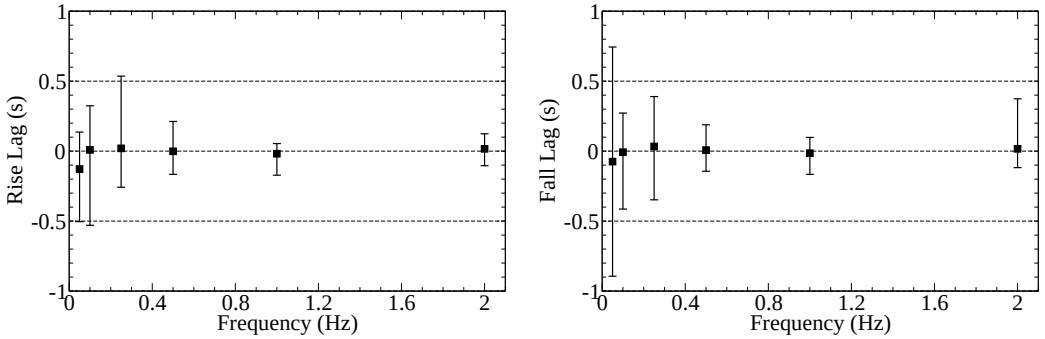

(a) Rise Lag *(b) Fall Lag*

Figure 4.5: Lag decreased as a function of target frequency in fixed-angle sine-wave tracking experiments.

the test subject managed to maintain the normalized RMS error below 20% for all constant-angle sine-tracking tests attempted. As shown in Fig. 4.6(b), increasing the target frequency did have an impact on tracking performance. Unfortunately, because tests at target frequencies of 0.5 Hz or above were only conducted at 33% MVC, it is difficult to compare the effect of altering the MVC on test error, but at

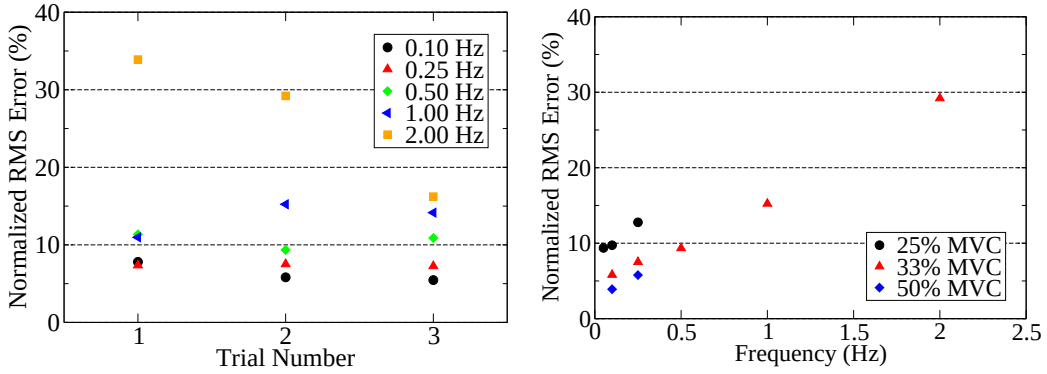

(a) All frequencies, 33% MVC *(b)* All efforts, best trial

Figure 4.6: Tracking error in fixed-angle sine-wave tracking tests increased as the target frequency increased. In general, results do not improve with additional experience, but the 2.00-Hz target frequency case is a notable exception.

low frequencies, tracking performance consistently improves as the required effort increases.

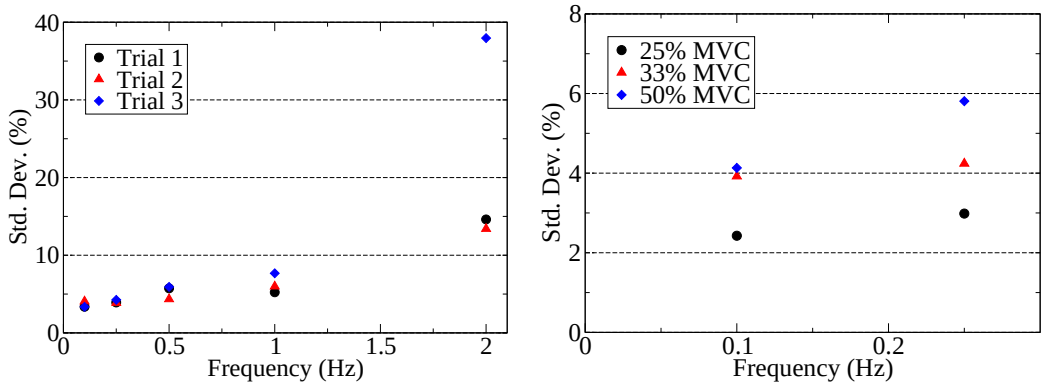

(a) Effect of learning *(b)* Effect of increasing %MVC

Figure 4.7: Fixed-angle sine wave tracking precision worsened as the target frequency increased and as the % MVC increased.

Plotting the standard deviation as a function of the target wave frequency, as shown in Fig. 4.7, revealed which conditions challenged the test subject's consistency. In both Fig. 4.7(a) and (b), the standard deviation steadily increases with

increasing target frequency. Although increased testing experience did appear to positively impact the force-tracking error in some fixed-angle tests, increased experience did not significantly impact the force-matching variation, as shown in Fig. 4.7(a).

Square waves

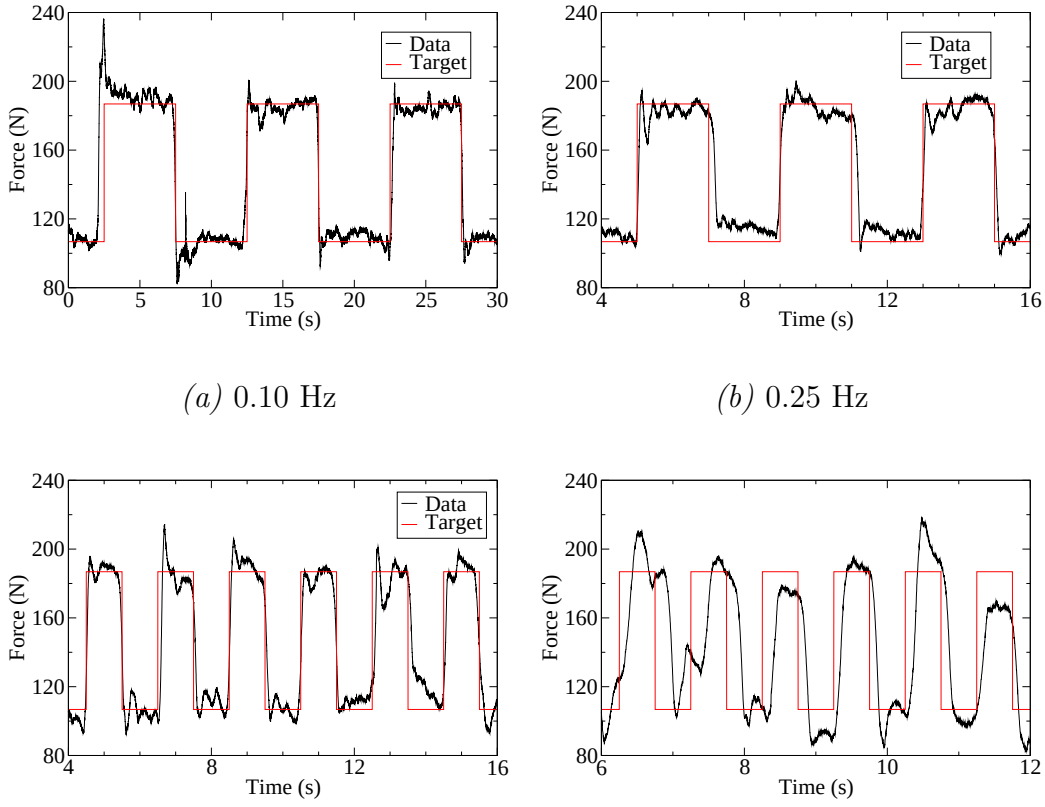

(a) 0.10 Hz

(b) 0.25 Hz

(c) 0.50 Hz

(d) 1.00 Hz

Figure 4.8: Typical results of square waveform matching at 33% MVC and various frequencies.

Figure 4.8 shows typical results of the square waveform matching experiments at 33% MVC with the frequency ranging from 0.10 Hz-1.00Hz. The four plots suggest that both error and lag increase as the frequency increases. Test results show the subject accurately tracked the target force profile with frequencies between 0.10 Hz and 0.50 Hz, with both the error and standard deviation increasing. Tracking the target square wave at 1.00 Hz proved far more difficult, with normalized RMS error more than doubling from the 0.50-Hz case at 10.78% to 23.86% at 1.00 Hz. Similarly, standard deviation increased from 9.84% at 0.50 Hz to 21.26% at 1.00 Hz. The dramatic change in error and variation is clearly depicted in Fig. 4.8, as qualitatively, the 0.10-Hz, 0.25-Hz, and 0.50-Hz cases are all similar, but the 1.00-Hz case shows considerable error and lag.

As the test frequency increased, the test subject found it more difficult to match the desired frequency accurately. In the sine- and triangle-wave constant angle tests, the subject's results would sometimes lead and other times lag the target waveform. In the square tests, on the other hand, as the target frequency increased, the test subject became far more likely to lag behind the target curve, as shown in Fig. 4.9. At a target frequency of 0.10 Hz, the subject led the target wave by 72 ms. Lag error was lowest at 0.25 Hz at only 6 ms lead and was highest at 1.00 Hz at 42 ms lag.

Figure 4.10 shows the test subject's mean response time in fixed-angle square-tracking tests. Target wave frequency was not expected to influence the response time, and, as shown in Fig. 4.10(a), this was the case. On the other hand, increasing the target force was expected to impact response time. As shown in Fig. 4.10(b), response time increased from 72 ms in the 25% MVC case to 250 ms in the 50% MVC case.

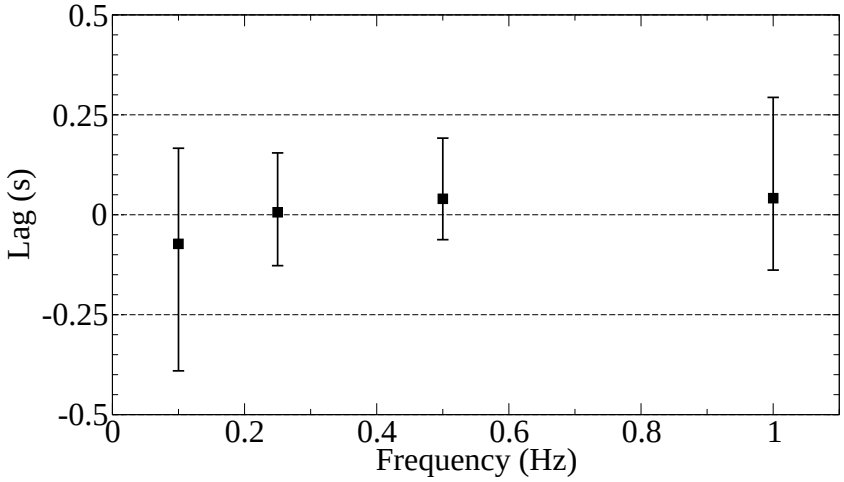

Figure 4.9: Frequency vs. lag for fixed-angle square wave tracking experiments.

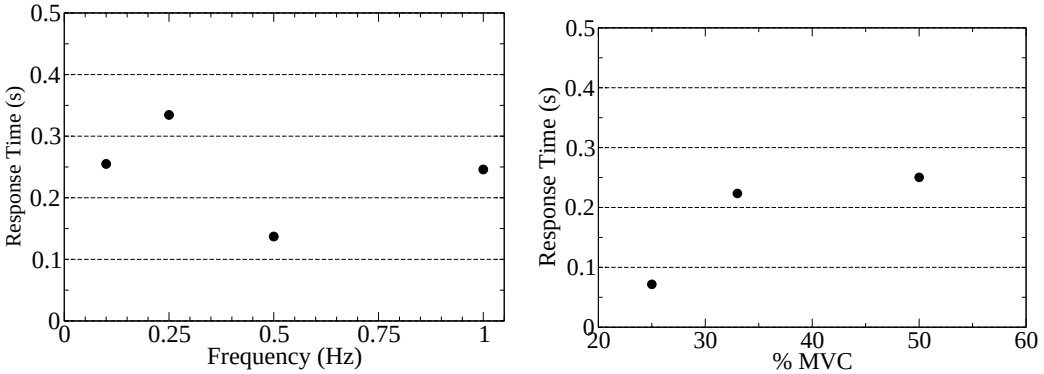

(a) Frequency dependency *(b)* Effort dependency

Figure 4.10: Time required to transition from the baseline force to the peak force in fixed-angle square-wave tracking experiments.

Overshoot was not related to target-wave frequency, as shown in Fig. 4.11(a). As shown in Fig. 4.11(b), overshoot was very high at 25% MVC, but the difference between overshoot at 33% and 50% MVC was insignificant. The high overshoot at 25% MVC could be the result of the order of the experiments or a simple byproduct of the test subject underestimating her strength.

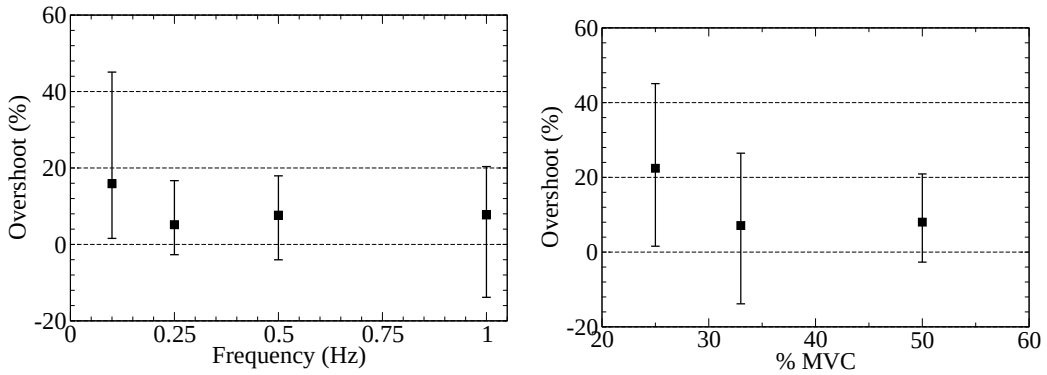

(a) Frequency dependency *(b)* Effort dependency

Figure 4.11: Target force overshoot decreased as a function of both target frequency and of effort in fixed-angle square-wave tracking experiments

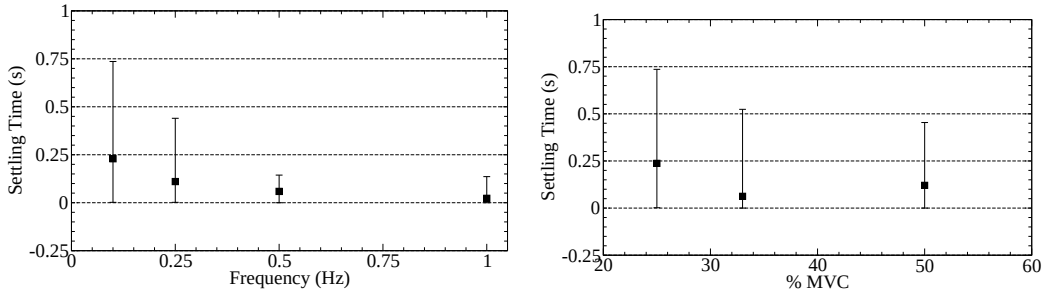

(a) Frequency dependency *(b)* Effort dependency

Figure 4.12: Settling time decreased as a function of both target frequency and of % MVC in fixed-angle square-wave tracking experiments

Settling time, shown in Fig. 4.12, decreased steadily with increasing frequency but did not show a strong correlation to the required effort. The frequency dependency illustrates one of the few benefits of requiring the test subject to track a square wave more quickly: because faster testing emphasized the importance of quickly relaxing, the settling time decreased, even though the difficulty of the test increased.

Normalized RMS error in fixed-angle square-wave tracking tests is plotted in Fig. 4.13. As shown in Fig. 4.13(a), for all cases except the 1.00-Hz experiment, increased experience did have a slight, beneficial effect on error. As the effort required to match the target force increased, so did the error, as shown in Fig. 4.13(b). Overall, fixed-angle square tracking tests were similar to fixed-angle sine tracking tests in terms of error. This can most easily be observed by comparing results in Tab. 4.2 or by comparing Figs. 4.6 and 4.13.

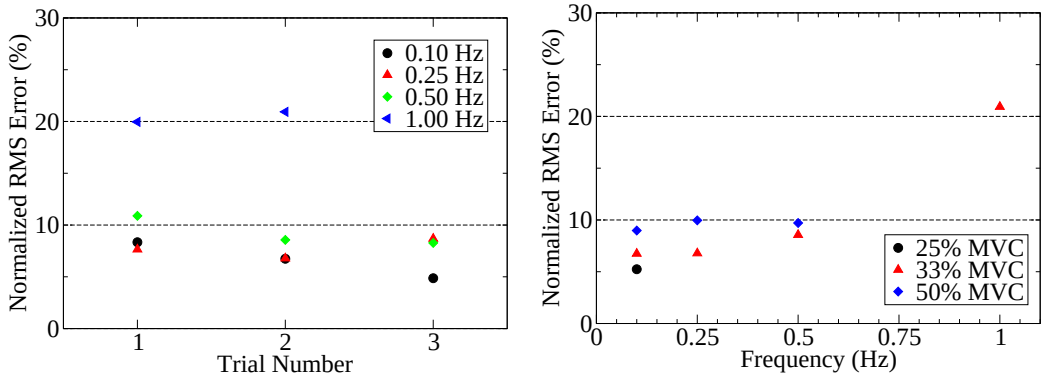

(a) All frequencies, 33% MVC *(b)* All efforts, best trial

Figure 4.13: Fixed-angle square-wave tracking error. Test results do not show any learning trends. Error increased slightly as the target frequency increased. In general, the larger the required effort, the larger the error.

As was the case for fixed-angle sine-wave matching experiments, the standard deviation steadily increased with increasing frequency in fixed-angle square-wave matching experiments. Increased testing experience had little effect on standard deviation, as shown in Fig. 4.14(a), while increasing the effort required did increase the standard deviation (Fig. 4.14(b)). It appears that, with the exception of "fast" tests, where the target frequency is at or above 1.00 Hz, only one or two trials are necessary to provide the test subject with the necessary experience to conduct the experiments reliably. Although error can be maintained at or below 10% for fixed-

angle experiments even at 50% MVC, increasing the effort negatively impacts the precision with which the subject tracks the desired force.

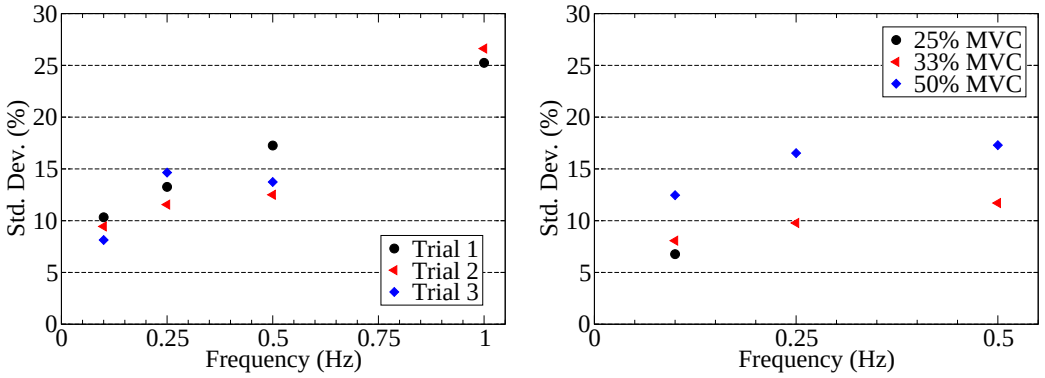

(a) Effect of learning *(b)* Effect of increased effort

Figure 4.14: Fixed-angle square-wave tracking precision decreased as target frequency increased. Learning did not significantly affect precision between trials. Tests performed at a higher percentage of the MVC had larger variation than those performed at a lower percentage of the MVC.

4.3.3 Variable-Angle experiment results

The fixed-angle force tracking experiments described in the previous chapter revealed the human machine is quite capable of generating a desired force profile under fixed-angle conditions. But this tells us little about how well a human can independently generate a desired force profile while not under control of the position of his or her legs. Thus, we developed experiments designed to find out whether and under what conditions a person can match a desired force profile as his or her leg was moved by a machine.

The test subject experienced mixed results in tracking forces while her leg was oscillated by the motor. Figure 4.15 shows typical results obtained when tracking

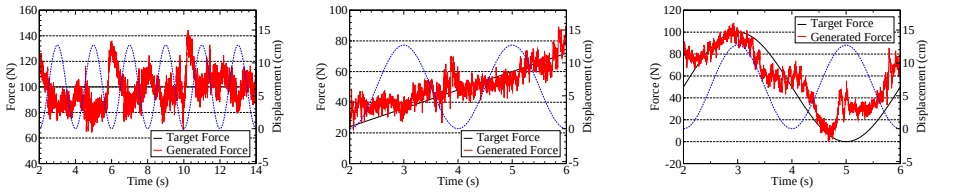

(a) $F_t = 100$ N *(b)* $F_t = 12$ N/s *(c)* $F_t = 50$ N $\sin(\pi t/2)$ + 50 N

Figure 4.15: Typical results for variable leg angle experiments with leg oscillations of 0.50 Hz, where F_t is the target force function and the dashed line is the leg displacement.

a constant, ramp, or sine force as the test leg was oscillated at a frequency of 0.50 Hz. The results of all variable-angle tests are shown in Table 4.3, which presents the mean normalized RMS error in addition to the normalized standard deviation for each fixed-angle experiment.

The subject had the most success tracking constant forces (9.06%-26.30% error) and the least success tracking $F_t = 25N \sin(\pi t) + 25N$ (30.44%-47.69% error). Increasing the required effort generally improved force-matching results. This effect was particularly dramatic in ramp-matching tests, discussed in more detail in Sec. 4.3.3, where the mean normalized RMS error for 12 N/s cases was approximately half the normalized RMS error for the 6 N/s case. In general, increasing the forcing frequency increased error. Increased practice did not impact test results as significantly as it improved fixed-angle test results; this is discussed in more detail in the following sections.

Matching a constant force

Figure 4.16 shows typical results for the constant force-matching tests at (a) 0.25 Hz and (b) 0.50 Hz.

Table 4.3: Variable-Angle force-tracking results

Target	*Condition*	*Error (%)*	*0.25 Hz*	*0.50 Hz*	*1.00 Hz*
Constant - 50 N		Mean	10.65	18.91	26.30
		Std. Dev.	10.35	16.14	25.27
Constant - 100 N		Mean	9.06	11.94	
		Std. Dev.	8.07	11.93	
Ramp - 6 N/s		Mean	31.33	38.63	50.73
		Std. Dev.	34.23	36.52	50.95
Ramp - 12 N/s		Mean	15.95	14.11	25.05
		Std. Dev.	17.84	16.42	27.56
Sine - 50 N	0.25 Hz	Mean	20.09	25.07	34.70
		Std. Dev.	17.36	19.12	26.94
	0.50 Hz	Mean	47.69	30.44	36.94
		Std. Dev	34.88	25.92	25.16
Sine - 100 N	0.25 Hz	Mean	18.37	19.79	20.58
		Std. Dev.	18.07	17.80	20.10
	0.50 Hz	Mean	19.67	16.08	22.22
		Std. Dev	19.17	16.77	21.42

At first glance, it seems clear that while the test subject succeeded in maintaining an average force approximately equal to the desired 50 N, the variation increased as the frequency at which the subject's leg was moved increased. It also appears that the frequency at which the subject's leg was moved had a direct impact on the error. The force exceeded the desired force as the leg was pulled back to the 90° starting position, and it often fell short of the desired force when the leg was extended.

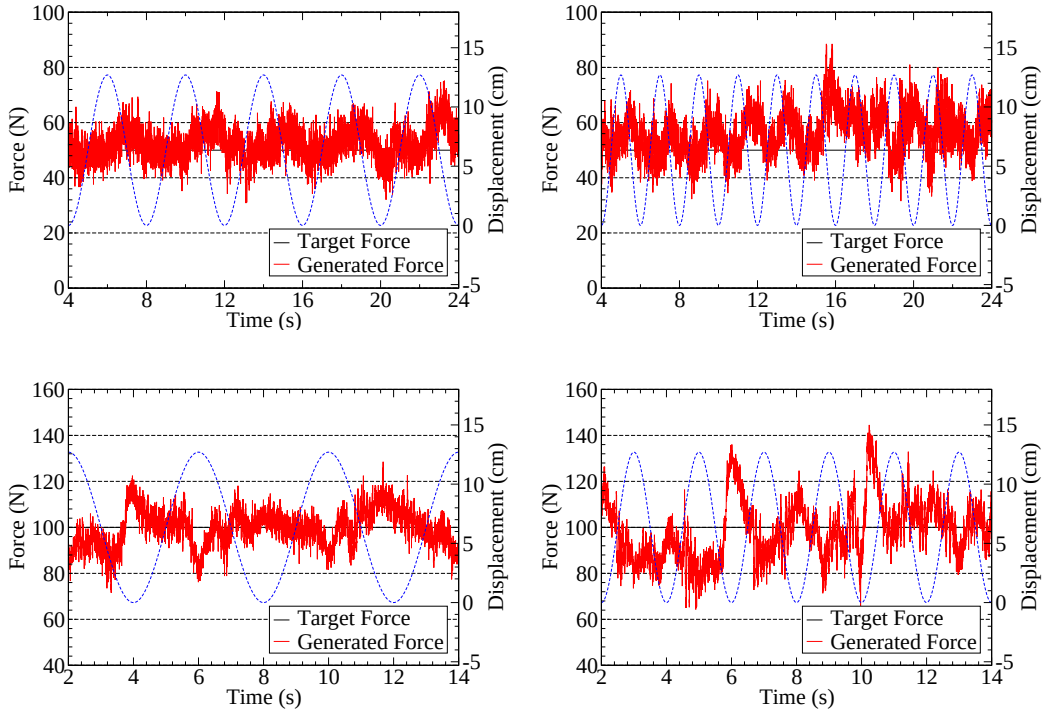

(a) 0.25 Hz *(b)* 0.50 Hz

Figure 4.16: Typical results of a constant-force tracking test as the test subject's leg (whose position is shown with the dashed line) was moved at different frequencies.

Figure 4.17 shows the normalized RMS error recorded over the course of the dynamic-leg-angle constant-force experiments. Error was less for the 100-N target force than it was for the 50-N target force. Gaining practice produced a slight error improvement. The largest factor in tracking error for constant target forces was the frequency at which the test subject's leg was oscillated. For all trials conducted with constant trial forces, error increased as the forcing frequency increased. For the 50-N case, the results were particularly dramatic, with error at 1.00 Hz nearly three times greater than error at 0.25 Hz.

The force-matching standard deviation for constant target forces of 50 N and 100 N is plotted versus forcing frequency in Fig. 4.18. It is clear that for all cases,

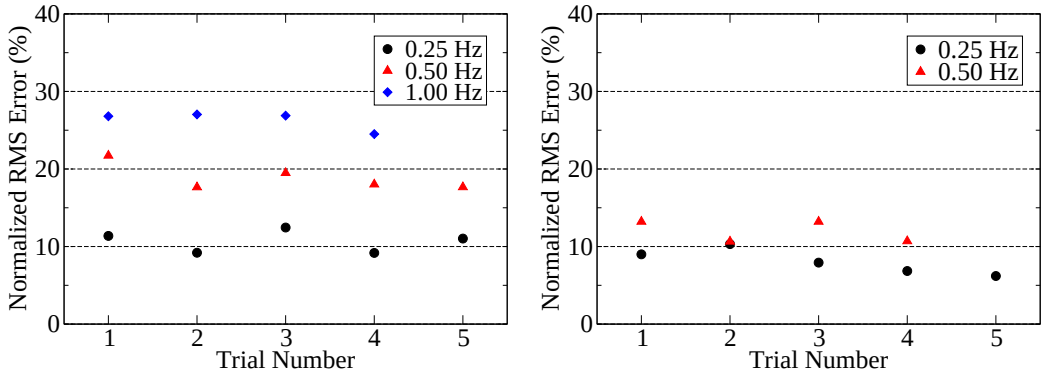

(a) $F_t = 50$ N *(b)* $F_t = 100$ N

Figure 4.17: Normalized RMS error in dynamic-leg-angle constant-force-matching experiments. As the forcing frequency increased from 0.25 Hz to 1.00 Hz, RMS error increased. Learning had a minor, positive effect on 100-N force-matching tests but was insignificant in 50-N force-matching tests.

there was a strong relationship between standard deviation and forcing frequency. The 50-N experiments had greater standard deviation than the 100-N case. Finally, increased practice did have a positive effect on standard deviation, as for almost all cases, the final trial had the smallest standard deviation.

Matching a ramp force

Figure 4.19 shows typical results for the ramp force-matching tests. Two rates were attempted: 6 N/s and 12 N/s. Each rate was attempted with the leg subjected to a forcing frequency of 0.25 Hz, 0.50 Hz, or 1.00 Hz. Qualitatively, the results from the ramp-matching tests appear to be better than those from the constant-force tests. Also, the ramp tests conducted at 12 N/s seem to have lower error than tests conducted at 6 N/s. The test subject reported that she felt the 12 N/s tests were easier than the 6 N/s tests. Increasing the forcing frequency seems to have a direct impact on the tracking error for both 6 N/s and 12 N/s tests.

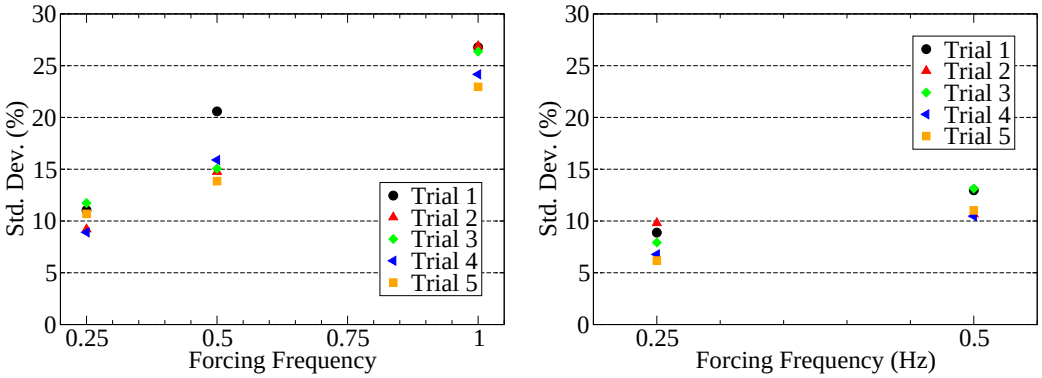

(a) $F_t = 50$ N *(b)* $F_t = 100$ N

Figure 4.18: Standard deviation in dynamic-leg-angle constant-force-matching experiments. As the forcing frequency increased, the precision decreased. Learning had a slight, positive effect on precision.

Ramp tracking proved to be far more challenging than constant-force tracking. Normalized RMS force-tracking error for ramp forces is shown in Fig. 4.20. Unlike the constant-force tracking experiments, the ramp-tracking experiments show no improvement with increased practice. Changes in forcing frequency also had a reduced impact in ramp-tracking experiments. It is, however, clear that the subject struggled more to match the 6 N/s test than she did to match the 12 N/s test.

Figure 4.21 shows the standard deviation of ramp-tracking results as a function of frequency. Variation generally increases with increasing frequency. Despite the lack of improvement of error with increased practice, the test subject gained some precision with more practice, as earlier trials generally have a higher standard deviation than later trials.

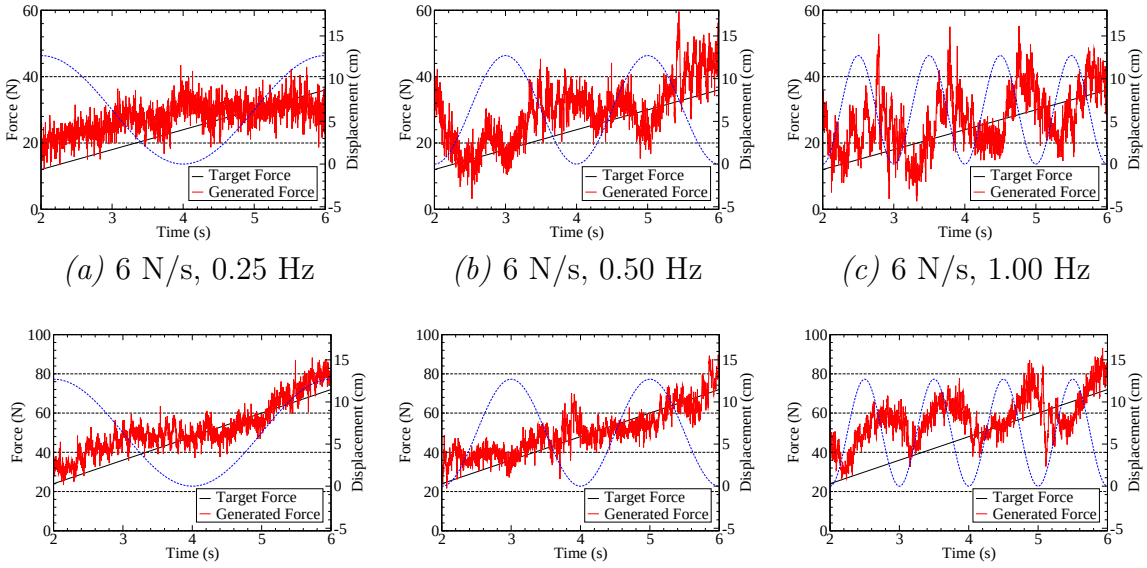

(a) 6 N/s, 0.25 Hz *(b)* 6 N/s, 0.50 Hz *(c)* 6 N/s, 1.00 Hz

(d) 12 N/s, 0.25 Hz *(e)* 12 N/s, 0.50 Hz *(f)* 12 N/s, 1.00 Hz

Figure 4.19: Typical ramp-tracking performance as the slope increased from 6 N/s to 12 N/s and as the forcing frequency increased from 0.25 Hz to 1.00 Hz. The dashed line shows leg displacement.

Matching a sinusoidal force

Finally, the test subject attempted to track a sine wave. Typical results are shown in Fig. 4.22. The test subject reported that the sine-wave tracking experiment was the most difficult of all the variable-angle and fixed-angle experiments. Sine-tracking tests were conducted with two maximum amplitudes: 50 N and 100 N. As in other variable-angle tests, the position forcing frequency (f_f) was 0.25-, 0.50-, or 1.00 Hz in each trial. The target force wave (F_t) had a frequency (f_t) of either 0.25 Hz or 0.50 Hz. Thus, in some of the variable-angle sine tracking tests, the subject worked perfectly in phase with the movement of her leg. Other tests challenged the subject to contract her muscles considerably faster or slower than her legs were being moved.

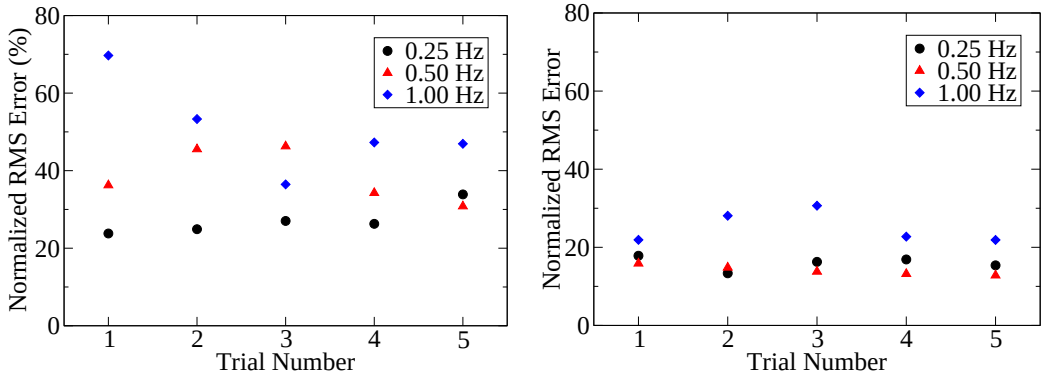

(a) $F_t = (6\text{ N/s})t$ *(b)* $F_t = (12\text{ N/s})t$

Figure 4.20: Normalized RMS error for variable-angle ramp-tracking experiments. Learning did not impact force-tracking accuracy, while increased forcing frequency decreased accuracy and increased force magnitude increased accuracy.

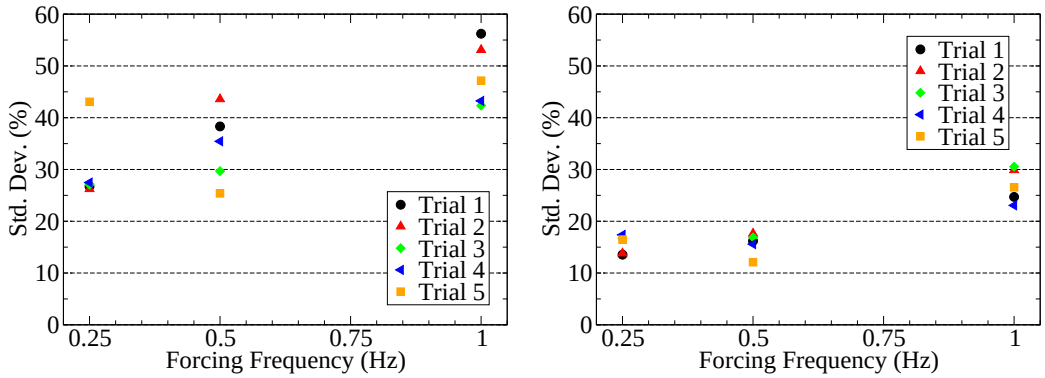

(a) $F_t = (6\text{ N/s})t$ *(b)* $F_t = (12\text{ N/s})t$

Figure 4.21: Standard deviation for variable-angle ramp-tracking experiments. Precision decreased as the forcing frequency increased. Both increased effort and increased experience improved precision.

As shown in Fig. 4.23, the subject struggled to track a sinusoidal force as her leg was being oscillated by a motor. Few of the sine-tracking experiments improved with increased practice, but one notable exception is the $F_t = 50N\sin(\pi t) + 50N$ test conducted with a forcing frequency of 1.00 Hz. In this case, error steadily

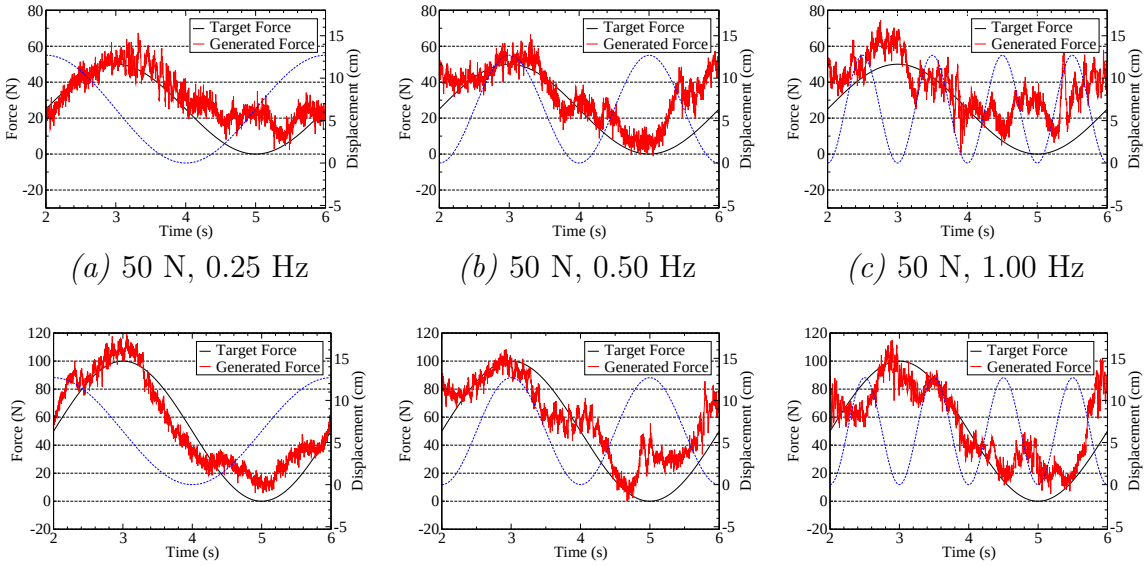

(a) 50 N, 0.25 Hz *(b)* 50 N, 0.50 Hz *(c)* 50 N, 1.00 Hz

(d) 100 N, 0.25 Hz *(e)* 100 N, 0.50 Hz *(f)* 100 N, 1.00 Hz

Figure 4.22: Typical variable-angle sine-tracking performance with a target frequency of 0.25 Hz. The dashed line shows leg displacement.

decreased with increased experience through the fourth trial. As in the other dynamic-leg-angle tests, the subject had more success tracking forces with a large maximum magnitude. In general, tracking results were best when the forcing frequency matched the target frequency. The experiment which showed the lowest error also showed the least variation from a forcing frequency of 0.25 Hz to 1.00 Hz, while the test with the greatest error showed the greatest variation in error from a forcing frequency of 0.25 Hz to 1.00 Hz, as shown in Figs. 4.23(c) and (b), respectively.

Because the test subject observed that the motor frequency, which controlled the position of her leg, had a great impact on her ability to accurately track forces, error was plotted again in Fig. 4.24, this time to highlight the relationship between target frequency and forcing frequency on the error. In all experiments, there was

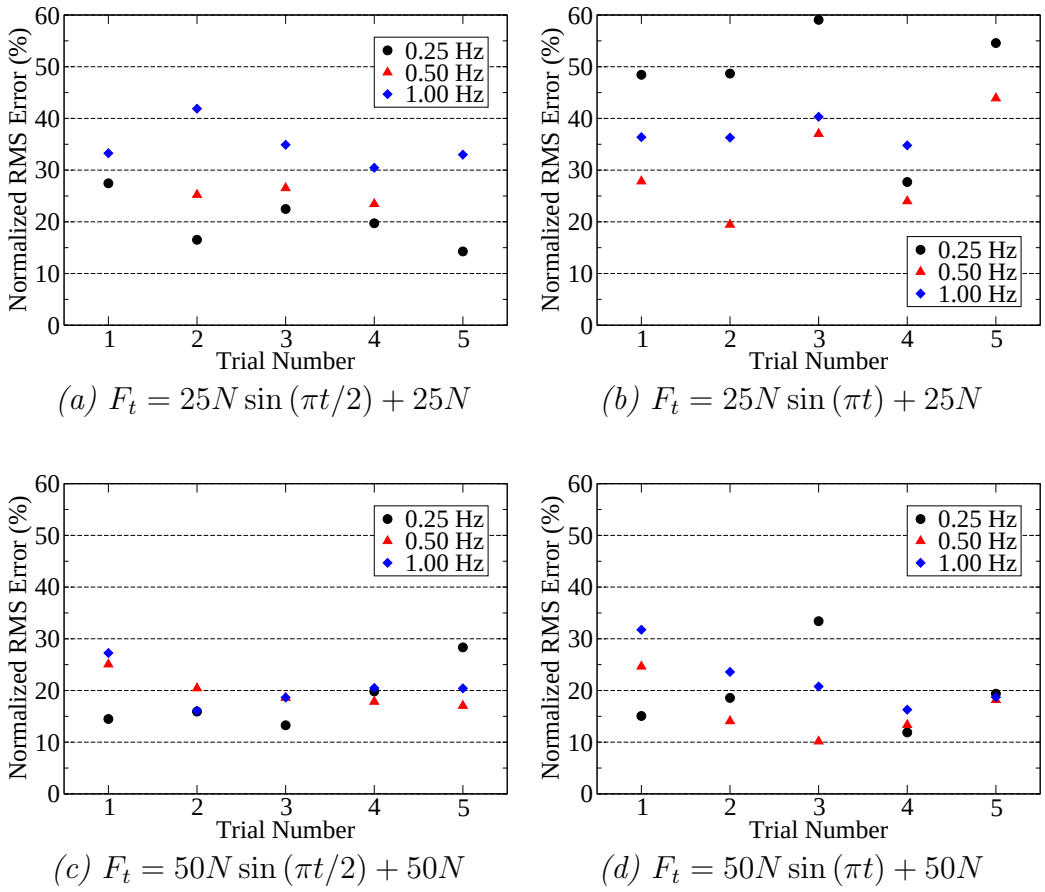

(a) $F_t = 25N \sin(\pi t/2) + 25N$ (b) $F_t = 25N \sin(\pi t) + 25N$

(c) $F_t = 50N \sin(\pi t/2) + 50N$ (d) $F_t = 50N \sin(\pi t) + 50N$

Figure 4.23: Normalized RMS error in variable leg angle sinusoidal-force-tracking experiments. Error was lower at higher amplitudes and was generally lowest when the forcing frequency matched the target frequency. Increased experience did not typically improve accuracy.

a 90° phase shift between the target frequency and the forcing frequency. At the beginning of the tests, the subject's leg was at its most accute angle of 90°. The target force was at its mid-range value. As the test subject contracted her muscles to meet the increasing target function, the motor was allowing her leg to extend. For both the 50-N and the 100-N amplitude tests, the error was lowest when the target frequency matched the forcing frequency. It appears that it was very difficult for the test subject to match a sine wave while her leg was being moved at a slower

frequency than the target force frequency. Error generally increased as the forcing frequency increased, especially in the 50-N amplitude experiments.

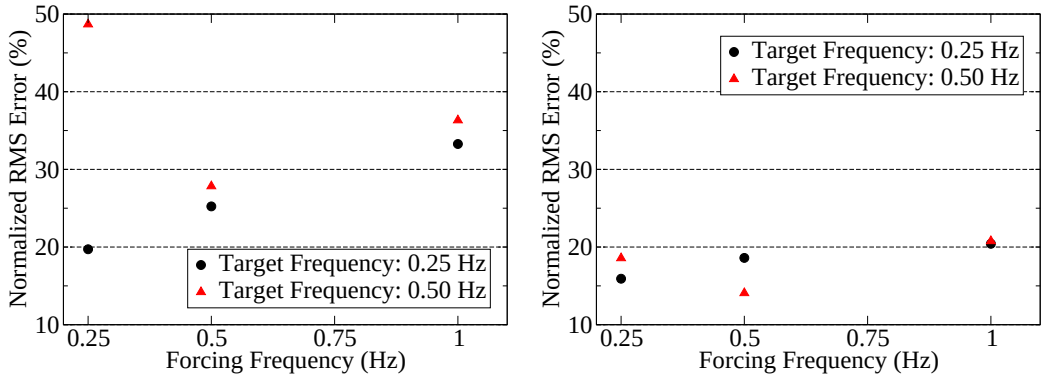

(a) Amplitude = 50 N *(b)* Amplitude = 100 N

Figure 4.24: Normalized RMS error in variable leg angle sinusoidal-force-tracking experiments.

Figure 4.25 shows the standard deviation of the dynamic-leg-angle sinusoidal force-tracking results. In general, the standard deviation is high for all sine tests, indicating that the subject's tracking was inconsistent. Neither forcing frequency nor experience is a significant factor in standard deviation. On average, the standard deviation, like the normalized RMS error, is lower for the tests with a maximum force of 100 N than for tests with a maximum force of 50 N. The standard deviation was, on average, higher for the variable-angle sine-matching tests than it was for all other experiments.

4.4 Discussion

It is difficult to find force-tracking experiments in the literature, but Srinivasan and Chen do provide some results that can be compared to the experiments presented

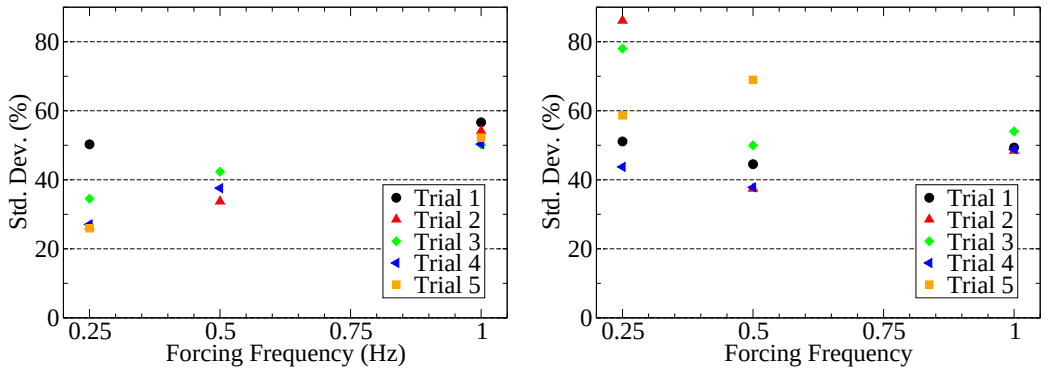

(a) $F_t = 25N \sin(\pi t/2) + 25N$

(b) $F_t = 25N \sin(\pi t) + 25N$

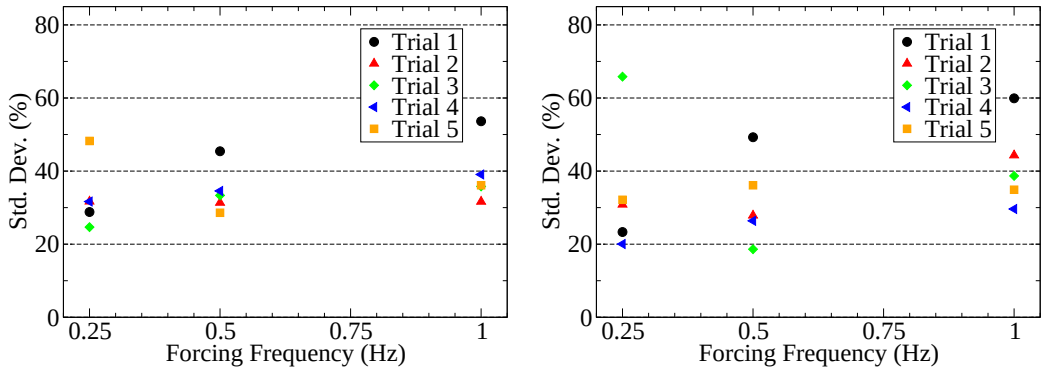

(c) $F_t = 50N \sin(\pi t/2) + 50N$

(d) $F_t = 50N \sin(\pi t) + 50N$

Figure 4.25: Standard deviation in variable leg angle sinusoidal-force-tracking experiments. Precision generally improved with increased experience. Forcing frequency did not impact precision as significantly as it did for other experiments.

in this thesis. In their experiments, Srinivasan and Chen asked test subjects to use their fingertips to match constant, sinusoidal, and ramp forces under fixed nominal knee angle conditions. When given visual feedback, average force-tracking error was typically between 11% and 15% [Srinivasan and Chen, 1993]. In this study, error in fixed-leg-angle force tracking experiments was generally between 7% and 11%. The resolution experiments conducted by Tan *et al.* indicated that force-matching precision is better for muscles near the torso (proximal muscles) than for muscles near the ends of the limbs (distal muscles) [Tan et al., 1994]. This

phenomenon may help explain why the results from this study, performed on the leg extensor muscles, show better tracking performance than Srinivasan and Chen's fingertip experiments.

Although some tracking tests proved more challenging than others, the force-tracking experiments showed that it is possible use the thigh muscles to track target forces accurately under both fixed-knee-angle and variable-knee-angle circumstances. The test subject tracked almost all fixed-angle target functions with less than 15% error, struggling only in the case of square waves at 33% MVC and a target frequency of 1.00 Hz. Variable-knee-angle tests proved a much more challenging exercise, and normalized RMS error in many target functions exceeded 25%. Still, the test subject was able to track constant forces with less than 15% error at 50 N when her leg was moved at a frequency of 0.25 Hz and at 100 N when her leg was moved at a frequency of less than 1.00 Hz. The subject was generally able to track target forces despite having no control over the position of her leg for constant profiles and for $F_t = 12N/s$ and $F_t = 50N\sin(n\pi t) + 50N$ (where $n = 1/2$ or $n = 1$). All other variable-angle tracking tests had very high (greater than 25%) error.

For variable-angle tests, it appears that the test subject did attempt to capitalize on the movement of her leg, which was beyond her control, to help better match the target force. When the subject's leg was being pulled back toward the 90° starting point, the force the test subject generated frequently rose above the target force in all variable-angle experiments. On the other hand, when the subject's leg was being extended, the generated force often dipped below the target force. This effect was generally more pronounced for faster forcing frequencies.

Among all the experiments, increasing the maximum target force generally improved test results. Increasing either the target or the forcing frequency increased tracking error and standard deviation. Gaining more testing experience by repeating trials had mixed results. These trends are discussed in more detail in the following sections.

4.4.1 Effect of increasing effort

For all tests except the fixed-angle square-wave tracking experiment, as the required effort increased, the normalized RMS error decreased. The effort required to track fixed-angle sine waves seemed to produce a trade-off between accuracy and precision: as the effort increased from 25% MVC to 50% MVC, the subject tracked the force more accurately but less precisely. For dynamic-knee-angle experiments, increasing the required effort improved both accuracy and precision. Variable-Angle tests were calibrated so that the maximum effort required would be approximately 50 N for the low-effort tests or 100 N for the high-effort tests. This corresponds to 8.8% MVC and 17.6% MVC, respectively. For humans, the "just noticeable difference" (JND) for distinguishing among forces is approximately 7% [Srinivasan and Chen, 1993]. It is possible that the reason the dynamic-knee-angle test results improved dramatically with increased effort requirements is that the test subject struggled to sense differences in the 50-N tests. It is likely that the rapid transition from low region to high region in the square-wave tests (and the associated increase in rise times) accounts for the test results that did not improve with increasing % MVC.

For future experiments, target forces should be chosen so that variations generally surpass the JND and so that the maximum effort required is at least 15%

Table 4.4: Effect of increasing effort on error and standard deviation

	Target	RMS Error (%)	Std. Dev. (%)
Fixed Angle Experiments	Sine	Improved	Worsened
	Square	Worsened	Worsened
Variable-Angle Experiments	Constant	Improved	Improved
	Ramp	Improved	Improved
	Sine	Improved	Improved

MVC. Maximum forces of 33% to 50% MVC will generally help to minimize error. Because 50% MVC constitutes a considerable effort, especially when maintained for more than several seconds, experiments conducted at this level should only be completed by athletes and the physically fit. An effort of 33% MVC presents a good compromise between easily generated and maintained but difficult to perceive forces and efforts that are easier to control but more difficult to maintain.

4.4.2 Effect of increasing frequency

In fixed-leg-angle tests, the subject was challenged to match the target force frequency, while in dynamic-leg-angle tests, the subject's leg was moved at a forced frequency beyond her control. Additionally, for the sinusoidal variable-angle tests, the subject was challenged to meet a target frequency as her leg was moved at a potentially different frequency. For the fixed-angle tests, target frequency could be viewed as a measure of how quickly a subject can generate and maintain the desired force and of how well she can perform each exercise consistently. For variable-angle tests, on the other hand, the forcing frequency measures how well the subject can track a force despite negative external influences.

For almost all tests, an increase in frequency (be it target frequency or forcing frequency) resulted in a decrease in overall performance, witnessed by increases in both normalized RMS error and standard deviation. The only exception occurred in dynamic-knee-angle sinusoidal tests, where the error and standard deviation was generally lowest when the forcing frequency matched the target frequency, allowing the test subject to contract her muscles in sync with their movement.

Table 4.5: Effect of increasing frequency on error and standard deviation

	Target	RMS Error (%)	Std. Dev. (%)
Fixed Angle Experiments	Sine	Worsened	Worsened
	Square	Worsened	Worsened
Variable-Angle Experiments	Constant	Worsened	Worsened
	Ramp	Worsened	Worsened
	Sine	Worsened	Varied

Target and forcing frequency have direct implications about future energy and locomotion experiments. If tests will be conducted at fixed knee angle, then any frequency up to and possibly including 2.00 Hz (given some practice) should work if the target force profile is smooth. If a square wave profile is used, then the frequency should be restricted to 1.00 Hz or less. For variable knee angle tests, constant forces can be used with a forcing frequency of 1.00 Hz or less provided the target force is at least 100 N. Ramp forces are a possibility if the slope is at least 12 N/s, and the frequency is below 1.00 Hz. If a test is desired that will really increase the pulse, then a dynamic-knee angle sine test could be used, possibly even with a forcing frequency of 2.00 Hz, provided the forcing frequency is a multiple of the target frequency.

4.4.3 Effect of increasing experience

Multiple trials were conducted for each force-tracking experiment. It was expected that with increased experience, force-tracking error and standard deviation would decrease. Actual experiments showed mixed results.

Among fixed-angle sine-tracking experiments, the 2.00-Hz target-frequency case showed dramatic improvement over the course of the three attempted trials, while the 0.10-Hz and 0.25-Hz cases improved slightly and the 0.50-Hz and 1.00-Hz cases showed no appreciable change. Additional attempts tracking square-waves conducted at fixed leg angle resulted in lower normalized RMS error for the 0.10-Hz and the 0.50-Hz experiments, but not for the 0.25-Hz or 1.00-Hz tests. None of the fixed-angle tests showed significant change in standard deviation with increased experience.

Among variable-angle experiments, additional experience decreased error in only a few cases ($F_t = 100$ N, $f_f = 1.00$ Hz; $F_t = 6$ N/s t, $f_f = 1.00$ Hz; $F_t = 25N \sin(\pi t/2) + 25N$, $f_f = 0.25$ Hz; $F_t = 50N \sin(\pi t) + 50N$, $f_f = 1.00$ Hz). In most variable-angle experiments, the standard deviation decreased with increased experience.

Generally, conducting additional trials of the same force-matching experiment produced positive results for high-frequency tests but had negligible results for low-frequency tests. This could indicate that at slower speeds, the test subject was easily able to adapt to the target force and optimize her performance. For future experiments, especially those conducted at higher frequencies, multiple practice trials should be conducted in advance of data collection to help ensure the subject

Table 4.6: Effect of increasing experience on error and standard deviation

	Target	RMS Error (%)	Std. Dev. (%)
Fixed Angle Experiments	Sine	Improved	Insignificant
	Square	Improved	Insignificant
Variable-Angle Experiments	Constant	Insignificant	Improved
	Ramp	Insignificant	Improved
	Sine	Insignificant	Improved

is comfortable with the testing and is performing as well as possible within a reasonable amount of time.

CHAPTER 5

CONCLUSIONS

We still have much to learn about human locomotion. One path to improving our understanding of locomotion is to investigate the performance capabilities and mechanics of *in vivo* muscle. To that end, I developed a muscle group isolation chair and conducted tests to determine how well humans can track forces using their leg extensor muscles under both fixed-angle and variable-angle conditions.

The muscle isolation chair was composed of a racing seat mounted onto a steel skeleton. A four-point seat belt and a set of custom-molded shoulder restraints prevented the test subject from moving her torso and limited the test subject's ability to recruit the core muscles to aid the leg extensors in force production. The test subject's leg was placed in a swing designed to constrain the rotation and transverse motion of the leg. Her foot was secured using molded plastic heel and forefoot cups. Stiff foam backing on the swing helped to push the subject's shin against an aluminum and plastic shin brace, which connected the shin to the load cell and motor via a 1/8-in cable. The test subject was able to evaluate and adapt her performance by watching and listening to a force-feedback system on a computer positioned approximately one meter away. For fixed-angle tests, a pretension load of 89 N was applied, helping to ensure a more rigid connection between the subject and the load cell at the beginning of each test. When the subject applied force to the chair during fixed-angle experiments, movement consisting of approximately 5 mm downward movement at the knee occurred at the beginning of each trial. After this initial deflection, no additional movement was observed during any fixed-angle test.

Both fixed-angle and variable-angle force tracking tests were conducted. For fixed-angle tests, square, sine, and triangle waves were chosen as target force profiles. The test subject had little difficulty tracking these forces, and her maximum error for all fixed-angle tests was only 23.86%±21.26%.

The test subject was not as successful in tracking forces during variable-angle tests. She experienced great difficulty, both qualitatively and quantitatively, tracking forces for sine waves with an amplitude of 50 N and ramp functions with a force rate of 6 N/s. The variable-angle tests did show, however, that it is possible to use leg extensor muscles to track a force with some accuracy and precision while not in control of the position of the leg. With a driving frequency of 0.25 Hz, the test subject tracked a 100-N constant target force with an error of only 9.06%±8.07%.

In general, increasing the required effort improved both fixed- and variable-angle test results. For fixed-angle results, increasing the maximum target force from 25% MVC to 50% MVC resulted in less precise results. Increasing the required effort had a positive effect on both accuracy and precision in variable-angle tests. Increasing the target frequency in fixed-angle tests and the forcing frequency in variable-angle tests resulted in decreased overall performance. Learning effects were not present in all tests, but they were often apparent in tests at higher frequencies that the subject found challenging to track.

In the future, the fixed- and variable-angle force tracking experiments could be expanded to include ramp tracking tests at higher force rates and to perform more trials of all experiments to see whether learning effects could be determined. It would also be beneficial to investigate the relationship between the phase of the forcing frequency and the target frequencies. The muscle isolation chair could be improved by developing a better foot swing to better align with the center of

rotation of the test subject's knee and to be slightly more rigid. A rigid link could be used instead of a cable to enhance the ability of the test subject to conduct eccentric force tracking tests. The racing seat could be replaced with a rigid plastic seat to reduce the effects of compliance. Also, EMG could be used to investigate how effectively the chair actually isolates the leg extensor muscles.

Before we can understand human locomotion, we must first master the performance capabilities and mechanics of muscle *in vivo*. The work presented here addressed this need by quantifying how well humans can match force waveforms using their leg extensor muscles under both fixed- and variable-angle conditions. I also developed a system of limiting undesired motion through the application of rigid constraints. This system should aid in future muscle mechanics research and may even help advance our understanding of muscle energetics.

APPENDIX A

MUSCLE ANATOMY AND PHYSIOLOGY

Skeletal muscle, the type of muscle of interest in this study, is composed of bundles of single-cell units called muscle fibers. Connective tissue binds these fibers together and provides an avenue for nerve fibers and bodily fluids to service the muscle. The primary constituent of this connective tissue is collagen. Muscles are connected to the bone or to fascia via tendons [Gray, 1918].

Skeletal muscle contracts to create movement of the body, generally transmitting a force through the tendon to the bone, developing a joint torque which results in the angular displacement of a limb about a joint. When the muscle causes a limb to move toward the body, the action is dubbed *flexion*. A muscle contraction that causes a limb to move away from the body is known as an *extension*. To provide the body with control and support, and because of the geometric constraints of attaching tendon to bone, muscles frequently act at a large mechanical disadvantage to create motion and to lift loads. For example, the force generated in the biceps muscles of the arm to lift a load using the forearm is typically a factor of five or more greater than the load to be lifted [Vander et al., 1970].

A.1 Glossary of anatomical terms

Geometric vocabulary

- *Proximal:* nearer to the center of the body (e.g. The shoulder is proximal to the elbow.)
- *Distal:* farther from the center of the body (e.g. The fingers are distal to the arm.)

- *Medial:* near the body
- *Lateral:* to the side of the body
- *Anterior:* in front of
- *Posterior:* behind
- *Superior:* above
- *Inferior:* below

A.1.1 Planes of the body

- *Median:* The plane axis that equally divides the body into left and right halves.
- *Saggital:* A plane that divides the body into unequal left and right portions.
- *Transverse:* The plane that divides the body into upper and lower halves, the body's transverse cross-sectional plane.
- *Frontal:* The plane that divides the body into front and back halves (also known as the *coronal* plane.

A.1.2 Movement terms

- *Flexion:* A movement that creates an increasing bend.
- *Extension:* A movement that straightens a joint.
- *Abduction:* Lateral movement away from the body
- *Adduction:* Lateral movement toward the body

A.1.3 Types of muscle contractions

- *Concentric contraction:* A contraction in which a muscle is actively shortened (e.g. a biceps curl).
- *Eccentric contraction:* A muscle response in which a muscle is actively lengthened.
- *Passive lengthening:* A muscle stretch at approximately zero tension.
- *Isometric contraction:* A "contraction" in which the length of the muscle remains constant.
- *Isotonic contraction:* A contraction in which the muscle contracts under a constant tension.
- *Isokinetic contraction:* A contraction in which the muscle contracts at a constant velocity.

A.2 Anatomy of muscle

Humans are born with all the muscle fibers they will ever have in their lifetimes. Instead of developing new muscle fibers, when a person practices weight-lifting or body-building activities, he increases the diameter of the muscle fiber [Zajac, 1989, Kandel et al., 2000]. This is known as hypertrophy. During human limb movement, muscle fibers reversibly change length by $\pm 10\%$ [Hunter and Lafontaine, 1992]. Isolated from the joint and surrounding tissue, human muscles can change length by ± 50 % [Zajac, 1989, Buchanan et al., 2004].

A whole muscle is a collection of long cells known as muscle fibers. Muscle fibers are composed of myofibrils, which are fibers generally around 2 μm in di-

ameter that span the length of the muscle fiber [Hunter and Lafontaine, 1992]. Myofibrils are composed of 1-μm bundles of thick and think protein strands called myofilaments [Enoka, 1998]. Myosin and actin are the primary constituent of the thick and thin myofilaments, respectively. These proteins interact to form the contraction machinery of muscle. The basic building block of muscle is the *sarcomere*. Sarcomeres are segments of the myofibril defined by an interlocking thick and thin myofilaments. Each sarcomere has a resting length of approximately 2.5 μm [Enoka, 1998].

Muscles have varied appearances and different properties according to their *insertion* and *origin* points and to the arrangement of the muscle fibers that comprise an individual muscle. A muscle is attached to the bone or to tissue at the *origin*, the more proximal point, and at the *insertion*, located along the joint that the muscle acts to move. Muscle fibers are arranged in many different ways in the body. A muscle whose fibers run parallel to their attachment tendons and that connect the origin and insertion directly is a *quadrilateral* muscle; if the fibers are not perfectly parallel, but are instead curved so that the muscle tapers to its origin and insertion points, the muscle is called *fusiform*. Fusiform and quadrilateral muscles have similar actions. *Triangular* muscles have fibers that run from a broad origin to a narrow insertion, such as the *gluteus maximus*. In some muscles, the fibers lie at an angle to the line segment created from the origin and insertion points. These muscles are *pennate* muscles; if the fibers attach to an oblique tendon, they are *unipennate*, and if they attach to a central tendon, they are *bipennate*. The *rectus femoris*, one of the muscles of the quadriceps group, is a bipennate muscle. Figure A.1 shows muscle fiber architecture in each of a fusiform, unipennate, and bipennate muscle [Gray, 1918].

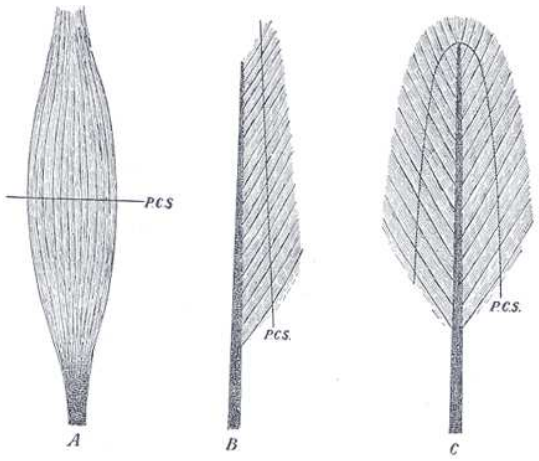

Figure A.1: Fiber arrangement in muscles: *A)* fusiform muscle, *B)* unipennate muscle, *C)* bipennate muscle (*PCS* represents the physiological cross-section) *Figure copied from [Gray, 1918]*

Most human muscles have pennation angles ranging from 0 to 2.3° [Enoka, 1998]. Pennate muscles lend the body strength in a compact way: within a given volume, a pennate muscle has a greater number of parallel fibers (and thus a larger cross-sectional area) than a fusiform muscle [Enoka, 1998]. Because of the pennation angle, geometry dictates the contribution of each muscle fiber to the force along the line of action is reduced to the cosine of the pennation angle. During contraction, the volume of muscle remains approximately constant while the muscle shortens; as a result, the pennation angle changes [Enoka, 1998]. Figure A.2 shows the pennation angles present in the *rectus femoris*, which is a bipennate muscle that belongs to the quadriceps group.

Fusiform and quadrilateral muscles, which have relatively long muscle fibers with a large number of sarcomeres in series, can attain higher shortening velocities and can produce greater length changes than pennate muscles, which have shorter muscle fibers but larger cross-sectional areas and a large number of sarcomeres in parallel. The body capitalizes on this difference between serial and parallel muscle

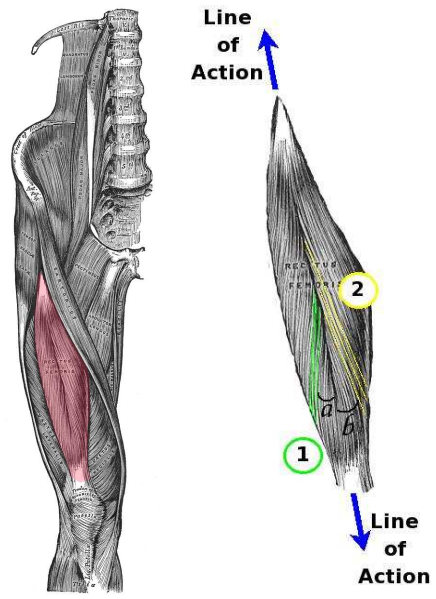

(a) *(b)*

Figure A.2: The *rectus femoris* (highlighted in *(a)*) is an example of a bipennate muscle. The line of action of the muscle and the pennation angle of the muscle fibers are shown in *(b)*. The alignment of the fibers on the lateral side of the muscle are highlighted at *1*, and the pennation angle of the lateral fibers is α. The medial fiber alignment is identified by *2*, and the pennation angle of these fibers is β. *Rectus femoris and quadriceps group images from [Gray, 1918]*

fibers, featuring pennate muscles in muscle groups that must be strong without occupying too much space (such as the quadriceps, which maintain posture against the effects of gravity) and fusiform muscles when rapid movement is desired, but strength is not as important a factor (such as in the hamstrings) [Enoka, 1998]. In general, long muscle fibers tend to give a muscle a high range of movement at the expense of power; the opposite is true of muscles composed of numerous, short fibers [Gray, 1918]. Thus the *sartorius* (the tailor's muscle), the longest muscle in the human body, is weak but contracts to help people cross their legs, while the bipennate *rectus femoris* (see Fig. A.2(a)), a leg flexor, helps people power through jumps, etc.

A.3 Muscle physiology

The *motor unit*, which consists of a motor neuron and the muscle fibers the neuron innervates, is the basic unit of the motor system. Thanks to the a large variety of motor units in the human body, our muscles can provide strength, dexterity, and speed. Each of our muscles is composed of a number of motor units, generally ranging from 100 to 1000 [Enoka, 1998]. Each motor neuron that defines a motor unit innervates between 10 and 2000 muscle fibers [Enoka, 1998]. The number of motor units contained within each muscle and of muscle fibers controlled by each motor neuron are key factors in overall muscle performance.

Small motor neurons have smaller input resistances but slower signal conduction speeds. As a result, small motor neurons are more excitable than larger motor neurons, but they generate and transmit action potentials (the signals that cause the muscles to contract) slower than larger motor neurons [Enoka, 1998]. In general, smaller motor neurons control groups of muscles that allow fine control and that have more fatigue resistance than large motor neurons, which allow strong, fatiguable contractions.

Like the size of the motor neuron, the innervation ratio–the number of muscle fibers innervated by a single motor neuron–plays an important role in muscle physiology. Muscles with small innervation ratios control fine movements. Muscles in the eye, for example, have innervation ratios as small as ten. On the other hand, muscles with high innervation ratios are not as precise, but they can be more powerful. For example, the powerful calf muscle can have an innervation ratio of 1:1900 [Enoka, 1998].

The muscle fibers controlled by a single motor neuron are concentrated near each other in the muscle. As a result, different parts of a muscle can be composed of distinct groups of motor units [Enoka, 1998]. These areas are known as neuromuscular compartments. The density of these groups can change with time as some motor neurons die, and the surrounding motor units grow new dendrites to help compensate, reducing the number of neuromuscular compartments. The existence of neuromuscular compartments complicates the study of muscle mechanics, as exacting models must account for innervation patterns and muscle architecture along with normal contraction dynamics and other factors [Enoka, 1998].

In general terms, muscle contraction is the result of a sequence of events beginning with a stimulus and ending with the sliding of myosin and actin proteins past each other in the sarcomere. The first step in the sequence is motor neuron stimulation. If the net input to the motor neuron is sufficiently high, the motor neuron responds by generating an electrical pulse, called an action potential [Enoka, 1998, Kandel et al., 2000]. This potential then travels along the nerve axon to the sarcolemma of the muscle fiber. The conversion of the signal from the axon to a sarcolemmal command is known as *neuromuscular propagation* [Enoka, 1998] The sarcolemmal command is also known as the muscle action potential, and it is this signal that directly initiates muscle contraction in the sarcomere [Enoka, 1998]. The process by which a neural signal is generated and propagated to the muscle and the subsequent processes that cause muscle contraction are known as *excitation-contraction coupling* [Enoka, 1998]. For information about how excitation-contraction coupling is modeled, see Sec. B.1.

The sarcomere, which consists of alternating thin (actin) and thick (myosin) protein chains, is the muscle's basic contractile unit. The sarcomere contracts as

the myosin head, or "crossbridge," of the thick filament alternately attaches to and detaches from sites along the thin filament, resulting in a "ratcheting" mechanism as the protein filaments overlap one another [Enoka, 1998]. It is believed that each crossbridge generates a force of approximately 1 pN [Hunter and Lafontaine, 1992].

APPENDIX B

MECHANICS OF THE MUSCULOTENDON

Voluntary muscle contraction begins with the central nervous system. Neural signals activate the release of calcium from the sarcoplasmic reticulum, triggering muscle contraction. Once activated, muscle force production is governed by mechanical contraction dynamics. Together, activation dynamics and contraction dynamics control muscle performance [Kandel et al., 2000, Zajac, 1989].

B.0.1 Force-length relationships

Muscle tissue that has been excited long enough to attain steady-state is known as activated muscle tissue, while muscle tissue that has not been excited in some time is passive muscle tissue. Both activated and passive muscle tissue generate force when held isometrically. Active muscle force is the difference between the total load transmitted in the muscle and the load carried by passive muscle tissue. Isolated from surrounding tissue, active muscle force is generated between $0.5L_0^m$ and $1.5L_0^m$ [Buchanan et al., 2004] (this range is reduced to $\pm 10\%$ *in vivo* in humans [Hunter and Lafontaine, 1992]), where L_0^m is the optimum muscle length (which occurs when the sarcomeres are at their peak force-production length of 2.8μm) [Zajac, 1989].

Nondimensionalized equations are typically used to characterize both the active and the passive force-length relationship. Although some research [Buchanan et al., 2004] shows the force-length relationship is not so simple, the

nondimensionalized force-length relationship is often modeled as a quadratic relationship [Valero-Cuevas, 2007]:

$$f_l = 1 - \left(\frac{L^m - L_0^m}{\omega L_0^m} \right) \tag{B.1}$$

where L^m is the current muscle length and ω is a shape factor.

Shutte suggested the passive force-length relationship be modeled as shown in Eq. B.2 [Buchanan et al., 2004].

$$f_p = \frac{\exp\left[10\left(\frac{L^m}{L_0^m} - 1\right)\right]}{\exp(5)} \tag{B.2}$$

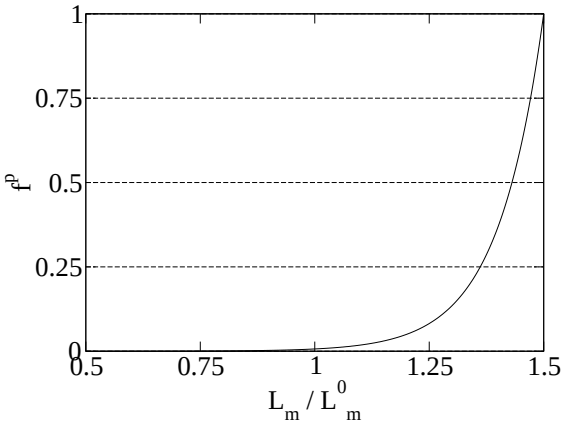

Figure B.1: Passive force-length relationship described by Eq. B.2.

B.0.2 Force-velocity relationships

Force-velocity relationships can be determined from the Hill equation, found empirically, or determined by integrating the force-length relationship [Zajac, 1989]. The maximum shortening velocity, v_m is the velocity at which a muscle at its optimum length can contract without bearing a load. A muscle's maximum power output occurs at approximately $0.3v_m$ [Zajac, 1989].

For concentric contractions, the force-velocity relationship can be modeled as shown in Eq. B.3, whereas the formula for the eccentric force-velocity relationship is shown in Eq. B.4.

$$f_v = \left(\frac{F_o^m b - a v^m}{b + v^m} \right) \tag{B.3}$$

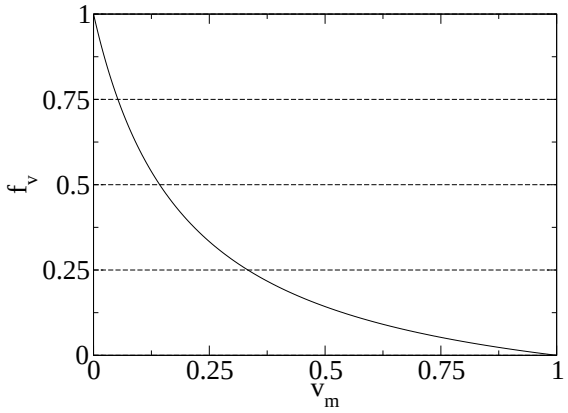

Figure B.2: Concentric force-velocity relationship described by Eq. B.3 with $F_o^m = 1$; $a = 0.2$; $b = 0.2$.

$$f_{v,ecc} = \frac{1}{F_o^m} \left(F_{ecc}^m F_o^m - (F_{ecc}^m - 1) \frac{F_o^m b' + a' v^m}{b' - v^m} \right) f_l \tag{B.4}$$

B.0.3 Maximum isometric force

The maximum isometric force that can be generated within a muscle is a function of the muscle's cross-sectional area, orientation, and the stress that can be withstood by the tissue and is generally approximated:

$$F_o^m = PCSA \cdot \sigma_m \cos \alpha \tag{B.5}$$

where $PCSA$ is the muscle's physiological cross-sectional area, σ_m is the tensile strength of the muscle (typically between 300 and 350 kPa), and α is the muscle pennation angle [Valero-Cuevas, 2007].

Because few muscles have a pennation angle greater than 15° or 20°, pennation angle (see Sec. A.2 for more information about pennation angle) is often neglected in muscle models [Buchanan et al., 2004]. When pennation angle is included, it can be modeled either as a constant angle throughout the full range of motion, or it can be assumed to vary as the muscle contracts. Physiologically, the pennation angle increases during a muscle contraction [Scott and Winter, 1991, Enoka, 1998]. In a study of three pennation angle assumptions, Scott and Winters found it is best to model the pennation angle as a function of muscle length and that models with a constant (non-zero) pennation angle assumption performed worst in estimating end-point muscle force [Scott and Winter, 1991]. Thus, some simple muscle models can neglect pennation without incurring too much error. Where more accuracy is desired, dynamic muscle pennation can be modeled simply as shown in Eq. B.6.

$$\alpha = \sin^{-1}\left(\frac{l_o^m \sin(\alpha_o)}{l^m(t)}\right) \tag{B.6}$$

where l_o^m is the optimal fiber length, $l^m(t)$ is the fiber length at time t, and α_o is the pennation angle at l_o^m [Buchanan et al., 2004].

A muscle's optimal isometric force depends on its cross-sectional area. Determining the actual cross-sectional area of a muscle requires measuring and summing the cross-sectional area of each muscle fiber along an axis perpendicular to the long axis of the muscle fiber [Enoka, 1998]. Because such a measurement is not currently possible *in vivo* and is infeasible to calculate for cadavers, an approximation, called the *physiological cross-sectional area*, or PCSA, is made. The PCSA is the ratio of the muscle's volume to its optimal fiber length. Barring the availability

of other measurement methods, muscle volume is generally calculated from the muscle mass [Buchanan et al., 2004, Yamaguchi et al., 1990]:

$$PCSA = \left\{ \begin{array}{ll} \dfrac{m}{\rho l} & \text{for fusiform muscles} \\ \dfrac{m}{2\rho t}\sin(2\alpha) & \text{for unipennate muscles} \end{array} \right\} \tag{B.7}$$

where m is the muscle mass; ρ is the muscle density (typically taken to be 1060 kg/m^3), l is the optimum muscle fiber length; t is the depth of the muscle pennation; and α is the pennation angle [Buchanan et al., 2004, Yamaguchi et al., 1990].

The use of the PCSA instead of the actual cross-sectional area of the muscle introduces errors in two ways. First, a number of PCSA models exist for different types of muscles, and the choice of model can impact the resulting PCSA calculation, as can using PCSAs determined using different methods in the same muscle model. Second, when the PCSA is used, it is assumed that noncontractile muscle elements are distributed evenly throughout muscle. Research indicates this is not the case, so results generated using PCSA should be viewed as estimates [Enoka, 1998].

B.1 Activation dynamics

Muscle contraction is triggered by muscle activation, which, in turn, is triggered by neural activation. Calcium dynamics plays a key role in the path from excitation to contraction and is generally approximated by first-order dynamics. Activation occurs more quickly than deactivation. Both activation and deactivation have saturation points, meaning that activation ranges from 0% to 100% [Zajac, 1989].

Because muscle systems are extremely complicated, and simple physiology dictates that we must make approximations of such key features as PCSA, muscle models are typically simplified to avoid computational complexity and to allow results to be compared with empirical data. For example, all the motor units of a particular muscle are typically given the same treatment using the following activation dynamics model:

$$\frac{da(t)}{dt} + \left[\frac{1}{\tau_{act}}\left(\beta + [1-\beta]u(t)\right)\right] a(t) = \left(\frac{1}{\tau_{act}}\right) u(t) \tag{B.8}$$

where $a(t)$ is the muscle activation; $u(t)$ is the neural excitation; τ_{act} is the time constant of the fully-excited muscle; and β is the ratio between the activation and deactivation time constants [Zajac, 1989].

In order to use empirical data in muscle models, electromyogram (EMG) data is often used to approximate activation dynamics. When used to model activation, EMG records are known as *interference patterns* because they represent the contributions of many motor units. EMG data that has been full-wave rectified and submitted to a low-pass filter, it corresponds roughly to generated force and can be used to approximate activation [Enoka, 1998].

The central nervous system has two methods to facilitate force generation: pulse-train frequency and motor-unit recruitment. As the frequency of one motor unit reaches saturation, additional motor units are recruited from the smallest to the largest [Kandel et al., 2000, Buchanan et al., 2004]. This process serves to ensure that we can precisely handle very small loads with our hands while maintaining the ability to produce large forces if needed [Kandel et al., 2000, Valero-Cuevas, 2007]. Because motor units have an activation saturation point, increasing the frequency in one motor unit will eventually cease to increase the force output from the innervated muscle fibers. Thus, there is a nonlinear relationship

between individual motor-unit force generation and motor-unit activation. When examining an entire muscle, however, the recruitment of additional motor units acts to offset the nonlinear nature of the activation-force relationship, resulting in a global linear relationship between activation and force [Buchanan et al., 2004].

B.2 Tendon mechanics

Because the tendon lies in series with the muscle, the force in the tendon is equal to the force in the muscle. Tendon mechanics can thus be used to simplify muscle models.

Tendons are passive elements composed primarily of collagen. At lengths shorter than the tendon slack length, l_s^t, the tendon does not transmit any force. As a tendon is stretched beyond its slack length, the force in the tendon can be determined as a function of tendon strain:

$$\epsilon^t = \frac{l^t - l_s^t}{l_s^t}. \tag{B.9}$$

where ϵ^t is the tendon strain and l^t is the current tendon length [Buchanan et al., 2004].

Under initial loading, tendons have a low stiffness because of the nature of the collagen fibers that comprise them. At low tensions, the force-strain relationship for tendons is nonlinear. Once the collagen fibers have untangled, however, tendons exhibit a linear force-strain relationship. The literature indicates that as the muscle approaches its maximum isometric force, the strain in the attached tendons is 3.3%. Failure in tendons occurs when the tendon strain reaches approximately 10% (and the muscle force is roughly $3.5F_o^m$) [Buchanan et al., 2004]. In

the elastic region, tendons have a Young's modulus of 1.2 GPa. This modulus can be normalized by the tendon stress at F_o^m, assumed to be 32 MPa, resulting in a normalized Young's modulus of 37.5 [Buchanan et al., 2004]. One model of the normalized tendon force as a function of tendon strain that captures this behavior is: [Buchanan et al., 2004]:

$$\bar{F}^t = \begin{cases} 0 & \epsilon \leq 0 \\ 1480.3\epsilon^2 & 0 < \epsilon < 0.0127 \\ 37.5\epsilon - 0.2375 & \epsilon \geq 0.0127 \end{cases}. \tag{B.10}$$

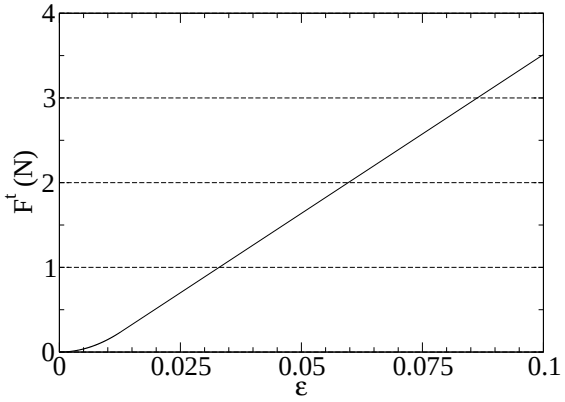

Figure B.3: Normalized tendon force as modeled by Eq. B.10.

B.3 A complete muscle model

One common, suitable muscle model is shown in Fig. B.4. The activation dynamics are determined, and the activation is fed as an input to the contraction dynamics, along with the muscle length and velocity.

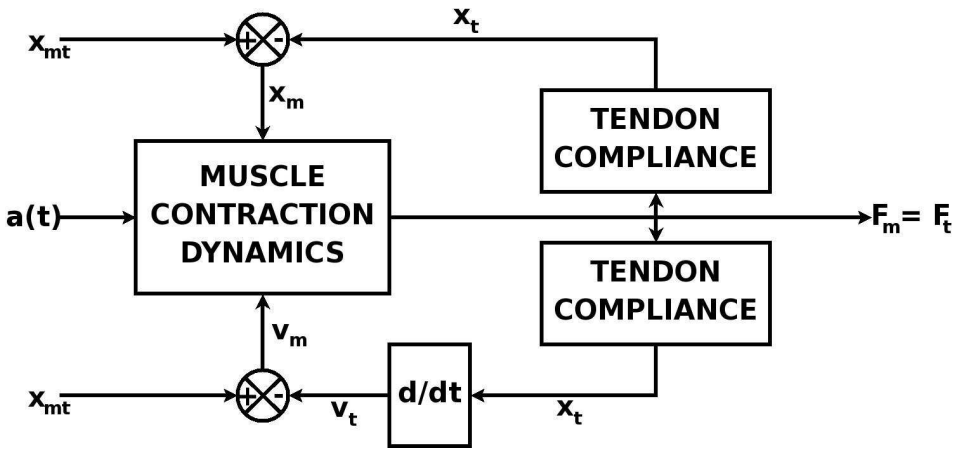

Figure B.4: Block diagram of muscle force generation.

The most prevalent model used to estimate muscle force is a Hill-type muscle model, which relates muscle output force to a muscle's maximum force, its activation, its length, and its velocity:

$$F^m(t) = (f_l)(f_v)(F_o^m)(a) \tag{B.11}$$

where F_m is the muscle force, f_l is the normalized force-length relationship, f_v is the normalized force-velocity relationship, a is the muscle activation, and F_o^m is the maximum possible muscle force.

This model includes the tendon along with the muscle, combining the two terms into the *musculotendon* (MT), shown in Fig. B.5. To determine the muscle force using this model, the length of the musculotendon unit (MT) is first determined. The length of the tendon is then determined, as is the velocity of the MT unit. Assuming an isometric contraction, the maximum force that can be generated by the muscle in question is determined using the current muscle length and activation. The contraction velocity is then determined from the inverse force-velocity curve. Finally, the velocity of the tendon is determined [Valero-Cuevas, 2007].

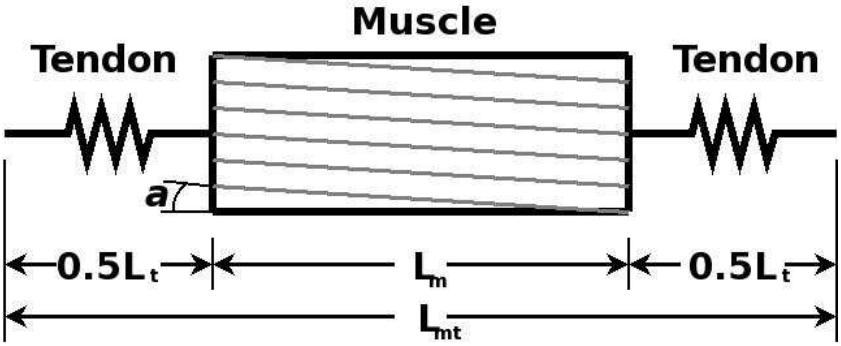

Figure B.5: Schematic of the musculotendon.

APPENDIX C

FORCE SENSING AND PROPRIOCEPTION

Bulk skeletal muscle includes two types of sensing organs. *Muscle spindles* are responsible for position and velocity sensing. The *Golgi tendon organ* detects and reports changes in muscle tension.

Muscle spindles, comprised of *intrafusal* muscle fibers, are located parallel to the power-generating *extrafusal* muscle fibers within skeletal muscle tissue. Extrafusal muscle fibers were described in Appendix A and are innervated by α-motor neurons. The intrafusal muscle fibers, which are wrapped with sensory receptors, are innervated by γ-motor neurons. Muscle spindles have both a sensory component, which capitalizes on the stretch sensitivity of the intrafusal muscle fibers, and a motor component, which is driven by the γ-motor-neuron response. Muscle spindles act to sense muscle length and velocity. Muscle length changes trigger the muscle spindles to send length-change information to both the central nervous system and the spinal cord and to send velocity information to the central nervous system. Because of the structure and mechanisms of muscle spindles, the central nervous system can independently adjust their dynamic and static sensitivity. Chemical changes within the muscle spindles affect the response of the muscle to a stretch stimulus [Kandel et al., 2000].

Golgi tendon organs are strands of collagen that connect the ends of the muscle fibers to the tendon. One *type 1b sensory afferent fiber* innervates each Golgi tendon organ. When the muscle shortens during contraction, the Golgi tendon organ is stretched, deforming the terminals of the 1b sensory afferent axon, opening cation channels and depolarizing the axon. This depolarization results in an action potential, signaling force development, which is sent to the central nervous system

via the spinal cord. A greater action potential pulse frequency signals a greater force application. Feedback from the Golgi tendon organ helps the body regulate force production [Kandel et al., 2000].

Force sensing is not dependent on the Golgi tendon organ alone. The effort required to complete a task affects perceived tension [Brockett et al., 1997, Weerakkody et al., 2003]. It is possible to sense tension in the absence of effort. Tests of the tonic vibration reflex, a muscle reflex to vibration, have shown that while the reflex tension is not accompanied by a sense of required effort, the force generated under the effect of the reflex can be matched through voluntary contraction of the untested limb [Weerakkody et al., 2003]. It has been shown, however, that both fatigue and effort affect force sensing [Brockett et al., 1997, Weerakkody et al., 2003].

In experiments where subjects attempted to match a torque generated with one arm under concentric contraction by producing an equivalent eccentric contraction with the other limb (or vice versa), the torque mismatch increased following the exercise, reaching error levels as high as approximately 40%, before returning to reference error levels of less than 10% four days later [Brockett et al., 1997]. Experiments to match a force using an exercised arm to a reference force held by an unexercised arm (or vice versa) show significantly higher error (13-14% mismatch) than control tests completed with both arms being unexercised [Weerakkody et al., 2003].

APPENDIX D

MUSCLE-RELATED ENERGY EXPENDITURE

D.1 Near Infrared Spectroscopy determination of $\dot{V}_{O_2}$

Near-infrared spectroscopy (NIRS) is a noninvasive technique capable of measuring information about tissue oxygenation. Originally used in studies of the brain, NIRS has found applications in a variety of areas and is considered an effective means of determining local $\dot{V}_{O_2}$ in skeletal muscle. Oxygen uptake, $\dot{V}_{O_2}$, is the difference between exhaled and inhaled oxygen and carbon dioxide levels and is often used to estimate energy consumption in muscles. When NIRS is used to determine oxygenation of tissues, near-infrared light is passed through the tissue. The amount of light the tissue absorbs is a function of the amount of oxygen present in the tissue. Changes in light absorption in the tissue are converted into measures of changes in oxyhemoglobin (O_2Hb) and deoxyhemoglobin (HHb) via a modified Lambert-Beer law [Praagman et al., 2003]. The Lambert-Beer law relates the absorption of light in a material to the properties of that material. Classically, it can be expressed

$$c = \frac{A}{\alpha l}, \tag{D.1}$$

where c is the concentration of the light in the material; A is the absorption of the light; $\alpha = \frac{4\pi k}{\lambda}$ relates the extinction factor to the wavelength of the light; and l is the optical path length (the distance the light travels through the medium). Modified for light-scattering materials such as tissue, the Lambert-Beer equation becomes:

$$c = \frac{A - A_r}{\alpha l f_l}, \tag{D.2}$$

where A_r represents light lost through scattering, and f_l, the differential pathlength factor, corrects for the increase in path length due to scattering. When a multichannel approach is taken, NIRS can be used to quantify heterogeneous metabolic responses to exercise, both within and among muscle groups [Quaresima et al., 2001].

The advantages of using NIRS in muscle energetics studies include:

- Discrimination between resting and active muscles
- Identification of varying levels of muscle activity
- Generation of localized data

Unfortunately, NIRS also has the following disadvantages:

- Dynamic testing is difficult because NIRS is sensitive to tissue temperature and because the volume of blood flowing to the area being tested must be constant [Praagman et al., 2003, de Ruiter et al., 2005].
- Determining the quantitative absolute oxygenation total is difficult because NIRS assumes body tissue is homogeneous[de Ruiter et al., 2005].
- Only superficial muscle tissue is sampled [de Ruiter et al., 2005].

Multichannel NIRS systems allow high spatial (0.1875 $1/\text{cm}^2$) and temporal resolution (100 ms), but they are still limited to isometric contractions [Quaresima et al., 2001].

NIRS seems to be an extremely useful tool for determining muscle energetics, but the combination of the increased cost and complexity of conducting experiments using NIRS and the disadvantages of NIRS testing itself suggest that for

the time being, it may not be feasible to include this technique. Still, NIRS is a technique that should be further investigated and possibly included in later experiments.

D.2 Initial transient oxygen consumption and $\dot{V}_{O_2}$ kinetics

Oxygen is delivered to active muscles as a response to adenosine triphosphate (ATP) production in tissues. If the oxygen supply is insufficient, the generation of ATP depends on anaerobic glycolysis. Systemic oxygen uptake ($\dot{V}_{O_2}$) is believed to indicate the change in oxidative enzymes in active tissues, reflecting both systemic oxygen transport and muscle metabolism [Xu and Rhodes, 1999].

In humans, oxygen uptake is a function of exercise intensity and can be sorted into three distinct domains. The first domain occurs during moderate exercise intensities with a work rate below the lactate threshold (LT). Next is the heavy exercise domain, occurring between the lactate threshold and the maximum lactate steady state. Finally, the severe intensity domain occurs beyond the maximum lactate steady state and is characterized by a systemic increase in blood lactate [Xu and Rhodes, 1999].

During exercise, $\dot{V}_{O_2}$ progresses through three phases. *Phase I* is characterized by a sharp rise in $\dot{V}_{O_2}$. This phase generally lasts 15-25 seconds (at moderate exercise) and is attributed to an increase in cardiac output and pulmonary blood flow. The effect of muscle metabolic change drives *Phase II*, in which $\dot{V}_{O_2}$ increases exponentially toward steady state. After approximately three minutes (when exercising moderately), $\dot{V}_{O_2}$ reaches steady state, achieving *Phase III*. At steady-state, $\dot{V}_{O_2}$ increases linearly with work rate [Xu and Rhodes, 1999].

In the moderate exercise domain, $\dot{V}_{O_2}$ can be expressed as a function of time as:

$$\Delta\dot{V}_{O_2}(t) = \Delta\dot{V}_{O_2}(ss)\left[1 - \exp\left(-\frac{t-\delta}{\tau}\right)\right] \tag{D.3}$$

where $\Delta\dot{V}_{O_2}(t)$ is the value of $\dot{V}_{O_2}$ relative to the reference value; $\Delta\dot{V}_{O_2}(ss)$ is the relative steady-state value of $\dot{V}_{O_2}$; δ is the time delay, and τ is the time constant [Xu and Rhodes, 1999].

Beyond moderate exercise, a "slow" component of $\dot{V}_{O_2}$, correlated with the onset of lactic acid accumulation, develops during *Phase II* after a few minutes of exercise. Because of the slow component, $\dot{V}_{O_2}$ continues to increase progressively, and steady-state oxygen uptake is reached later than at moderate exercise. Beyond heavy exercise, steady state cannot be achieved. Instead, $\dot{V}_{O_2}$ continues to increase until the subject becomes fatigued. As a result, the slow component is much larger at severe intensities [Xu and Rhodes, 1999].

One of the most frequently explored issues relating to $\dot{V}_{O_2}$ kinetics is deducing the limiting mechanism in *Phase II*. Generally, the mechanism is thought to be driven by one of two mechanisms:

1. Limitation in the body's ability to transport oxygen to the muscles
2. Limitation in the muscles' ability to use the delivered oxygen

Some evidence collected from tests on both humans and animals suggests that oxygen utilization is the limiting factor at moderate exercise levels [Xu and Rhodes, 1999]. Dynamic changes of phosphocreatine (PCr) are generally used to monitor muscle oxygen utilization in humans. At constant ATP levels, the rate of oxygen intake in muscle, $\dot{V}_{O_2mus}$, changes with change in PCr levels. One study, conducted at 65% of $\dot{V}_{O_2max}$, showed PCr levels decrease at the beginning of

exercise. This PCr depletion has been correlated with the response time of $\dot{V}_{O_2}$. A comparison of PCr and $\dot{V}_{O_2}$ kinetics by Barstow *et al.* suggested *Phase II* $\dot{V}_{O_2}$ kinetics, PCr dynamics, and the rate of muscle oxygen utilization occur at the same rate. Tests to decrease or increase blood flow before and during exercise have have not significantly affected $\dot{V}_{O_2}$ kinetics [Xu and Rhodes, 1999].

To date, there seems to be more evidence suggesting that oxygen utilization is the limiting factor at moderate intensities, but the subject is still a matter of debate [Xu and Rhodes, 1999]. Above moderate exercise intensities, oxygen transport seems to be the limiting factor. Paterson *et al.* found that $\dot{V}_{O_2}$ is highly correlated with femoral artery blood flow during heavy-intensity, single-leg exercise [Paterson et al., 2005]. This effect may be reflected in the slow component of $\dot{V}_{O_2}$ above the lactate threshold. Many potential mechanisms for controlling the slow component have been suggested, as listed below:

- Blood lactate
- Epinephrine
- Ventilation
- Body temperature
- Type-II fiber recruitment
- Physical training

Among these factors, Type II fiber recruitment is most likely to be the limiting factor. Skeletal muscles are are composed of Type I and Type-II fibers, where Type II fibers are further categorized into Type IIa and Type IIb based on their oxidative capacity. At a given force, Type IIb fibers consume more oxygen than other muscle fiber types. Application of Type IIb fibers is proportional to exercise

intensity. Xu and Montgomery found that post-exercise $\dot{V}_{O_2}$ was significantly larger when subjects completed a 90-minute track run at 80% of their $\dot{V}_{O_2max}$ than after completing a run of the same duration at 65% of their $\dot{V}_{O_2max}$. These results were attributed partially to muscle fatigue and subsequent recruitment of Type IIb muscle fibers. Barstow *et al.* found a negative correlation between the magnitude of the slow component of $\dot{V}_{O_2}$ and the proportion of Type I muscle employed in working muscles [Xu and Rhodes, 1999].

Despite some differences at heavy intensity, $\dot{V}_{O_2}$ kinetics in children are identical to those of adults. In senior citizens, $\dot{V}_{O_2}$ kinetics are affected by the decline of cardiorespiratory function and muscle oxidative capacity. Seniors seem to exhibit different $\dot{V}_{O_2}$ limiting mechanisms depending on the size of the muscle group exercising. Furthermore, physical fitness seems to be an important factor in the $\dot{V}_{O_2}$ kinetics of senior citizens [Xu and Rhodes, 1999].

D.3 Metabolic cost of isolated joint exercise

Ogita *et al.* sought to determine why one-legged cycling requires greater oxygen uptake at submaximal intensities than two-legged cycling and to evaluate whether the peak oxygen uptake during cycling is proportional to active muscle mass. In their experiments, Ogita et al. determined that $\dot{V}_{O_2}$ increases linearly with the increase in work rate in both one- and two-legged experiments, but that $\dot{V}_{O_2}$ rose faster during one-legged studies. The peak $\dot{V}_{O_2}$ attained was higher during two-legged tests, and the difference between the one-legged and two-legged responses was attributed to the circulatory response [Ogita et al., 2000]. The oxygen uptake for a one-legged test during peak exercise was found to be approximately 80% that

of two-legged cycling. The one-legged work rate was just under two-thirds the maximum two-legged work rate. Thus, the peak $\dot{V}_{O_2}$ was not proportional to active muscle mass [Ogita et al., 2000]. Vokac *et al.* studied the difference between oxygen uptake during leg and arm exercise and investigated the relationship between the oxygen uptake and pulse. Heart rate was found to exhibit a similar trend to $\dot{V}_{O_2}$ at lower intensities. Oxygen uptake in hand-cranking did not vary significantly between standing and sitting trials [Vokac et al., 1975].

D.4 Isometric muscle contraction

Hogan *et al.* investigated the effects of varying contraction durations on metabolic energy cost and fatigue. They found that short-duration contractions had higher $\dot{V}_{O_2}$, rate of ATP utilization, energy cost, and fatigue than long-duration contractions. The energy cost (ATP utilization/developed force) of short durations was 70% greater than that of long contractions. The cost of continuous muscle work was generally proportional to the amount of work being done [Hogan et al., 1998]. De Ruiter *et al.* found that oxygen consumption was lower or isometric contractions of the knee extensors at 30° than at 60° or at 90°. Oxygen uptake at 60° and 90° was nearly identical [de Ruiter et al., 2005].

D.5 Cost of breathing

Because we will be using $\dot{V}_{O_2}$ to predict the muscle energy cost of performing work, we need an estimate of how much oxygen uptake is devoted to breathing. Aaron *et al.* helped answer this question as they researched the existence of a critical venti-

lation point in heavy exercise. Using voluntary mimicking of the transpulmonary pressure-tidal volume loop and end-expiratory lung volume produced during a previously completed progressive exercise test, Aaron et al. analyzed the oxygen cost of exercise hyperpnea (hyperventilation). At heavy exercise levels, the relative oxygen cost accounted for 10% of the $\dot{V}_{O_2}$ on average and reached as high as 13-15% in some subjects. The relative cost of hyperpnea was correlated to the absolute cost of ventilation and to the work of breathing. Results were similar to those estimated by Saltin. For moderate exercise, the oxygen cost of exercise-induced rapid breathing was 3-6% of the total $\dot{V}_{O_2}$ [Aaron et al., 1992].

D.6 Large-scale energetics

Ellerby *et al.* studied how blood flow depends on exercise intensity. Blood flow at a variety of intensities was monitored by injecting guinea fowl with 15-μm polystyrene microspheres at four levels of effort: rest, walking at 0.5 m/s, running at 1.5 m/s, and running at 90% of $\dot{V}_{O_2max}$ (2.5-2.78 m/s). Throughout the test, blood was withdrawn at a rate of 1.0-1.75 mL/min, depending on exercise intensity. After the test, the birds were euthanized. The sphere concentrations were determined, the muscle mass was measured, and hemoglobin and lactate concentration levels were measured. The tests showed that cardiac output was proportional to $\dot{V}_{O_2}$ and that blood flow to leg muscles increased linearly with $\dot{V}_{O_2}$. The flow contributions to the legs and to the heart accounted for nearly all the increase in the cardiac output. Blood flow was not evenly distributed across muscles. In fact, three groups of muscles were identified:

Group I muscles preferentially used energy at lower speeds. Their fractional contribution was decreased at greater speeds. These muscles accounted for 25% of the leg muscle mass but contributed 57% of the energy increase as the guinea fowl progressed from rest to a walk. Group I muscles were only responsible for 14% of the energy contribution when the intensity was increased from 63% of $\dot{V}_{O_2max}$ to 90% of $\dot{V}_{O_2max}$.

Group II muscles preferentially used energy at high speeds. These muscles represented 46% of the leg muscle mass and contributed 58% of the increase from a readily sustainable run to 90% of $\dot{V}_{O_2max}$. They were responsible for only 15% of the energy increase from rest to walking.

Group III muscles provided a nearly constant energy contribution across exercise intensities and accounted for 28% of leg muscle mass.

Finally, blood flow to active muscles occurred in such a way that the rate of oxygen delivery was proportional to the metabolic rate [Ellerby et al., 2005].

APPENDIX E

LABVIEW CODE

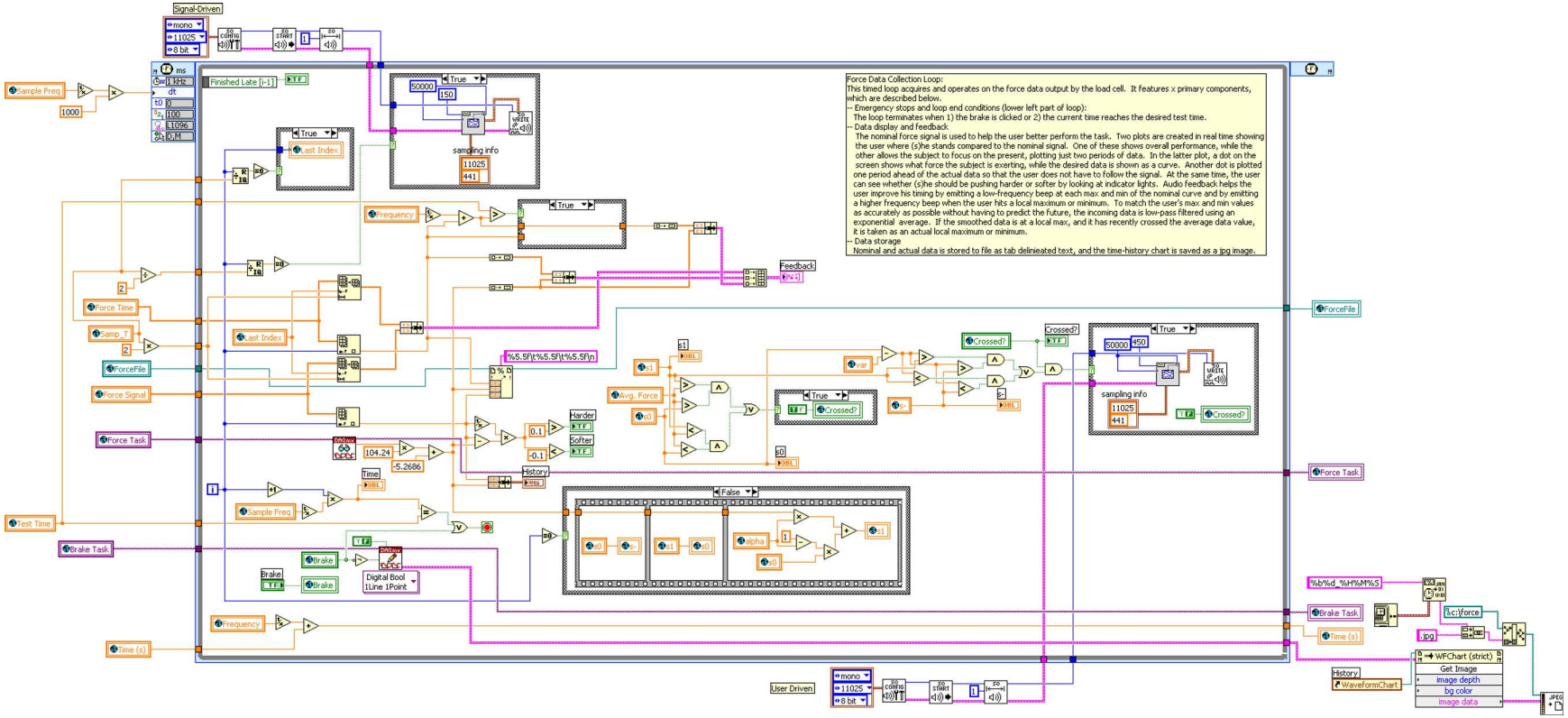

Figure E.1: LabVIEW schematic for force-tracking experiments

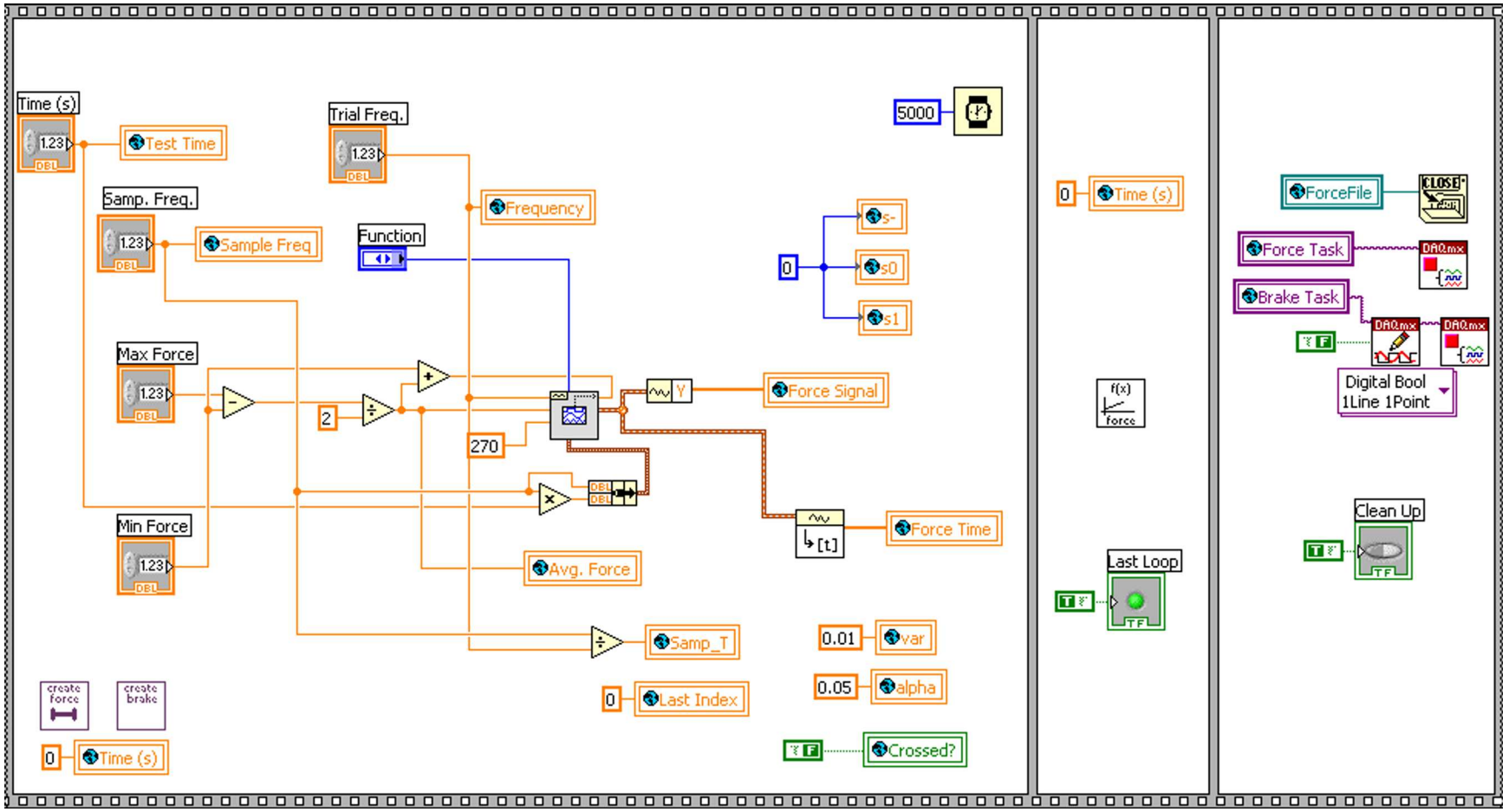

Figure E.2: LabVIEW schematic for force-tracking experiments

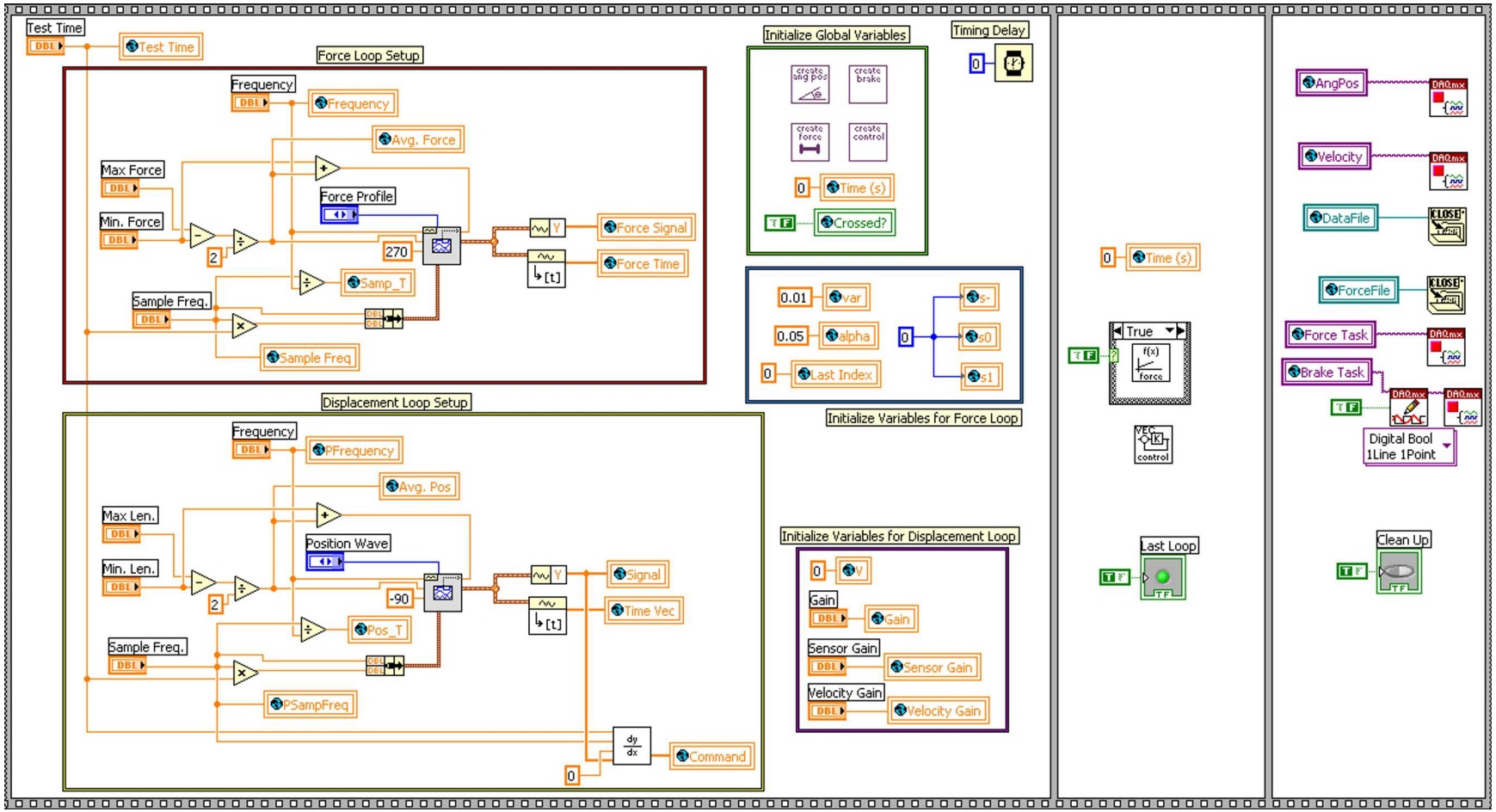

Figure E.3: LabVIEW motor control block diagram

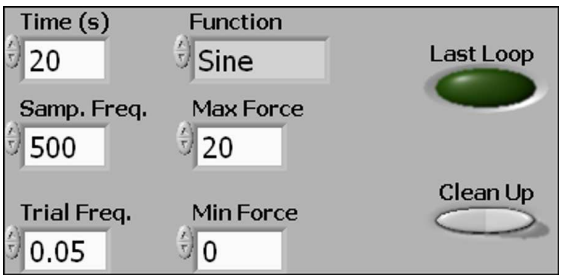

(a) Fixed-angle

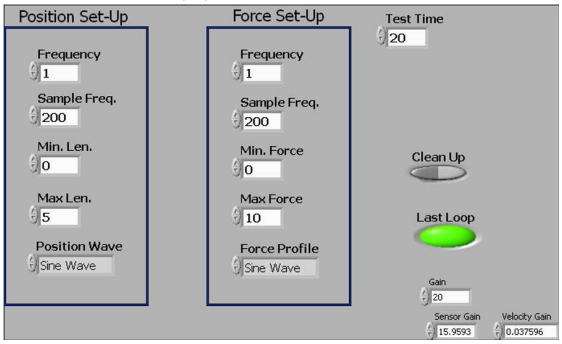

(b) Dynamic

Figure E.4: Front panel for fixed-angle and variable-angle main feedback programs.

APPENDIX F

DATA ANALYSIS CODE

Several Octave, Python, and Perl scripts were used to facilitate data processing and analysis. The key scripts are included here to expedite related endeavors.

All Octave scripts are Matlab compatible – simply replace the double quotes with single quotes, and replace any hash marks (#), which denote comments, to percent symbols (%). Also, delete the line:

```
#! /bin/octave -qf.
```

F.1 Data processing and analysis scripts

The following Octave scripts were used to separate raw data files into smaller, labeled, files.

F.1.1 Sine and triangle wave processing, fixed-angle tests

```
% Script to separate sine and triangle-wave files into individual
% curves. Finds how many full periods occur, then separates each
% period so that the maximum is centered in the file.

#! /bin/octave -qf    % Allows the file to be run from Octave

clear all;

% Import filename from the command line
x = argv();
if x
  fname = sprintf("%s",x(1));
```

```
else
  disp('Error: no command-line input given.')
    exit(1);
  num_trials = 3;
end

loadname = [fname ".csv"];            % Loadable name
fname = [fname "_"];                  % Form base for saved filename
fname_y = ["xy/complete/" fname "y.csv"];
fname_a = ["xy/complete/" fname "a.csv"];

data = load(loadname);                % Load data file

t = data(:,1);                        % Time vector
y = data(:,2) * 4.44822;              % Load cell data in Newtons
a = data(:,3) * 4.44822;              % Desired force vector in Newtons
yvec = [t y];
avec = [t a];
save("-ascii",fname_y,"yvec");
save("-ascii",fname_a,"avec");

max_a = max(a);                       % Maximum desired value
min_a = min(a);                       % Minimum desired value
avg_a = mean(a);                      % Average value

i = 1;                                % Counter
N = length(t);                        % Number of elements

% Define variables to count the number of periods
up_count = 0;
down_count = 0;

% Create vectors to store the index of each transition
up_ind(1) = 0;
down_ind(1) = 0;

% Loop over the number of elements, finding maxes and mins
for i = 1:N-1
  if a(i) >= avg_a && a(i+1) <= avg_a
    down_count = down_count + 1;
    down_ind(down_count) = i;
  end
```

```
  if a(i) <= avg_a && a(i+1) >= avg_a
    up_count = up_count + 1;
    up_ind(up_count) = i;
  end
end

% Ensure that each index ends in 1 (dumb bug fix)
for i = 1:length(up_ind)
  if mod(up_ind(i),5) == 0
    up_ind(i) = up_ind(i) + 1;
  end;
end;

for i = 1:length(down_ind)
  if mod(down_ind(i),5) == 0
    down_ind(i) = down_ind(i) + 1;
  end
end

% Average number of points between the max and the min
delta_ind = floor((up_ind(2) - down_ind(1))/2);

% Starting point index
ind = up_ind - delta_ind;

flag = 0;

% Loop over the elements, writing each period to file
% Periods are saved from min-to-min
for i = 1:length(ind)-1
  % Solve problems relating to a set ending mid-period
  if ind(i) > length(t)
    flag = 1;
    break;
  end;

  clear filename; clear data1;
  filename = [fname int2str(i) ".csv"];
  filename_y = ["xy/" fname int2str(i) "_y.csv"];
  filename_a = ["xy/" fname int2str(i) "_a.csv"];

  tnew(:,i) = t(ind(i):ind(i+1));
  tnewv(:,i) = t(ind(i):ind(i+1)) - t(ind(i));
  ynew(:,i) = y(ind(i):ind(i+1));
```

```
  anew(:,i) = a(ind(i):ind(i+1));

  data1 = [tnew(:,i) ynew(:,i) anew(:,i)];
  data1y = [tnewv(:,i) ynew(:,i)];
  data1a = [tnewv(:,i) anew(:,i)];

  save("-ascii",filename,"data1");
  save("-ascii",filename_y,"data1y");
  save("-ascii",filename_a,"data1a");
end

% If the end of the file wasn't the end of a period
% save the remaining data to file
if flag == 1
  tend = t(ind(i):length(t));
  tendv = t(ind(i):length(t)) - t(ind(i));
  yend = y(ind(i):length(t));
  aend = a(ind(i):length(t));
  data_end = [tend yend aend];
  data_endy = [tendv yend];
  data_enda = [tendv aend];

  filename = [fname int2str(i) ".csv"];
  filenamey = ["xy/" fname int2str(i) "_y.csv"];
  filenamea = ["xy/" fname int2str(i) "_a.csv"];

  save("-ascii",filename,"data_end");
  save("-ascii",filenamey,"data_endy");
  save("-ascii",filenamea,"data_enda");

  clear tend; yend; aend;
end

% Clear variables that could cause problems in later
% iterations
clear down_ind; clear up_ind; clear ind;
clear tnew; ynew; anew;
```

F.1.2 Sine and triangle wave analysis, fixed-angle tests

```
% Megan Thompson
```

```
% Last Revised: 7/17/07

% Script to analyze sine wave data.
% Determines lead/lag for rise and fall of sine wave
% Calculates average error

% Starting data consists of systematically named data files,
% each file representing one square wave.

% Files are assumed to be named as shown:
% sin_XXpct_FREQ_TRIALNUM_WAVENUM.csv
% tri_XXpct_FREQ_TRIALNUM_WAVENUM.csv

% Also work for triangle waves

#! /bin/octave -qf

clear all

% Import file name from the command line
x = argv();

if(x)
  disp("Received command line input.")
  fname = sprintf("%s",x(1));

else
  disp("No command line input.")
  exit(1)
end

filename = [fname "data.csv"];       % Saves calculated values
lagname = ["lag/" fname "lag.csv"];  % Saves lag data
aerrname = [fname "abs_err.csv"];    % Saves the absolute error.
perrname = [fname "pct_err.csv"];    % Saves the pct. error

fname = [fname ".csv"];              % File to be loaded
data = load(fname);

t = data(:,1) - data(1,1);           % Time
y = data(:,2);                       % Data
a = data(:,3);                       % Target

N = length(t);
```

```
y_avg = mean(y);
a_avg = mean(a);

ycounter = 0;
acounter = 0;

% Loop over the data, finding points where the curve crosses
% the halfway point
for i = 2:(N-1)
  if ((y(i-1) > y_avg && y(i+1) < y_avg)
     || (y(i-1) < y_avg && y(i+1) > y_avg))
     ycounter = ycounter + 1;
     y_ind_cross(ycounter) = i;
  end

  if ((a(i-1) > a_avg && a(i+1) < a_avg)
     || (a(i-1) < a_avg && a(i+1) > a_avg))
    acounter = acounter + 1;
    a_ind_cross(acounter) = i;
  end
end

N_half = floor(N/2); % Index of halfway point in the data

sum_y_ind0 = 0;
sum_y_indf = 0;
num_below = 0;
num_above = 0;

% Average crossover points to get a representative midpoint
for i = 1:length(y_ind_cross)
  if y_ind_cross(i) < N_half
     sum_y_ind0 = sum_y_ind0 + y_ind_cross(i);
     num_below = num_below + 1;
  else
    sum_y_indf = sum_y_indf + y_ind_cross(i);
    num_above = num_above + 1;
  end
end

% Find the index of the mean crossing point.
% If there is no crossing point, set the index to 1.
if num_below > 0
```

```
   i_cross_low_y = floor(sum_y_ind0 / num_below);
else
   i_cross_low_y = 1;
end

if num_above > 0
   i_cross_high_y = floor(sum_y_indf / num_above);
else
   i_cross_high_y = 1;
end

num_below = 0;
num_above = 0;
sum_a_ind0 = 0;
sum_a_indf = 0;

for i = 1:length(a_ind_cross)
  if a_ind_cross(i) < N_half
     sum_a_ind0 = sum_a_ind0 + a_ind_cross(i);
     num_below = num_below + 1;
  else
     sum_a_indf = sum_a_indf + a_ind_cross(i);
     num_above = num_above + 1;
  end
end

if num_below > 0
   i_cross_low_a = floor(sum_a_ind0 / num_below);
else
   i_cross_low_a = 1;
end

if num_above > 0
   i_cross_high_a = floor(sum_a_indf / num_above);
else
   i_cross_high_a = 1;
end

% Find crossing lag.  If there was no crossing point, set lag to -1
if i_cross_low_a > 0 && i_cross_low_y > 0
   tlag_rise = t(i_cross_low_a) - t(i_cross_low_y);
else
   tlag_rise = -1;
end
```

```
if i_cross_high_a > 0 && i_cross_high_y > 0
   tlag_fall = t(i_cross_high_a) - t(i_cross_high_y);
else
   tlag_fall = -1;
end

% Calculate error
for i = 1:N
    abs_err(i) = a(i) - y(i);
    pct_err(i) = abs_err(i) / a(i) * 100;
end

% Save newly computed data
vlag = [tlag_rise tlag_fall];
vabs_err = [t abs_err'];
vpct_err = [t pct_err'];

save("-ascii",lagname,"vlag");
save("-ascii",aerrname,"vabs_err");
save("-ascii",perrname,"vpct_err");
```

F.1.3 Square wave processing, fixed-angle tests

```
% Script to separate square waves into individual curves.
% Finds how many full periods occur, then separates each period
% so that the square wave is centered in each file.
#! /bin/octave -qf

clear all;
x = argv();
if x
  fname = sprintf("%s",x(1));
else
  disp('No command-line input.')
  exit(1);
end

loadname = [fname ".csv"];
fname = [fname "_"];
```

```
data = load(loadname);

t = data(:,1);
y = data(:,2) * 4.44822;
a = data(:,3) * 4.44882;
max_a = max(a);
min_a = min(a);

whole_a = [t a];
whole_y = [t y];
wholename_a = ["xy/complete/" fname "a.csv"];
wholename_y = ["xy/complete/" fname "y.csv"];
save("-ascii",wholename_a,"whole_a");
save("-ascii",wholename_y,"whole_y");

up_count = 0;
down_count = 0;
up_ind(1) = 0;
down_ind(1) = 0;

i = 1;

N = length(t);

for i = 1:N-1
  if a(i) == max_a && a(i+1) == min(a)
    down_count = down_count + 1;
    down_ind(down_count) = i;
  end

  if a(i) == min_a && a(i+1) == max(a)
    up_count = up_count + 1;
    up_ind(up_count) = i;
  end
end

nfile = min(up_count,down_count);

for i = 1:length(down_ind)
  if mod(down_ind(i),5) == 0
    down_ind(i) = down_ind(i) + 1;
  end;
end
```

```
for i = 1:length(up_ind)
  if mod(up_ind(i),5) == 0
    up_ind(i) = up_ind(i) + 1;
  end;
end;

delta_ind = (up_ind(2) - down_ind(1))/2;

ind = down_ind + delta_ind;

tnew(:,1) = t(1:ind(1)) - t(1);
ynew(:,1) = y(1:ind(1));
anew(:,1) = a(1:ind(1));

data_new = [tnew ynew anew];
data_newy = [tnew ynew];
data_newa = [tnew anew];

filename_start = [fname int2str(1) ".csv"];
filename_start_y = ["xy/" fname int2str(1) "_y.csv"];
filename_start_a = ["xy/" fname int2str(1) "_a.csv"];

save("-ascii",filename_start,"data_new");
save("-ascii",filename_start_y,"data_newy");
save("-ascii",filename_start_a,"data_newa");

i = 2;
flag = 0;

for i = 2:length(ind)
  if ind(i) > length(t)
    flag = 1;
    break;
  end;

  clear filename; clear data1;
  filename = [fname int2str(i) ".csv"];
  filenamey = ["xy/" fname int2str(i) "_y.csv"];
  filenamea = ["xy/" fname int2str(i) "_a.csv"];

  tnew(:,i) = t(ind(i-1):ind(i)) - t(ind(i-1));
  ynew(:,i) = y(ind(i-1):ind(i));
  anew(:,i) = a(ind(i-1):ind(i));
  data1 = [tnew(:,i) ynew(:,i) anew(:,i)];
```

```
  newy = [tnew(:,i) ynew(:,i)];
  newa = [tnew(:,i) anew(:,i)];

  save("-ascii",filename,"data1");
  save("-ascii",filenamey,"newy");
  save("-ascii",filenamea,"newa");
end

if flag == 1
  tend = t(ind(i-1):length(t)) - t(ind(i-1));
  yend = y(ind(i-1):length(t));
  aend = a(ind(i-1):length(t));
  data_end = [tend yend aend];
  data_end_y = [tend yend];
  data_end_a = [tend aend];

  filename = [fname int2str(i) ".csv"];
  filename_y = ["xy/" fname int2str(i) "_y.csv"];
  filename_a = ["xy/" fname int2str(i) "_a.csv"];

  save("-ascii",filename,"data_end");
  save("-ascii",filename_y,"data_end_y");
  save("-ascii",filename_a,"data_end_a");
end

clear tnew; clear ynew; clear anew;
clear tend; clear yend; clear aend;
clear newy; clear newa;
clear up_ind; clear down_ind; clear ind;
```

F.1.4 Square wave analysis, fixed-angle tests

```
# Megan Thompson
# Last Revised: 7/5/07

# Script to analyze square wave data.
# Determines lead/lag for rise and fall of square wave
# Finds average for high and low phases plus std. dev
# Calculates average error
# Determines rise time, fall time, and settling time
```

```
# Starting data consists of systematically named data files,
# each file representing one square wave.

# Files are assumed to be named as shown:
# square_XXpct_FREQ_TRIALNUM_WAVENUM.csv

#! /bin/octave -qf

clear all

x = argv();

if(x)
  disp("Received command line input.")
  fname = sprintf("#s",x(1));
  tbuffstring = sprintf("#s",x(2));
  tbuffer = str2num(tbuffstring);

else
  disp("No command line input.")
  exit(1);
end

filename = ["data/" fname "data.csv"]; # Saves calculated values
rplotname = ["xy/" fname "rplot.csv"]; # Saves rise portion
eplotname = ["xy/" fname "eplot.csv"]; # Saves fall portion

fname = [fname ".csv"];            # File to be loaded

data = load(fname);                # Load current data set

t = data(:,1);                     # Time data
y = data(:,2);                     # Recorded force data
a = data(:,3);                     # Desired curve

i = 1;                             # Counter index
N = length(t);                     # End-point index

tlow0 = 0;                         # Transition time for rise

# Using desired curve, find transition index from low-to-high
while a(i) == min(a)
  i = i + 1;
end
```

```
t_low0 = t(i) - t(1);              # Duration of low period
ind_trans1 = i;                    # Index of transition

# Using desired curve, find transition index from high-to-low
while a(i) == max(a)
  i = i + 1;
end

t_high = t(i) - t_low0;            # Duration of high period
ind_trans2 = i;                    # Index of second transition
t_low1 = t(length(t)) - t(i);      # Duration of ending low period

dt_low_on = tbuffer;               # Before initial averaging
dt_low_off = t_low0 - tbuffer;     # Stop initial averaging
dt_high_on = t_low0 + tbuffer;     # Start rise averaging
dt_high_off = t(i) - tbuffer - t(1); # Stop rise averaging
dt_low2_on = t(i) + tbuffer - t(1);  # Start fall averaging
dt_low2_off = t(length(t)) - tbuffer - t(1); #Stop fall avging

T_samp = t(2) - t(1);              # Sampling time

# Find indices relating to averaging periods
Tlow_init = floor(dt_low_on / T_samp);
Tlow_end = floor(dt_low_off / T_samp);

Thigh_init = floor(dt_high_on / T_samp);
Thigh_end = floor(dt_high_off / T_samp);

Tlow2_init = floor(dt_low2_on / T_samp);
Tlow2_end = floor(dt_low2_off / T_samp);

# Find average and standard deviations for low and high periods
avgLow = mean(y(Tlow_init:Tlow_end));
sdLow = std(y(Tlow_init:Tlow_end));
sdLow_pct = sdLow / avgLow * 100;

avgHigh = mean(y(Thigh_init:Thigh_end));
sdHigh = std(y(Thigh_init:Thigh_end));
sdHigh_pct = sdHigh / avgHigh * 100;

avgLow2 = mean(y(Tlow2_init:Tlow2_end));
sdLow2 = std(y(Tlow2_init:Tlow2_end));
sdLow2_pct = sdLow2 / avgLow2 * 100;
```

```
# Find maximum force attained and corresponding overshoot
maxHigh = max(y);
overshoot = (max(y) - max(a)) / max(a) * 100;

# Average of trial high and low segments
waveAvg = 0.5*(avgLow + avgHigh);

# Find first transition in data
i = 1;
while y(i) < waveAvg
  i = i + 1;
end

Ttrans1 = t(i);

# Find second  transition in data
i = Thigh_end;
while y(i) > waveAvg
  i = i + 1;
  if i == length(y)
    break;
  end;
end

Ttrans2 = t(i);

# Calculate error for high and low phases
high_err = max(a) - avgHigh;
high_pct_err = high_err / max(a) * 100;

low_err = min(a) - avgLow;
low_pct_err = low_err / min(a) * 100;

# Find lead/lag between actual data and desired curve
start_lag = t(ind_trans1) - Ttrans1;
end_lag = t(ind_trans2) - Ttrans2;

# Find settling time (not a good algorithm)
# Simply starts with maximum piont and iterates until
# current data point is less than the sum of the average
# high value and the standard deviation
i = 1;
while y(i) < max(y)
```

```
  i = i + 1;
  if i == length(y)
    disp('t_settle error at line 154');
    break;
  end
end

t1 = t(i);

while y(i) > avgHigh + sdHigh
  i = i + 1;
  if i == length(y)
    disp('t_settle error at line 164');
    break;
  end
end

t_settle = t(i) - t1;

# Find rise and fall time, trying to avoid local min/maxes
i = Tlow_end - Tlow_init;

if i <= 1;
  i = 2;
end;

while y(i) < (avgLow + 2*sdLow)
  i = i + 1;
end

avgLow
t_st_rise = t(i-1)
y_st_rise = y(i-1)
i_st_rise = i-1;

while y(i) < avgHigh
  i = i + 1;
end;

t_end_rise = t(i);
y_end_rise = y(i);
i_end_rise = i;

T_rise = t_end_rise - t_st_rise;
```

```
i = Thigh_end;
while y(i) > (avgHigh - 2*sdHigh)
  i = i + 1;
  if i == length(y)
    disp('Error at line 204')
    break;
  end;
end

t_st_fall = t(i);
y_st_fall = y(i);
i_st_fall = i;

while y(i) > avgLow2
  i = i + 1;
  if i == length(y)
    disp('Error at line 216.')
    break;
  end
end

t_end_fall = t(i);
y_end_fall = y(i);
i_end_fall = i;

T_fall = t_end_fall - t_st_fall;

# Plot waves with rise/fall data highlighted
#    plot(t,y); hold on;
#    plot(t,a);
#    plot(t(i_st_rise:i_end_rise),y(i_st_rise:i_end_rise),'b');
#    plot(t(i_st_fall:i_end_fall),y(i_st_fall:i_end_fall),'c');
#    pause(1);

# Save rising and falling data to file so it can be plotted externally
st_plot_data = [t(i_st_rise:i_end_rise) y(i_st_rise:i_end_rise)];
end_plot_data = [t(i_st_fall:i_end_fall) y(i_st_fall:i_end_fall)];

save("-ascii", rplotname, "st_plot_data");
save("-ascii", eplotname, "end_plot_data");

# Write data to file for later review
fref = fopen(filename,'a');
```

```
# The file referred to by fref (data/name.csv) will contain:
  # Rise lag (s): Duration between rising midpoints
  # Low average (N): Average force during the initial low phase
  # Low std. dev (N): Standard deviation of low phase
  # Low std. dev pct (percent): std. dev / average * 100
  # Pct. error (low): Error between desired and actual values

  # Fall lag (s):
  # High average (N):
  # High std. dev (N):
  # High std. dev pct (percent):
  # Pct. error (high):

  # Overshoot (percent):
  #    Overshoot between max actual and desired high point
  # Settling time (s):
  #    Time from max to average high value
  # Rise time (s):
  #    Time to transition from low to high
  # Fall time (s):
  #    Time to transition from high to low

fprintf(fref, 'Rise lag:\t%2.5f\nLow average:
        \t%2.5f\nLow std. dev:
        \t%2.5f\nLow std. dev pct: \t%2.5f\n
        Pct. Error (Low): \t%2.2f\n',start_lag,avgLow,
        sdLow,sdLow_pct,low_pct_err);

fprintf(fref,'\nFall lag: \t%2.5f\nHigh average:
        \t%2.5f\nHigh std. dev: \t%2.5f
        \nHigh std. dev pct.: \t%2.5f
        \nPct. Error (High): \t%2.2f\n',
        end_lag,avgHigh,sdHigh,sdHigh_pct,high_pct_err);

fprintf(fref,'\nOvershoot:\t%2.2f\nSettling Time
        \t%2.5f\nRise Time:\t%2.5f\nFall Time:
        \t%2.5f\n',overshoot,t_settle,T_rise,T_fall);

fclose(fref);
```

F.1.5 Dynamic wave processing and analysis

```
% Script to process and analyze data recorded from dynamics
% force-matching attempts

#! /bin/octave -qf

clear all

x = argv();

if (x)
  fname = sprintf("%s",x(1));
  % fname will be of the form xxN_yyyHz_z
  % where the x represent load
  %           y represent freq*1000
  %           z represent trial num
  T_cut = str2num(sprintf("%s",x(2))); % Time to shave off wave data

else
  disp("Error: No command line input.")
  exit(1);
end

% Input files
force_name = [fname ".csv"];
pos_name = [fname "p.csv"];

% Output files
fy_name = ["xy/" fname "_y.csv"];   % Recorded force
fa_name = ["xy/" fname "_a.csv"];   % Desired force
py_name = ["xy/" fname "_py.csv"];  % Recorded position
pa_name = ["xy/" fname "_pa.csv"];  % Desired position

ferr_name = ["err/" fname "_err.csv"];  % Force error
perr_name = ["err/" fname "_perr.csv"]; % Position error

fstat_name = ["stats/" fname "_fstats.csv"];   % Force stats
festat_name = ["stats/" fname "_festats.csv"]; % Force err stats
pestat_name = ["stats/" fname "_pestats.csv"]; % Pos err stats

% Load data files
force_data = load(force_name);
```

```
pos_data = load(pos_name);

% Break data into vectors
t_f_all = force_data(:,1);
y_f_all = force_data(:,2);
a_f_all = force_data(:,3);

t_p_all = pos_data(:,1);
y_p_all = pos_data(:,2);
a_p_all = pos_data(:,3);

% Trim data to include only the middle 20 sec.
dt_force = floor(1/t_f_all(2));
dt_pos = floor(1/t_p_all(2));

Nf = length(t_f_all);
Np = length(t_p_all);

f_ind0 = dt_force * T_cut + 1;
f_indf = Nf - (dt_force * T_cut) + 1;
p_ind0 = dt_pos * T_cut + 1;
p_indf = Np - (dt_pos * T_cut) + 1;

t_f = t_f_all(f_ind0:f_indf);
y_f = y_f_all(f_ind0:f_indf);
a_f = a_f_all(f_ind0:f_indf);

t_p = t_p_all(p_ind0:p_indf);
y_p = y_p_all(p_ind0:p_indf);
a_p = a_p_all(p_ind0:p_indf);

% Calculate percent error
% f_error = (a_f - y_f) ./ a_f * 100;
f_error = (a_f - y_f);
p_error = (a_p - y_p);

% Calculate statistics
f_stats = statistics(y_f);
p_err_stats = statistics(p_error);
f_err_stats = statistics(f_error);

fy_data = [t_f y_f];
fa_data = [t_f a_f];
py_data = [t_p y_p];
```

```
pa_data = [t_p a_p];

f_err_data = [t_f f_error];
p_err_data = [t_p p_error];

f_stats_data = [f_stats(3) f_stats(4) f_stats(2) f_stats(5)
                f_stats(1)];
p_stats_data = [p_err_stats(3) p_err_stats(4) p_err_stats(2)
                p_err_stats(5) p_err_stats(1)];
fe_stats_data = [f_err_stats(3) f_err_stats(4) f_err_stats(2)
                 f_err_stats(5) f_err_stats(1)];

save("-ascii", fy_name, "fy_data");
save("-ascii", fa_name, "fa_data");
save("-ascii", py_name, "py_data");
save("-ascii", pa_name, "pa_data");

save("-ascii", ferr_name, "f_err_data");
save("-ascii", perr_name, "p_err_data");

save("-ascii", fstat_name, "f_stats_data");
save("-ascii", festat_name, "fe_stats_data");
save("-ascii", pestat_name, "p_stats_data");
```

F.1.6 Script to compile statistical information from the data

```
clear all;

x = argv();

if(x)
  fname = sprintf("%s",x(1));

else
  disp("Error: no command line input.");
  exit(1);
end
```

```
statname = ["stats/" fname "_stats.csv"];
filename = [fname "pct_err.csv"];

data = load(filename);
y = data(:,2);

stats = statistics(y);

fref = fopen(statname,'a');
for i = 1:9
  fprintf(fref,'%f6\t',stats(i));
end

fprintf(fref,'\n');
fclose(fref);
```

F.2 Python scripts used to automate processing

These short Python scripts can be run from the shell of a Linux system or emulator, decreasing the time and effort required to process and analyze the data using the Octave scripts.

F.2.1 Fixed-Angle data processing automation

```
import os, os.path, sys

for fname in sys.argv[1:]:
    print 'Executing loop body'
    wave = fname.split('_')[0]
    trial1 = fname.split('_')[-1]
    midname = fname.split('_')[1]
    freqname = fname.split('_')[2]
    trial = trial1[0].split('\w')[0]

    octname = wave + '_' +  midname + '_' + freqname + '_' + trial
```

```
    if wave == 'square':
        print 'Executing square script.'
        print octname
        os.system('octave --silent ~/data/sq_process_metric.m %s %s'
                  % (octname,fname))
    elif wave in ('sin','tri'):
        print 'Executing sin/tri script'
        print octname
        os.system('octave --silent ~/data/sin_process_metric.m %s %s'
                  % (octname,fname))
    else:
        raise Exception('Bad filename')
```

F.2.2 Fixed-Angle data analysis automation

```
import os, os.path, sys

for fname in sys.argv[1:]:
    print 'Executing loop body:'
    wave = fname.split('_')[0]
    octname = str(fname.split('.')[0])
    freqname = fname.split('_')[2]

    if freqname == '5hundredth':
        t_var = '0.5';
    elif freqname == 'tenth':
        t_var = '0.33';
    elif freqname == 'quarter':
        t_var = '0.25';
    elif freqname == 'one':
        t_var = '0.1';
    else:
        t_var = '0.05';

    if wave == 'square':
        print "Executing Square Script."
        print octname
        print freqname
        os.system('octave --silent ~/data/sq_anal_metric.m %s %s'
                  % (octname,t_var))
    elif wave in ('sin','tri'):
```

```
        print "Executing Sin/Tri Script."
        print octname
        print freqname
        os.system('octave --silent ~/data/sin_anal_metric.m %s %s'
                  % (octname,t_var))
    else:
        raise Exception('Bad filename')
```

F.2.3 Sort and compile square-wave data

```
import os, os.path, sys

alldata = open('compiled/all.csv','a')

# Effort-based files
eff25data = open('compiled/eff25.csv','a')
eff33data = open('compiled/eff33.csv','a')
eff50data = open('compiled/eff50.csv','a')
eff66data = open('compiled/eff66.csv','a')

# Frequency-based files
freq5hundredthdata = open('compiled/freq_5hund.csv','a')
freqtenthdata = open('compiled/freq_tenth.csv','a')
freqquarterdata = open('compiled/freq_quarter.csv','a')
freqhalfdata = open('compiled/freq_half.csv','a')
freqonedata = open('compiled/freq_one.csv','a')
freqtwodata = open('compiled/freq_two.csv','a')

# Trial-based files
trial1data = open('compiled/trial1.csv','a')
trial2data = open('compiled/trial2.csv','a')
trial3data = open('compiled/trial3.csv','a')
trial4data = open('compiled/trial4.csv','a')

# Wave-based files
sindata = open('compiled/sin_data.csv','a')
tridata = open('compiled/tri_data.csv','a')
sqdata = open('compiled/sq_data.csv','a')

for fname in sys.argv[1:]:
    f = open(fname,'r');
```

```
currentline = f.readline();
wave = fname.split('_')[0]
effort1 = fname.split('_')[1]
freq = fname.split('_')[2]
trial = fname.split('_')[3]
lastbit = fname.split('_')[-1]
wavenum1 = lastbit.split('lag')[0]
effort = effort1.split('pct')[0]

alldata.write(currentline);

if effort == '25':
    eff25data.write(currentline);
elif effort == '33':
    eff33data.write(currentline);
elif effort == '50':
    eff50data.write(currentline);
else:
    eff66data.write(currentline);

if wave == 'sin':
    sindata.write(currentline);
elif wave == 'tri':
    tridata.write(currentline);
else:
    sqdata.write(currentline);

if trial == '1':
    trial1data.write(currentline);
elif trial == '2':
    trial2data.write(currentline);
elif trial == '3':
    trial3data.write(currentline);
else:
    trial4data.write(currentline);

if freq == '5hundredth':
    freq5hundredthdata.write(currentline);
elif freq == 'tenth':
    freqtenthdata.write(currentline);
elif freq == 'quarter':
    freqquarterdata.write(currentline);
elif freq == 'half':
    freqhalfdata.write(currentline);
```

```
    elif freq == 'one':
        freqonedata.write(currentline);
    else:
        freqtwodata.write(currentline);

    f.close();

# Close open data files
eff25data.close();
eff33data.close();
eff50data.close();
eff66data.close();
freq5hundredthdata.close()
freqtenthdata.close()
freqquarterdata.close()
freqhalfdata.close()
freqonedata.close()
freqtwodata.close()
trial1data.close()
trial2data.close()
trial3data.close()
trial4data.close()
sindata.close()
tridata.close()
sqdata.close()
alldata.close()
```

F.2.4 Run the error analysis script

```
import os, os.path, sys

for fname in sys.argv[1:]:
    filename = fname.split('pct_err')[0];
    os.system('octave --silent ~/data/erranal.m %s' % (filename))
```

F.2.5 Run the dynamic processing and analysis script

```
import os, os.path, sys
```

```
for fname in sys.argv[1:-1]:
    filename = fname.split('.')[0];
    print 'Processing ' + filename
    T_cut = sys.argv[-1];
    os.system('octave --silent ~/dyndata/process_constant.m %s %s'
              % (filename,T_cut))
```

F.2.6 Dynamic results sorting script

```
import os, os.path, sys, re

for fname in sys.argv[1:]:
    force1 = fname.split('_')[0];
    force = force1.split('N')[0];
    freq1 = fname.split('_')[1];
    freq = freq1.split('Hz')[0];
    trial = fname.split('_')[2];
    stype1 = fname.split('_')[3];
    stype = stype1.split('.csv')[0];

    f = open(fname,'r');

    stat_data = f.readline();
    stat_data = stat_data.strip();

    freq_x = str(float(freq) * 0.01);

    force_name = 'processed/' + stype + '/force.csv';
    freq_name = 'processed/' + stype + '/freq.csv';
    trial_name = 'processed/' + stype + '/trial.csv';

    fo_name = 'processed/' + stype + '/force_' + fname;
    fr_name = 'processed/' + stype + '/freq_' + fname;
    tr_name = 'processed/' + stype + '/trial_' + fname;

    w_force = open(force_name,'a');
    w_freq = open(freq_name,'a');
    w_trial = open(trial_name,'a');

    w_fo = open(fo_name,'a');
```

```
    w_fr = open(fr_name,'a');
    w_tr = open(tr_name,'a');

    force_str = force + ' ' + stat_data + '\n';
    freq_str = freq_x + ' ' + stat_data + '\n';
    trial_str = trial + ' ' + stat_data + '\n';

    w_force.write(force_str);
    w_freq.write(freq_str);
    w_trial.write(trial_str);

    w_fo.write(force_str);
    w_fr.write(freq_str);
    w_tr.write(trial_str);

    w_force.close();
    w_freq.close();
    w_trial.close();

    w_fo.close();
    w_fr.close();
    w_tr.close();
    f.close();
```

F.2.7 Compile dynamic results to find the effects of increasing forcing frequency

```
freq_compressed = open('freq_compiled.csv','a');
fname = open('freq.csv','r');

f025mean = 0;
f050mean = 0;
f100mean = 0;

f025min = 0;
f050min = 0;
f100min = 0;

f025max = 0;
```

```
f050max = 0;
f100max = 0;

f025q1 = 0;
f050q1 = 0;
f100q1 = 0;

f025q3 = 0;
f050q3 = 0;
f100q3 = 0;

f025count = 0;
f050count = 0;
f100count = 0;

for line in fname:
    currentline = line;
    data = currentline.split(' ');
    freq = float(data[0]);
    if freq == .25:
        f025mean = f025mean + float(data[1]);
        f025q3 = f025q3 + float(data[2]);
        f025q1 = f025q1 + float(data[3]);
        f025max = f025max + float(data[4]);
        f025min = f025min + float(data[5]);
        f025count = f025count + 1;
    if freq == .50:
        f050mean = f050mean + float(data[1]);
        f050q3 = f050q3 + float(data[2]);
        f050q1 = f050q1 + float(data[3]);
        f050max = f050max + float(data[4]);
        f050min = f050min + float(data[5]);
        f050count = f050count + 1;
    if freq == 1.00:
        f100mean = f100mean + float(data[1]);
        f100q3 = f100q3 + float(data[2]);
        f100q1 = f100q1 + float(data[3]);
        f100max = f100max + float(data[4]);
        f100min = f100min + float(data[5]);
        f100count = f100count + 1;

f025flag = 0;
f050flag = 0;
f100flag = 0;
```

```
if f025count > 0:
    f025mean = f025mean / f025count;
    f025q3 = f025q3 / f025count;
    f025q1 = f025q1 / f025count;
    f025max = f025max / f025count;
    f025min = f025min / f025count;
    f025flag = 1;

if f050count > 0:
    f050mean = f050mean / f050count;
    f050q3 = f050q3 / f050count;
    f050q1 = f050q1 / f050count;
    f050max = f050max / f050count;
    f050min = f050min / f050count;
    f050flag = 1;

if f100count > 0:
    f100mean = f100mean / f100count;
    f100q3 = f100q3 / f100count;
    f100q1 = f100q1 / f100count;
    f100max = f100max / f100count;
    f100min = f100min / f100count;
    f100flag = 1;

if f025flag == 1:
    L1str = '0.25 ' + str(f025mean) + ' ' + str(f025q3) + ' '
                    + str(f025q1) + ' ' + str(f025max) + ' '
                    + str(f025min) + '\n';
    freq_compressed.write(L1str);

if f050flag == 1:
    L2str = '0.50 ' + str(f050mean) + ' ' + str(f050q3) + ' '
                    + str(f050q1) + ' ' + str(f050max) + ' '
                    + str(f050min) + '\n';
    freq_compressed.write(L2str);

if f100flag == 1:
    L3str = '1.00 ' + str(f100mean) + ' ' + str(f100q3) + ' '
                    + str(f100q1) + ' ' + str(f100max) + ' '
                    + str(f100min) + '\n';
    freq_compressed.write(L3str);

freq_compressed.close();
```

```
fname.close();
```

F.2.8 Compile dynamic results to find the effects of increasing target frequency

```
ffreq_compressed = open('ffreq_compiled.csv','a');
fname = open('ffreq.csv','r');

f025mean = 0;
f050mean = 0;

f025min = 0;
f050min = 0;

f025max = 0;
f050max = 0;

f025q1 = 0;
f050q1 = 0;

f025q3 = 0;
f050q3 = 0;

f025count = 0;
f050count = 0;

for line in fname:
    currentline = line;
    data = currentline.split(' ');
    ffreq = float(data[0]);
    if ffreq == .25:
        f025mean = f025mean + float(data[1]);
        f025q3 = f025q3 + float(data[2]);
        f025q1 = f025q1 + float(data[3]);
        f025max = f025max + float(data[4]);
        f025min = f025min + float(data[5]);
        f025count = f025count + 1;
    if ffreq == .50:
        f050mean = f050mean + float(data[1]);
```

```
        f050q3 = f050q3 + float(data[2]);
        f050q1 = f050q1 + float(data[3]);
        f050max = f050max + float(data[4]);
        f050min = f050min + float(data[5]);
        f050count = f050count + 1;

f025flag = 0;
f050flag = 0;


if f025count > 0:
    f025mean = f025mean / f025count;
    f025q3 = f025q3 / f025count;
    f025q1 = f025q1 / f025count;
    f025max = f025max / f025count;
    f025min = f025min / f025count;
    f025flag = 1;

if f050count > 0:
    f050mean = f050mean / f050count;
    f050q3 = f050q3 / f050count;
    f050q1 = f050q1 / f050count;
    f050max = f050max / f050count;
    f050min = f050min / f050count;
    f050flag = 1;

if f025flag == 1:
    L1str = '0.25 ' + str(f025mean) + ' ' + str(f025q3) + ' '
                    + str(f025q1) + ' ' + str(f025max) + ' '
                    + str(f025min) + '\n';
    ffreq_compressed.write(L1str);

if f050flag == 1:
    L2str = '0.50 ' + str(f050mean) + ' ' + str(f050q3) + ' '
                    + str(f050q1) + ' ' + str(f050max) + ' '
                    + str(f050min) + '\n';
    ffreq_compressed.write(L2str);

ffreq_compressed.close();
fname.close();
```

F.2.9 Compile dynamic results to find the effects of learning

```
trial_compressed = open('trial_compiled.csv','a');
fname = open('trial.csv','r');

tr1mean = 0;
tr2mean = 0;
tr3mean = 0;
tr4mean = 0;
tr5mean = 0;

tr1min = 0;
tr2min = 0;
tr3min = 0;
tr4min = 0;
tr5min = 0;

tr1max = 0;
tr2max = 0;
tr3max = 0;
tr4max = 0;
tr5max = 0;

tr1q1 = 0;
tr2q1 = 0;
tr3q1 = 0;
tr4q1 = 0;
tr5q1 = 0;

tr1q3 = 0;
tr2q3 = 0;
tr3q3 = 0;
tr4q3 = 0;
tr5q3 = 0;

tr1count = 0;
tr2count = 0;
tr3count = 0;
tr4count = 0;
tr5count = 0;
```

```
for line in fname:
    currentline = line;
    data = currentline.split(' ');
    trial = float(data[0]);
    if trial == 1:
        tr1mean = tr1mean + float(data[1]);
        tr1q3 = tr1q3 + float(data[2]);
        tr1q1 = tr1q1 + float(data[3]);
        tr1max = tr1max + float(data[4]);
        tr1min = tr1min + float(data[5]);
        tr1count = tr1count + 1;

    if trial == 2:
        tr2mean = tr2mean + float(data[1]);
        tr2q3 = tr2q3 + float(data[2]);
        tr2q1 = tr2q1 + float(data[3]);
        tr2max = tr2max + float(data[4]);
        tr2min = tr2min + float(data[5]);
        tr2count = tr2count + 1;

    if trial == 3:
        tr3mean = tr3mean + float(data[1]);
        tr3q3 = tr3q3 + float(data[2]);
        tr3q1 = tr3q1 + float(data[3]);
        tr3max = tr3max + float(data[4]);
        tr3min = tr3min + float(data[5]);
        tr3count = tr3count + 1;

    if trial == 4:
        tr4mean = tr4mean + float(data[1]);
        tr4q3 = tr4q3 + float(data[2]);
        tr4q1 = tr4q1 + float(data[3]);
        tr4max = tr4max + float(data[4]);
        tr4min = tr4min + float(data[5]);
        tr4count = tr4count + 1;

    if trial == 5:
        tr5mean = tr5mean + float(data[1]);
        tr5q3 = tr5q3 + float(data[2]);
        tr5q1 = tr5q1 + float(data[3]);
        tr5max = tr5max + float(data[4]);
        tr5min = tr5min + float(data[5]);
        tr5count = tr5count + 1;
```

```
tr1mean = tr1mean / tr1count;
tr1q3 = tr1q3 / tr1count;
tr1q1 = tr1q1 / tr1count;
tr1max = tr1max / tr1count;
tr1min = tr1min / tr1count;

tr2mean = tr2mean / tr2count;
tr2q3 = tr2q3 / tr2count;
tr2q1 = tr2q1 / tr2count;
tr2max = tr2max / tr2count;
tr2min = tr2min / tr2count;

tr3mean = tr3mean / tr3count;
tr3q3 = tr3q3 / tr3count;
tr3q1 = tr3q1 / tr3count;
tr3max = tr3max / tr3count;
tr3min = tr3min / tr3count;

tr4mean = tr4mean / tr4count;
tr4q3 = tr4q3 / tr4count;
tr4q1 = tr4q1 / tr4count;
tr4max = tr4max / tr4count;
tr4min = tr4min / tr4count;

tr5mean = tr5mean / tr5count;
tr5q3 = tr5q3 / tr5count;
tr5q1 = tr5q1 / tr5count;
tr5max = tr5max / tr5count;
tr5min = tr5min / tr5count;

L1str = '1 ' + str(tr1mean) + ' ' + str(tr1q3) + ' ' + str(tr1q1)
             + ' ' + str(tr1max) + ' ' + str(tr1min) + '\n';

L2str = '2 ' + str(tr2mean) + ' ' + str(tr2q3) + ' ' + str(tr2q1)
             + ' ' + str(tr2max) + ' ' + str(tr2min) + '\n';

L3str = '3 ' + str(tr3mean) + ' ' + str(tr3q3) + ' ' + str(tr3q1) + ' '
             + str(tr3max) + ' ' + str(tr3min) + '\n';

L4str = '4 ' + str(tr4mean) + ' ' + str(tr4q3) + ' ' + str(tr4q1) + ' '
             + str(tr4max) + ' ' + str(tr4min) + '\n';

L5str = '5 ' + str(tr5mean) + ' ' + str(tr5q3) + ' ' + str(tr5q1) + ' '
             + str(tr5max) + ' ' + str(tr5min) + '\n';
```

```
trial_compressed.write(L1str);
trial_compressed.write(L2str);
trial_compressed.write(L3str);
trial_compressed.write(L4str);
trial_compressed.write(L5str);

trial_compressed.close();
fname.close();
```

F.3 Perl scripts used to sort files and automate graph creation

The following Perl scripts were used to further automate data processing. The open-source program xmgrace was used to generate the graphs included in this thesis. Aside from producing visually appealing graphs, xmgrace can be automated using a number of "gracebat" commands, which make the process slightly less time-consuming when dealing with uniform x- and y-axes.

F.3.1 Data compilation scripts

The following two scripts concatenated data files so that the effects of increasing trial frequency, target frequency, and trial number could be compared.

Frequency file compilation

```
@files = @ARGV;
foreach $file (@files)
{
    $file =~ m/^(\w*_\d*N_)\d*Hz_(\d)_(\w*).csv$/;
```

```
    $wavestring = $1;
    $trialstring = $2;
    $typestring = $3;

    $f1 = $wavestring . "025Hz_" . $trialstring . "_" .
          $typestring . ".csv";
    $f2 = $wavestring . "050Hz_" . $trialstring . "_" .
          $typestring . ".csv";
    $f3 = $wavestring . "100Hz_" . $trialstring . "_" .
          $typestring . ".csv";

    $outfile = $wavestring . $trialstring . "_" . $typestring . ".csv";

    system("(cat ${f1}; cat ${f2}; cat ${f3};) > ${outfile}");
}
```

Trial file compilation

```
@files = @ARGV;
foreach $file (@files)
{
    $file =~ m/^(\w*_\d*N_\d*Hz)_\d_(\w*).csv$/;
    $wavestring = $1;
    $typestring = $2;

    $f1 = $wavestring . "_1_" . $typestring . ".csv";
    $f2 = $wavestring . "_2_" . $typestring . ".csv";
    $f3 = $wavestring . "_3_" . $typestring . ".csv";
    $f4 = $wavestring . "_4_" . $typestring . ".csv";
    $f5 = $wavestring . "_5_" . $typestring . ".csv";

    $outfile = $wavestring . "_" . $typestring . ".csv";

    system("(cat ${f1}; cat ${f2}; cat ${f3}; cat ${f4}; cat ${f5};)
             > ${outfile}");
}
```

F.3.2 Sample graphing automation script

All graphing scripts have a similar format and could easily be generated using one such script as a template.

```
foreach $file (@files)
{
    $file =~ m/^(\d*R_\d*Hz_\d)_\w.csv$/;
    $wavestring = $1;
    $pafile = $wavestring . "_pa.csv";
    $pyfile = $wavestring . "_py.csv";
    $fafile = $wavestring . "_a.csv";
    $fyfile = $wavestring . "_y.csv";

    $poutfile = $wavestring . "_p.agr";
    $pprintfile = $wavestring . "_p.eps";
    $foutfile = $wavestring . "_f.agr";
    $fprintfile = $wavestring . "_f.eps";

    $ptopstring = "ptop";
    $ftopstring = "ftop";
    system("(cat ${ptopstring}; cat ${pafile}; cat middle; cat ${pyfile};
            echo \"&\") > ${poutfile}");
    system("gracebat -hardcopy -printfile ${pprintfile} -hdevice EPS
           ${poutfile}");
    system("(cat ${ftopstring}; cat ${fafile}; cat middle; cat ${fyfile};
           echo \"%\") > ${foutfile}");
    system("gracebat -hardcopy -printfile ${fprintfile} -hdevice EPS
           ${foutfile}");
}
```

BIBLIOGRAPHY

[Aaron et al., 1992] Aaron, E. E., Seow, K. C., Johnson, B. D., and Depmsey, J. A. (1992). Oxygen cost of exercise hyperpea: implications for performance. *Journal of Applied Physiology*, 72:1818–1825.

[Alkner et al., 2000] Alkner, B. A., Tesch, P. A., and Berg, H. E. (2000). Quadriceps emg/force relationship in knee extension and leg press. *Medicine and Science in Sports and Exercise*, 32(2):459–463.

[Allum and Young, 1976] Allum, J. H. J. and Young, L. R. (1976). The relaxed oscillation technique for the determination of the moment of inertia of limb segments. *Journal of Biomechanics*, 9:21–25.

[Brockett et al., 1997] Brockett, C., Warren, N., Gregory, J. E., Morgan, D. L., and Proske, U. (1997). A comparison of the effects of concentric versus eccentric exercise on force and position sense at the human elbow joint. *Brain Research*, 771:251–258.

[Buchanan et al., 2004] Buchanan, T. S., Lloyd, D. G., Manal, K., and Besier, T. F. (2004). Neuromusculoskeletal modeling: Estimation of muscle forces and joint moments and movements from measurements of neural command. *Journal of Applied Biomechanics*, 20(4):367–395.

[de Luca and Mambrito, 1987] de Luca, C. J. and Mambrito, B. (1987). Voluntary control of motor units in human antagonist muscles: Coactivation and reciprocal activation. *Journal of Neurophysiology*, 58(3):525–542.

[de Ruiter et al., 2005] de Ruiter, C. J., de Boer, M. D., Spanjaard, M., and de Haan, A. (2005). Knee angle-dependent oxygen consumption during isometric contractions of the knee extensors determined with near-infrared spectroscopy. *Journal of Applied Physiology*, 99:579–586.

[Doke et al., 2004] Doke, J., Donelan, J. M., and Kuo, A. D. (2004). Mechanics and energetics of swinging the human leg. *The Journal of Experimental Biology*, 208:439–445.

[Ellerby et al., 2005] Ellerby, D. J. et al. (2005). Blood flow in guinea fowl *Numida meleagris* as an indicator of energy expenditure by individual muscles during walking and running. *Journal of Physiology*, 564:631–648.

[Enoka, 1998] Enoka, R. M. (1998). *Neuromechanical Basis of Kinesiology*. Human Kinetics Publishers, second edition.

[Gray, 1918] Gray, H. (1918). *Anatomy of the Human Body*. Lea and Febiger, 20th edition. Bartleby.com, 2000.

[Hill, 1938] Hill, A. V. (1938). The heat of shortening and the dynamic constants of muscle. *Proceedings of the Royal Society of London*, 126(843):136–195.

[Hogan et al., 1998] Hogan, M. C., Ingham, E., and Kurdak, S. S. (1998). Contraction duration affects metabolic energy cost and fatigue in skeletal muscle. *American Journal of Physiology*, 274:E397–E402.

[Hunter and Lafontaine, 1992] Hunter, I. W. and Lafontaine, S. (1992). A comparison of muscle with artificial actuators. *Solid-State Sensor and Actuator Workshop*, pages 178–185.

[Kandel et al., 2000] Kandel, E. R., Schwartz, J. H., and Jessell, T. M., editors (2000). *Principles of Neural Science*. McGraw-Hill, fourth edition.

[Kilbreath and Gandevia, 1993] Kilbreath, S. L. and Gandevia, S. C. (1993). Neural and biomechanical specializations of human thumb muscles revealed by matching weights and grasping objects. *Journal of Physiology*, 472:537–556.

[Norssell, 2000] Norssell, U. (2000). Magnus gustaf blix (1849-1904); neurophyisological, physiological, and engineering virtuoso. *Journal of the History of the Neurosciences*, 9(3):238–249.

[Ogita et al., 2000] Ogita, F. et al. (2000). Oxygen uptake in one-legged and two-legged exercise. *Medicine and Science in Sports and Exercise*, pages 1737–1742.

[Paterson et al., 2005] Paterson, N. D., Kowalchuk, J. M., and Paterson, D. H. (2005). Kinetics of $\dot{V}_{O_2}$ and femoral artery blood flow during heavy-intensity, knee-extension exercise. *Journal of Applied Physiology*, 99:683–690.

[Peyton, 1986] Peyton, A. J. (1986). Determination of the moment of inertia of limb segments by a simple method. *Journal of Biomechanics*, 19(5):405–410.

[Praagman et al., 2003] Praagman, M., Veeger, H. E. J., Chadwick, E. K. J., Colier, W. N. J. M., and van der Helm, F. C. T. (2003). Muscle oxygen consumption, determined by nirs, in relation to external force and emg. *Journal of Biomechanics*, 36:905–912.

[Quaresima et al., 2001] Quaresima, V., Colier, W. N. J. M., van der Sluijs, M., and Ferrari, M. (2001). Nonuniform quadriceps o_2 consumption revealed by near infrared multipoint measurements. *Biochemical and Biophysical Research Communications*, 285:1034–1039.

[Scott and Winter, 1991] Scott, S. H. and Winter, D. A. (1991). A comparison of three muscle pennation assumptions and their effect on isometric and isotonic force. *Journal of Biomechanics*, 24(2):163–167. Technical Note.

[Slifkin et al., 2000] Slifkin, A. B., Vaillancourt, D. E., and Newell, K. M. (2000). Intermittency in the control of continuous force production. *Journal of Neurophysiology*, 84:1708–1718.

[Srinivasan and Ruina, 2006] Srinivasan, M. and Ruina, A. (2006). Computer optimization of a minimal biped model discovers walking and running. *Nature*, 439:72–75.

[Srinivasan and Chen, 1993] Srinivasan, M. A. and Chen, J.-S. (1993). Human performance in controlling normal forces of contact with rigid objects. In Kazerooni, H., Colgate, J. E., and Adelstein, B. D., editors, *Advances in Robotics, Mechatronics and Haptic Interfaces, 1993*, pages 119–125. ASME.

[Tan et al., 1994] Tan, H. Z., Srinivasan, M. A., Eberman, B., and Cheng, B. (1994). Human factors for the design of force-relating haptic interfaces. *ASME DSC*, 55(1):353–359.

[Valero-Cuevas, 2007] Valero-Cuevas, F. (2007). MAE 463 Class Notes.

[Vander et al., 1970] Vander, A. J., Sherman, J. H., and Luciano, D. S. (1970). *Human Physiology: The Mechanisms of Body Function*. McGraw-Hill, second edition.

[Vokac et al., 1975] Vokac, Z., Bell, H., Bautz-Holter, E., and Rodahl, K. (1975). Oxygen uptake/heart rate relationship in leg and arm exercise, sitting and standing. *Journal of Applied Physiology*, 39:54–59.

[Weerakkody et al., 2003] Weerakkody, N., Percival, P., Morgan, D. L., Gregory, J. E., and Proske, U. (2003). Matching different levels of isometric torque in elbow flexor muscles after eccentric exercise. *Experimental Brain Research*, 149:141–150.

[Wilkie, 1950] Wilkie, D. R. (1950). The relation between force and velocity in human muscle. *Journal of Physiology*, 110:249–280.

[Xu and Rhodes, 1999] Xu, F. and Rhodes, E. C. (1999). Oxygen uptake kinetics during exercise. *Journal of Sports Medicine*, 27:313–327.

[Yamaguchi et al., 1990] Yamaguchi, G. T., Sawa, A.-U., Moran, D. W., Fessler, M. J., and Winters, J. M. (1990). Appendix: A survey of human musculotendon actuator properties. In Winters, J. M. and Woo, S.-Y., editors, *Multiple Muscle Systems: Biomechanics and Movement Organization*. Springer-Verlag.

[Zajac, 1989] Zajac, F. E. (1989). Muscle and tendon: properties, models, scaling, and application to biomechanics and motor control. *Critical Reviews in Biomedical Engineering*, 17(4):359–411.